te technical note techn

Airport Surveillance Radar (ASR) Solid-State Transmitter Demonstration Final Report

Thomas A. Healy

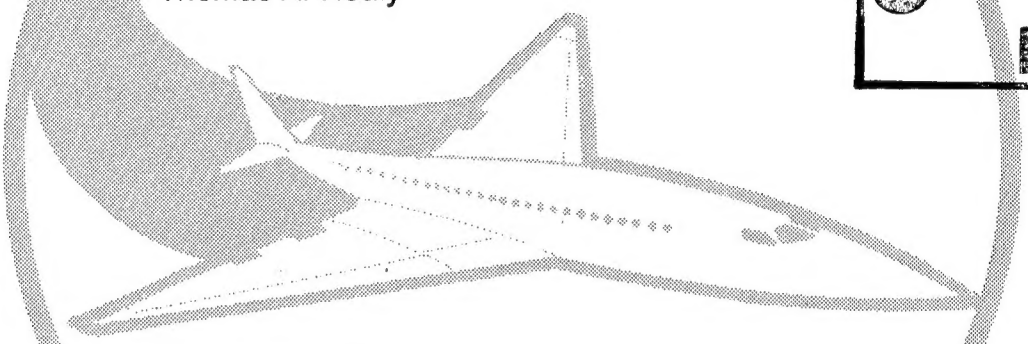

December 1994

DOT/FAA/CT-TN94/11

U.S. Department of Transportation
Federal Aviation Administration

Technical Center
Atlantic City Airport, NJ 08405

NOTICE

This document is disseminated under the sponsorship of the U.S. Department of Transportation in the interest of information exchange. The United States Government assumes no liability for the contents or use thereof.

The United States Government does not endorse products or manufacturers. Trade or manufacturers' names appear herein solely because they are considered essential to the objective of this report.

Technical Report Documentation Page

1. Report No.	2. Government Accession No.	3. Recipient's Catalog No.
DOT/FAA/CT-TN94/11		

4. Title and Subtitle	5. Report Date
AIRPORT SURVEILLANCE RADAR (ASR) SOLID-STATE TRANSMITTER DEMONSTRATION FINAL REPORT	September 1994
	6. Performing Organization Code
7. Author(s) Thomas A. Healy, Richard L. Ferranti, MIT Lincoln Laboratories	8. Performing Organization Report No. DOT/FAA/CT-TN94/11
9. Performing Organization Name and Address U.S. Department of Transportation Federal Aviation Administration Technical Center Atlantic City International Airport, NJ 08405	10. Work Unit No. (TRAIS)
	11. Contract or Grant No.
12. Sponsoring Agency Name and Address U.S. Department of Transportation Federal Aviation Administration Research and Development Service, ARD-90 Washington, DC 20591	13. Type of Report and Period Covered Technical Note
	14. Sponsoring Agency Code

15. Supplementary Notes

16. Abstract

Present versions of the Federal Aviation Administration (FAA) Airport Surveillance Radar (ASR) use either magnetron or klystron radar transmitter configurations. These radars transmit a simple pulse waveform and use the peak power capabilities in the detection process. Solid-state technology does not allow for transmission of high-peak power pulses in the S-band. As a consequence, the solid-state transmitter uses the average power capabilities of the transmitted pulses. A longer, lower peak power pulse is transmitted. The pulse is coded to increase the bandwidth of the transmitted waveform. Upon reception of the echo, the long pulse is compressed to provide the range resolution of a shorter pulse.

This report presents results of tests of a solid-state transmitter system developed by ITT and Thomson-CSF under a Cooperative Research and Development Agreement (CRDA) with the FAA. The demonstration system was tested at the ASR-9 test facility at the FAA Technical Center, Atlantic City International Airport, NJ. The tests performed were divided into three major categories; transmitter tests, receiver tests, and system tests. The transmitter tests included measurements of the waveforms and operating frequencies; the output power; the output spectrum; and a maintainability demonstration. The receiver tests included measurements of the noise figure, dynamic range, bandwidth, and waveform characteristics at the output of the pulse compressor. The system tests included measurements of the pulse compression time sidelobe performance, stability, detection performance, and range resolution.

17. Key Words	18. Distribution Statement
Solid-state Pulse Compression Stability Detection Resolution	Document is available to the public through the National Technical Information Service, Springfield, VA 22161

19. Security Classif. (of this report)	20. Security Classif. (of this page)	21. No. of Pages	22. Price
Unclassified	Unclassified	158	

Form DOT F 1700.7 (8-72) Reproduction of completed page authorized

TABLE OF CONTENTS

LIST OF ILLUSTRATIONS

LIST OF ILLUSTRATIONS (Continued)

LIST OF ILLUSTRATIONS (Continued)

LIST OF TABLES

EXECUTIVE SUMMARY

This report details the results of tests performed on a solid-state transmitter system developed jointly by ITT and Thomson-CSF, the Cooperative Research Organization (CRO), for integration into the Airport Surveillance Radar, model 9 (ASR-9).

The tests performed were divided into three major categories; transmitter tests, receiver tests, and system tests. The transmitter tests included measurements of the waveforms and operating frequencies; the output power; the output spectrum; and a maintainability demonstration. The maintainability demonstration included transmitter built-in test (BIT); fail-soft operation; module replacement; and transmitter remote monitoring capabilities.

The receiver tests were subdivided into three categories: receiver measurements, pulse compression measurements, and stability measurements. Receiver measurements of the noise figure; dynamic range at the in-phase and quadrature (I and Q) outputs; receiver bandwidth at the I and Q outputs; I and Q phase and amplitude errors were performed. Pulse compression measurements included waveform characteristics measurements at the pulse compression output relative to doppler, range position, and input level.

The system tests were designed to evaluate the performance of the demonstration equipment with the ASR-9. The system tests included measurements of the pulse compression time sidelobe performance; stability; detection performance, and range resolution.

It should be noted that data collected at the demonstration receiver is 18-bit data whereas the ASR-9 moving target detection (MTD) processor is a 12-bit processor. The interface of the demonstration receiver to the MTD processor introduced a reduction in the dynamic range of the demonstration system. Therefore, the full capabilities of the demonstration system may not be seen in data collected at the output of the ASR-9. Poor performance as measured at the output of the radar during some of the tests may be due to the dynamic range reduction and will not be attributed solely to the demonstration equipment.

1. OBJECTIVES.

This report presents the results of the test and evaluation of a solid-state transmitter and receiver system developed to interface with the Airport Surveillance Radar, model 9 (ASR-9). The purpose of the effort was to evaluate the suitability of a solid-state transmitter coupled with digital pulse compression techniques for an S-band ASR.

2. BACKGROUND.

The FAA ASR is designed to provide coverage within a 60-nautical mile (nmi) radius of the radar for 360° below 25000 feet elevation. Present versions of the FAA ASRs use either magnetron or klystron radar transmitter configurations. These radars transmit a simple pulse waveform and use the peak power capabilities in the detection process.

Since solid-state technology does not allow for transmission of high peak power pulses in the S-band, the solid-state transmitter uses the average power capabilities of the transmitted pulses. A longer, lower peak power pulse is transmitted. The pulse is coded to increase the bandwidth of the transmitted waveform. Upon reception of the echo, the long pulse is compressed to provide the range resolution of a shorter pulse.

Under a Cooperative Research and Development Agreement (CRDA), ITT Gilfillan, a unit of ITT Defense and Electronics (ITT), and Thomson-CSF (TCSF) developed a solid-state transmitter and receiver system for interface to existing ASR-9 equipment. The transmitter and receiver performance was evaluated at the FAA Technical Center ASR-9 facility, Atlantic City International Airport, NJ. The demonstration transmitter and receiver replaced the ASR-9 channel A klystron transmitter and radio frequency (rf)/intermediate frequency (if) receiver during testing.

The demonstration system transmits a dual pulse waveform as shown in figure 2-1. A 75-microsecond (μs) long pulse is followed by a 1-μs short pulse with a 1-μs separation between the two pulses. The pulses are transmitted at different frequencies. Nonlinear frequency modulation (FM) codes the waveform to increase the bandwidth and lower the pulse compression time sidelobes. The long pulse enables the solid-state transmitter to operate at a lower peak power than the klystron transmitter while achieving the needed energy on target. The short pulse is required for detection at short range.

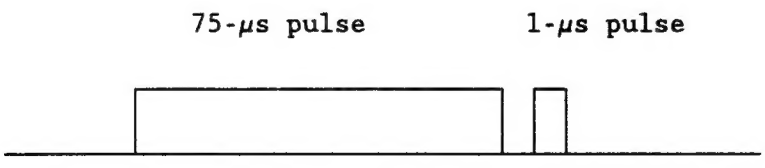

FIGURE 2-1. TRANSMITTED PULSE WAVEFORM

Several performance issues must be addressed when designing a pulse compression system for a terminal radar environment:

a. The level of the pulse compression time sidelobes must be low in order to resolve two targets in range.

b. The system stability must be high in order to detect gust fronts and small targets in clutter.

c. The radar must provide continuous coverage when short and long pulses are used.

d. The choice of pulse code for the long pulse must allow for the detection of weather events.

3. RELATED DOCUMENTATION.

a. Test Plan for the ITT Gilfillan/Thomson-CSF Solid State Airport Surveillance Radar Transmitter System, Massachusetts Institute of Technology Lincoln Laboratory, Lexington, Massachusetts.

b. Test Plan for Solid State Transmitter CRDA Demonstration Equipment, ITT Gilfillan, Van Nuys, California.

c. CRDA Demonstration Test Plan, Thomson-CSF, Meudon, France.

d. Airport Surveillance Radar (ASR-9), DOT, FAA Specification, FAA-E-2704.

e. ASR-9 System Manuals, Westinghouse Electric Corporation, Baltimore, Maryland.

4. DEMONSTRATION EQUIPMENT DESCRIPTION.

A block diagram of the solid-state transmitter is shown in figure 4-1. The transmitter employs several stages of amplification. The synthesized RF pulse is fed through a preamplifier into class C driver and final stage amplifiers. The transmitter has two preamplifier/driver channels.

An input switch to the preamplifier/driver channels was used to switch the synthesized RF pulse into the desired channel because only one synthesizer channel was available for the demonstration. In a full-up ASR configuration, this input switch is not required, as the synthesized RF pulse for each of the two preamplifier/driver channels is fed from two synthesizers. Channel switching is designed to be done automatically in the event of channel failure, but can also be performed manually for maintenance.

The output of the active channel is switched into a final stage consisting of 40 identical driver modules. The final stage modules are the same type as the driver modules in each channel.

Twelve identical 43-volt power supply modules (not shown in figure 4-1) provide the direct current (dc) power for the transmitter. The transmitter was designed so that loss of up to three power supply modules should not affect transmitter operation.

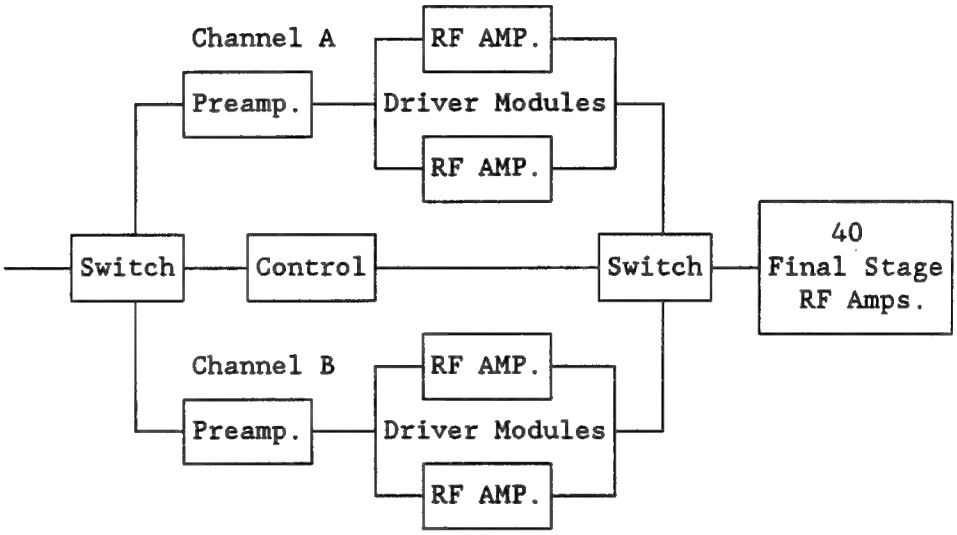

FIGURE 4-1. SOLID-STATE TRANSMITTER BLOCK DIAGRAM

The receiver/synthesizer block diagram is shown in figure 4-2. The synthesizer generates the RF drive pulse for amplification by the transmitter and provides 31 megahertz (MHz) timing to the receiver.

The receiver has two channels; one processes long-pulse returns and the other processes short-pulse returns. After down conversion, the analog video is converted to digital video and detected. The long pulse is also digitally pulse compressed. The receiver then time aligns the digital video. The resultant digital video is 18-bit I and Q data. Note that the 18 bits are truncated to 12 bits for interface to the ASR-9 processor as described in the next section.

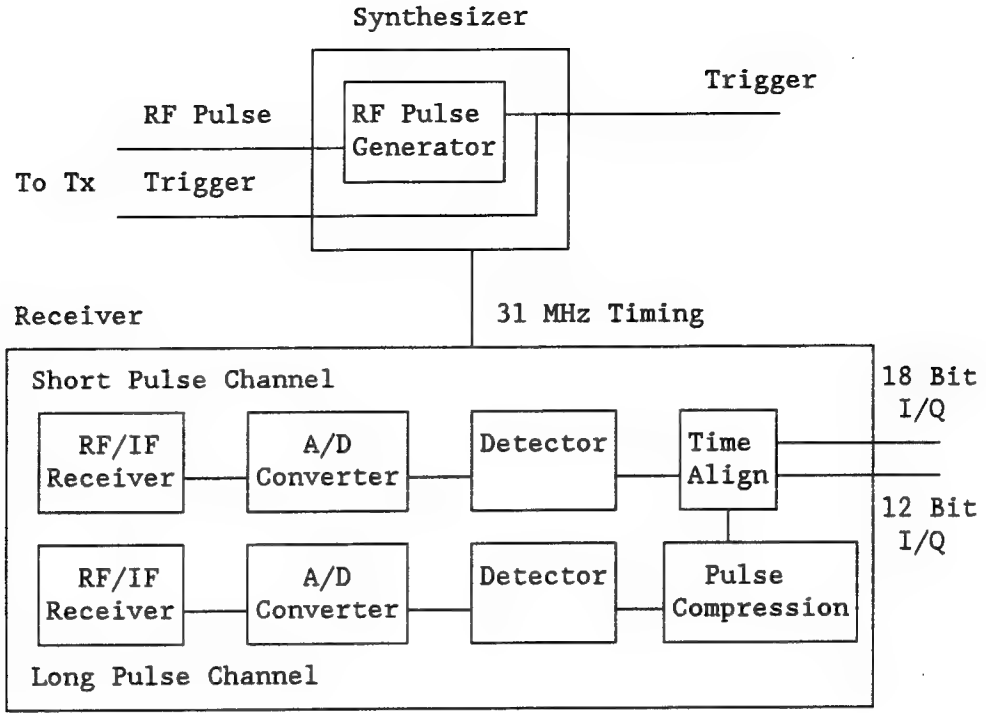

FIGURE 4-2. DEMONSTRATION RECEIVER/SYNTHESIZER BLOCK DIAGRAM

5. DEMONSTRATION EQUIPMENT INTERFACE TO THE ASR-9.

A block diagram of the demonstration transmitter and receiver interface to the ASR-9 is shown in figure 5-1.

The receiver/synthesizer used the existing modcharge trigger generated by the ASR-9 receiver/processor. The modcharge trigger was properly delayed to account for differences in the demonstration waveform and that of the ASR-9. The synthesizer then generated the RF pulse and sent it to the solid-state transmitter for amplification.

The ASR-9 channel A klystron transmitter was physically disconnected from the system during the demonstration. The solid-state transmitter was connected through a dual bandpass filter (used for spectrum control) to the ASR-9 waveguide in the transmit path.

The demonstration receiver was connected to Channel A of the ASR-9 at the output of the Low Noise Amplifier (LNA) and replaced the existing ASR-9 RF/IF receiver. After detection and digital pulse compression, the receiver aligned data from the short pulse and the long pulse and sent 12-bit in-phase and quadrature (I and Q) data to the post processor at a 772 nanosecond (ns) rate. The 31-MHz coherent oscillator (COHO) signal was supplied to the ASR-9 processor from the receiver/synthesizer. The receiver/synthesizer also controlled the ASR-9 Sensitivity Time Control (STC) and high/low beam switch.

There was a hard limit introduced in the reduction of the data from 18 bits to 12 bits for the interface to the ASR-9 processor. The most significant 6 bits were eliminated to preserve the system linearity. Therefore, strong radar returns limit the dynamic range of the demonstration system when it is interfaced to the ASR-9.

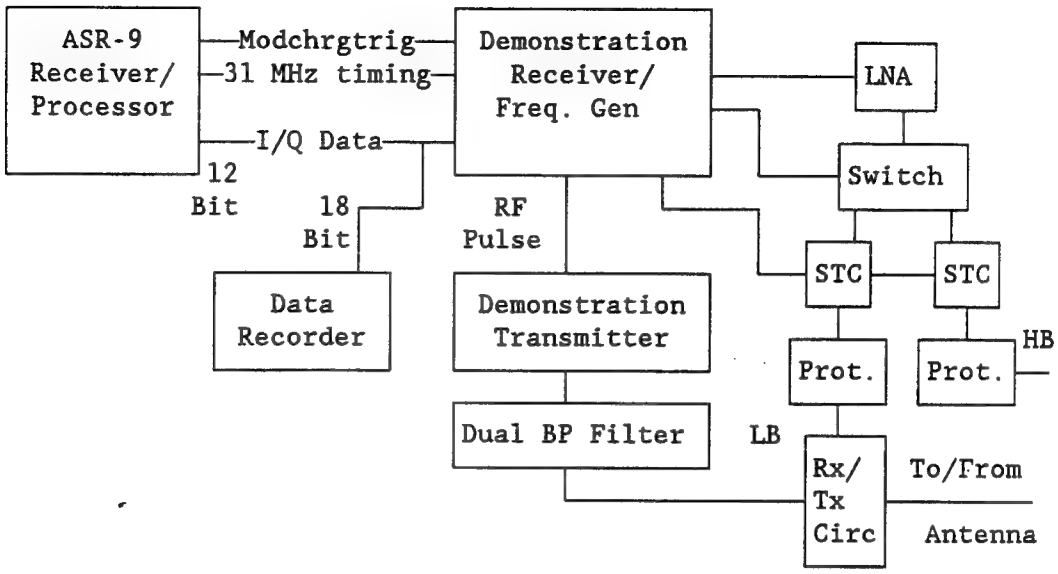

FIGURE 5-1. DEMONSTRATION EQUIPMENT INTERFACE TO THE ASR-9

6. DATA RECORDING CAPABILITIES.

The Cooperative Research Organization (CRO) supplied a personal computer based data recording capability at the demonstration receiver. Predetection data or post-detection data could be recorded from the long or short pulse. Long-pulse data could also be recorded before or after pulse compression.

The CRO data recorder was limited to 16 kilobytes (Kb) of data per scan. The record window was adjustable in range and azimuth. For example, data could be collected for 1024 range cells (1/16 nmi) and 16 pulse repetition intervals (PRI), or 512 range cells and 32 PRIs, etc. The small recording capacity limited the effectiveness of the recorder for use in flight tests (i.e., the aircraft was often not in the record window) or weather data collection.

The personal computer (PC) could present the recorded data in several ways:

a. The mean power (i.e., $(I^2 + Q^2)^{1/2}$) at each range cell was computed and plotted versus the range. The computation was made for a user selectable number of PRIs, for any burst selection (high pulse repetition frequency (PRF), low PRF, or both). This presentation showed the level of the time sidelobes relative to the main pulse.

b. The pulse spectrum was presented for a chosen range cell with a user selectable number of points in the Fast Fourier Transform (FFT) for any burst selection.

c. The phase was plotted versus the PRI. This information was used in the phase stability measurement.

In addition to the calculations performed with the PC, the data recorded on the CRO recorder was analyzed at Lincoln Laboratory. The following analyses were completed:

a. System stability using the moving target simulator (MTS).

b. Time sidelobe levels for the aircraft in available clutter. Note that the Atlantic City area is not a severe clutter environment.

c. Time sidelobe levels as a function of transmit module changes and transmitter temperature, using a long delay line.

d. Detection performance for aircraft crossing the long-/short-pulse boundary.

Data was also recorded at the output of the ASR-9 and analyzed using the Integrated Radar Evaluation System (IRES) developed by the weather/primary surveillance division (ACW-200C) at the Federal Aviation Administration (FAA) Technical Center. Primary and secondary surveillance (beacon) reports were collected with IRES. The beacon reports provided a source of truth for aircraft positions during flight tests.

The IRES is a PC based tool containing a custom circuit board for data recording and software programs for data analysis. IRES presents results in tabular or plotted form (histograms, range-azimuth plots). The software analysis programs include a filter program for isolating data of interest, an alpha beta tracker for false alarm analysis, and percent detection and resolution programs.

It should be noted that data collected at the demonstration receiver is 18-bit data whereas the ASR-9 MTD is a 12-bit processor. The interface of the demonstration receiver to the moving target detection (MTD) processor introduced a reduction in the dynamic range of the demonstration system. Therefore, the full capabilities of the demonstration system may not be seen in data collected at the output of the ASR-9. Poor performance as measured at the output of the radar during some of the tests may be due to the dynamic range reduction and will not be attributed solely to the demonstration equipment.

Data was also recorded using the ASR-9 Digital Recorder Interface (DRI). The DRI records primitive reports at the input to the ASR-9 Correlation and Interpolation (C&I) processor. The primitive reports include range, azimuth, and amplitude information for each PRI.

7. SOLID-STATE TRANSMITTER DEMONSTRATION.

The solid-state transmitter demonstration included measurements of the waveforms and operating frequencies, output power, input power variation, spectrum, and a maintainability demonstration. The maintainability demonstration included Built-In Test (BIT), fail soft operation, module replacement, and remote monitoring capabilities of the transmitter.

7.1 WAVEFORMS AND OPERATING FREQUENCIES.

The purpose of this test was to verify that the solid-state transmitter outputs a dual pulse waveform consisting of a 75-μs nonlinear FM coded pulse followed by a 1-μs uncoded pulse. The pulse characteristics including the pulse widths, rise times, and fall times, were also measured.

The test configuration is shown in figure 7.1-1. The synthesizer generated a pulsed signal of fixed PRF (1000 hertz (Hz)) to drive the transmitter. The transmitter output was monitored at a spectrum analyzer and oscilloscope after being appropriately coupled and amplitude detected. The Tektronix 2782A spectrum analyzer (with counter) was used to measure the frequencies of the long and short pulses. Frequency measurements were made when the long pulse transmitted on 2815 MHz and the short pulse transmitted on 2725 MHz. The measured frequencies are shown in table 7.1-1.

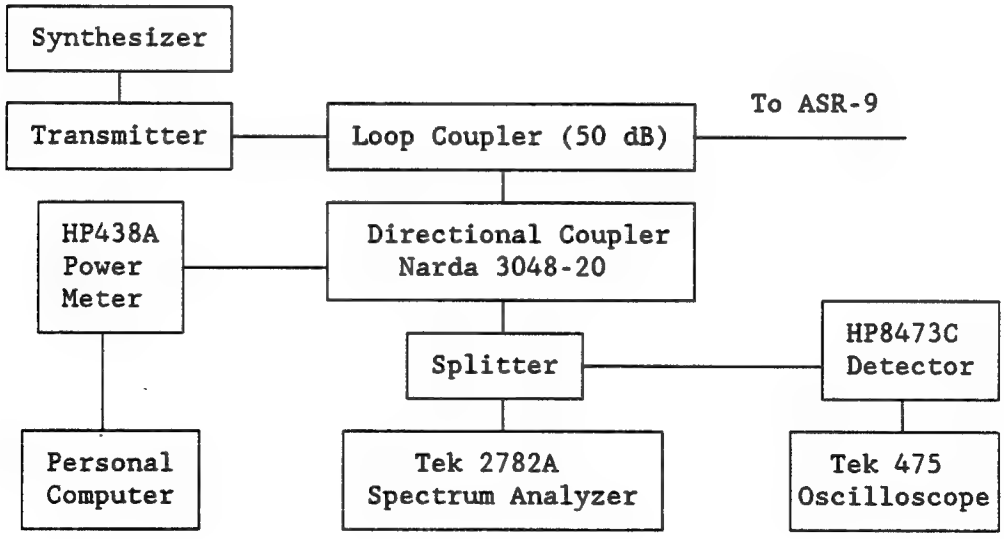

FIGURE 7.1-1. TRASMITTER DEMONSTRATION CONFIGURATION

The dual pulse waveform, pulse widths, rise times, and fall times were measured using a Tektronix 475 oscilloscope after the signal had been amplitude detected using a HP8473C diode detector. On a 10 μs/division scale, the scope showed the dual pulse waveform consisting of nominally 75 μs pulse followed by a 1 μs pulse. With a smaller scope time scale, the pulse width measurements were made at the 50-percent amplitude points of each pulse and the rise and fall times were measured between the 10 percent and 90 percent amplitude points. The measured values can also be found in table 7.1-1.

TABLE 7.1-1. WAVEFORMS AND OPERATING FREQUENCIES

	Pulse Width (μs)	Rise Time (ns)	Fall Time (ns)	Frequency (MHz)
Long Pulse (2815 MHz)	74.2	240	72	2814.765
Long Pulse (2725 MHz)	74.2	150	60	N/A
Short Pulse (2815 MHz)	.88	100	65	N/A
Short Pulse (2725 MHz)	.86	100	72	2724.735

7.2 OUTPUT POWER.

The purpose of this test was to measure the peak output power of the long and short pulses at the two radar operating frequencies, with each of Channel A and Channel B drivers selected.

The configuration for this test is shown in figure 7.1-1. The power of the solid-state transmitter was measured at the coupled outputs of a calibrated ITT loop coupler (with attenuations of 51.62 decibel (dB) at 2.815 gigahertz (GHz) and 52.035 dB at 2.725 GHz) and a Narda 4038-20 directional coupler (measured 20.35 dB) into a power meter (HP438A). The directional coupler was removed for short-pulse power measurements because the added attenuation was not needed. The synthesizer drove the transmitter with a fixed 1000-Hz PRF signal in order to keep the meter stable.

Table 7.2-1 shows the results of the measurements. The power was measured for each transmitter driver channel for each operating frequency. The pulse widths are the same as presented in the previous section.

TABLE 7.2-1. TRANSMITTER OUTPUT POWER

		Short Pulse			Long Pulse		
		Meter Power (μW)	Pulse Width (μs)	Peak Power (kW)	Meter Power (μW)	Pulse Width (μs)	Peak Power (kW)
2.815 GHz	Chan. A	108.00	.84	18.7	109.50	74.25	23.3
	Chan. B	110.30	.835	19.1	106.70	74.25	22.6
2.725 GHz	Chan. A	105.20	.85	19.8	94.0	74.25	21.9
	Chan. B	104.65	.85	19.7	93.4	74.25	21.8

The peak output power of the transmitter can be calculated using the equation:

Peak Power = Meter Power(dBW) + Coupling Loss(dB) + Duty Factor(dB)

For example, the peak power for the short pulse (SP) and the long pulse (LP) at 2.815 GHz (Channel A) is calculated as shown:

$$\text{Peak Power}_{SP} = 10 \log(108 \times 10^{-6}) + 51.62 + 10 \log(10^{-3}/.84\times10^{-6})$$
$$= -39.67 + 51.62 + 30.76 = 42.7 \text{ dBW} = 18.7 \text{ kW}$$

$$\text{Peak Power}_{LP} = 10 \log(109.5 \times 10^{-6}) + 71.97 + 10 \log(10^{-3}/74.25\times10^{-6})$$
$$= -39.6 + 71.97 + 11.29 = 43.66 \text{ dBW} = 23.3 \text{ kW}$$

The average power for the long pulse for a 1000 μs PRI is

$$\text{Avg. Power}_{LP} = 43.66 \text{ dBW} + 10\log(74.25\times10^{-6}/10^{-3}) = 32.36 \text{ dBW}$$
$$= 1724.6\text{kW}$$

The average power of the ASR-9 klystron for peak power of 1.3 MW and pulse width of 1.03 μs is:

$$\text{Avg. Power}_{ASR\text{-}9} = 61.13 \text{ dBW} + 10 \log (1.03 \times 10^{-6}/10^{-3}) = 31.25 \text{ dBW}$$
$$= 1336 \text{ kW}$$

7.3 INPUT POWER VARIATION.

The purpose of this test was to measure the effects on the transmitter output power and dc bus voltage when the input line voltage was varied.

This measurement was made at ITT Gilfillan in Van Nuys, California, prior to shipment of the equipment to the FAA Technical Center. The current on each phase, the dc bus voltage, and transmitter rf output power were monitored while the line voltage was varied using a variac. Table 7.3-1 shows the current measured on each phase, the dc bus voltage, and the RF power out of the transmitter as the input voltage was adjusted. The coupling factor for the power measurement was 83.17 dB and the duty cycle was 7.5 percent.

TABLE 7.3-1. TRANSMITTER INPUT POWER VARIATION

Line Voltage (Vac)	RF (MHz)	Phase A Current (Amps rms)	Phase B Current (Amps rms)	Phase C Current (Amps rms)	DC Bus Voltage (volts)	RF Power (μW)
102/177	2815	37.00	35.50	34.00	43.12	110.10
120/208	2815	31.00	30.00	30.00	43.12	110.10
138/239	2815	27.00	26.00	25.50	43.12	110.10

The results show no adverse effects on the output power or the dc bus voltage when the line voltage was varied.

7.4 OUTPUT SPECTRUM.

The purpose of this test was to measure the output spectrum of the solid-state transmitter's short-pulse and long-pulse waveforms, and compare it with the National Telecommunications and Information Administration (NTIA) Radar Spectrum Emissions Criteria (RSEC) requirements.

The output spectrum of the transmitter was monitored at the coupled output of a directional coupler in the waveguide path following the dual bandpass filter with a spectrum analyzer. The dual bandpass filter was installed in the waveguide between the loop coupler at the transmitter output and the ASR-9 waveguide to limit the significant transmitted energy to the two radar operating frequencies. The two cavities in the dual bandpass filter were designed to pass energy at the operating frequencies (2725 MHz and 2815 MHz).

The NTIA RSEC requirements for the long pulse at 2815 MHz and the short pulse at 2725 MHz are shown in table 7.4-1. The attenuation is relative to the peak amplitude. The RSEC bandwidths were calculated using a 72 ns fall time (the smaller of the pulse rise or fall time) taken from table 7.2-1. The bandwidth values in table 7.4-1 correspond to the configuration with the dual bandpass filter installed.

TABLE 7.4-1. RSEC BANDWIDTH REQUIREMENTS

	Long Pulse 72 ns falltime			Short Pulse 72 ns falltime		
Atten. (dB)	Start Freq. (MHz)	Stop Freq. (MHz)	RSEC BW (MHz)	Start Freq. (MHz)	Stop Freq. (MHz)	RSEC BW (MHz)
-40	2810.71	2819.29	8.58	2713.45	2736.55	23.10
-45	2810.04	2819.96	9.92	2711.66	2738.34	26.68
-50	2809.28	2820.72	11.44	2709.59	2740.41	30.82
-55	2808.39	2821.61	13.22	2707.21	2742.79	35.58
-60	2807.37	2822.63	15.26	2704.46	2745.54	41.08
-65	2806.19	2823.81	17.62	2701.28	2748.72	47.44
-70	2804.82	2825.18	20.36	2697.60	2752.40	54.80
-75	2803.25	2826.75	23.50	2693.36	2756.64	63.28
-80	2801.43	2828.57	27.15	2688.47	2761.53	73.06

Figures 7.4-1 through 7.4-4 show the measured spectra for the short pulse at 2725 MHz and the long pulse at 2815 MHz for each transmitter driver selected. The measurements were made on 100 MHz and 50 MHz spans, respectively, while both pulses were transmitted.

Comparison of the measured spectra for the short pulse (with each driver channel selected) in figures 7.4-1 and 7.4-2 with the bandwidth values in table 7.4-1 shows compliance with NTIA RSEC limits. The bandwidths at the higher attenuations (i.e., -75 and -80 dB) cannot be seen in the plot due noise floor limitations of the spectrum analyzer.

Comparison of the measured spectra for the long pulse in figures 7.4-3 and 7.4-4 with the bandwidth values in table 7.4-1 shows that the measured values slightly exceed the NTIA requirements at several attenuation levels. This is not seen as a significant event since the requirements in table 7.4-1 were calculated using the measured pulse fall time (72 ns). The fall time value is dependent on the detector used in the measurement and some margin for error should be allowed. As a result there is a margin of error in the calculated values in table 7.4-1.

Figures 7.4-5 through 7.4-12 show the spectra with the transmitter outputting one pulse at frequency (f1). The measurements were made with a 150-MHz span. The energy at both radar operating frequencies is shown in each figure. The energy at the "untransmitted" frequency (f2) is that which leaked through the passband of the dual bandpass filter. The maximum power level at f2 for all the figures is approximately -37 decibel below the carrier (dBc).

The leakage is not considered a significant spectrum issue since all of the energy is transmitted at the allocated radar frequencies.

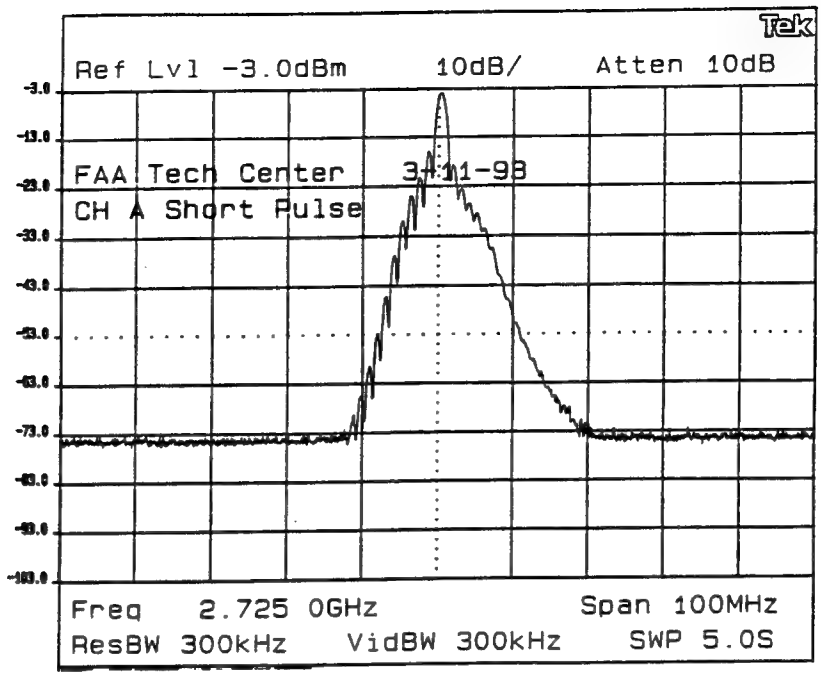

FIGURE 7.4-1. SHORT PULSE SPECTRUM - CHANNEL A - BOTH PULSES TRANSMITTED

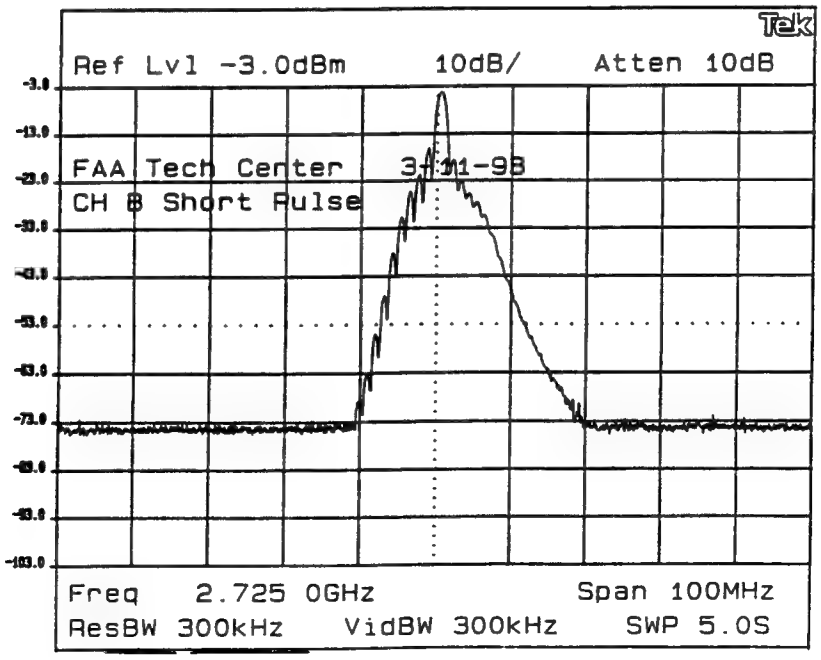

FIGURE 7.4-2. SHORT PULSE SPECTRUM - CHANNEL B - BOTH PULSES TRANSMITTED

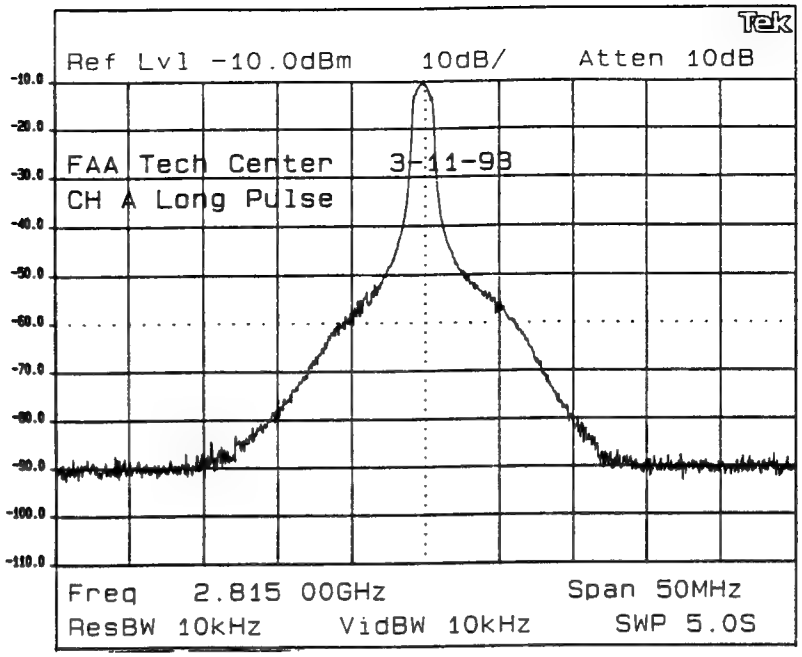

FIGURE 7.4-3. LONG PULSE SPECTRUM - CHANNEL A - BOTH PULSES TRANSMITTED

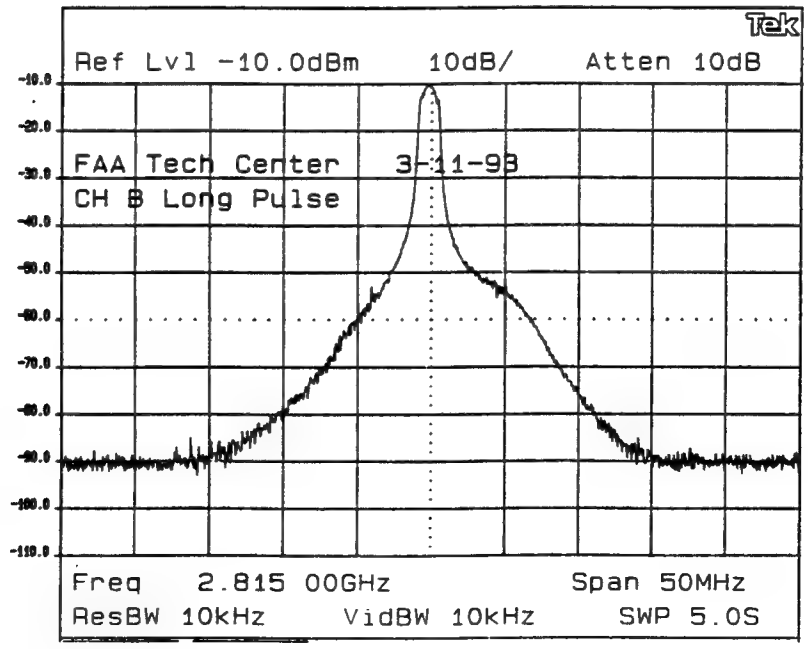

FIGURE 7.4-4. LONG PULSE SPECTRUM - CHANNEL B - BOTH PULSES TRANSMITTED

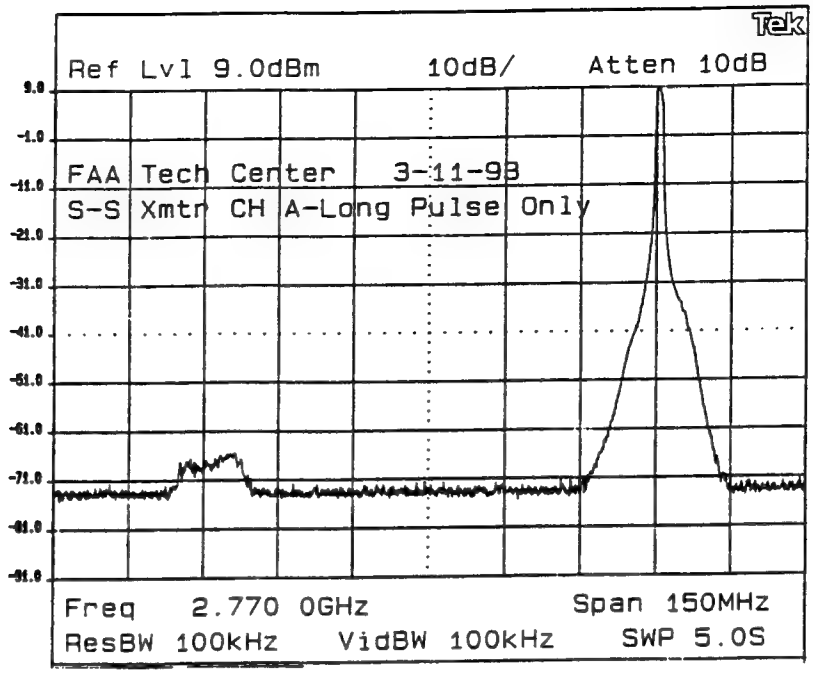

FIGURE 7.4-5. TRANSMITTED SPECTRUM - CHANNEL A - LONG PULSE ONLY

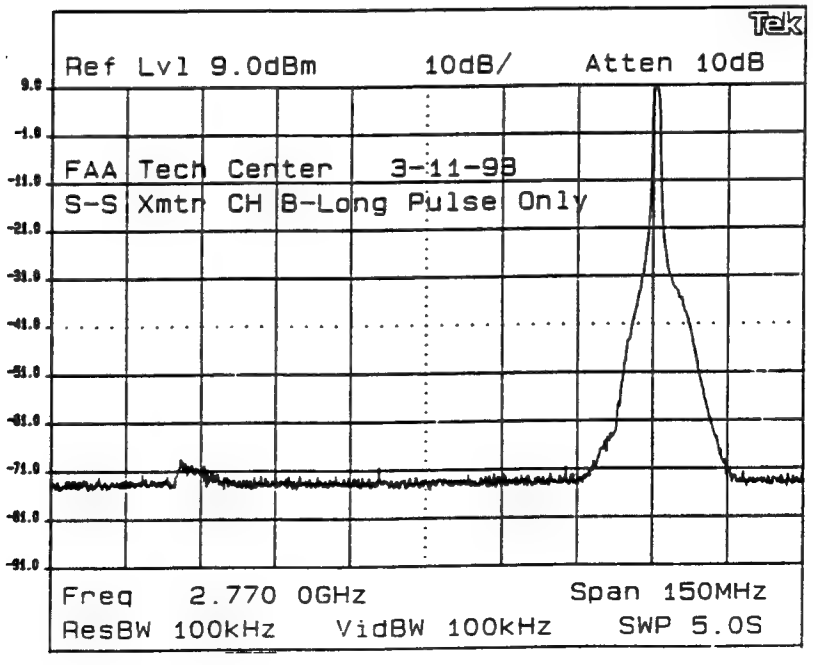

FIGURE 7.4-6. TRANSMITTED SPECTURM - CHANNEL B - LONG PULSE ONLY

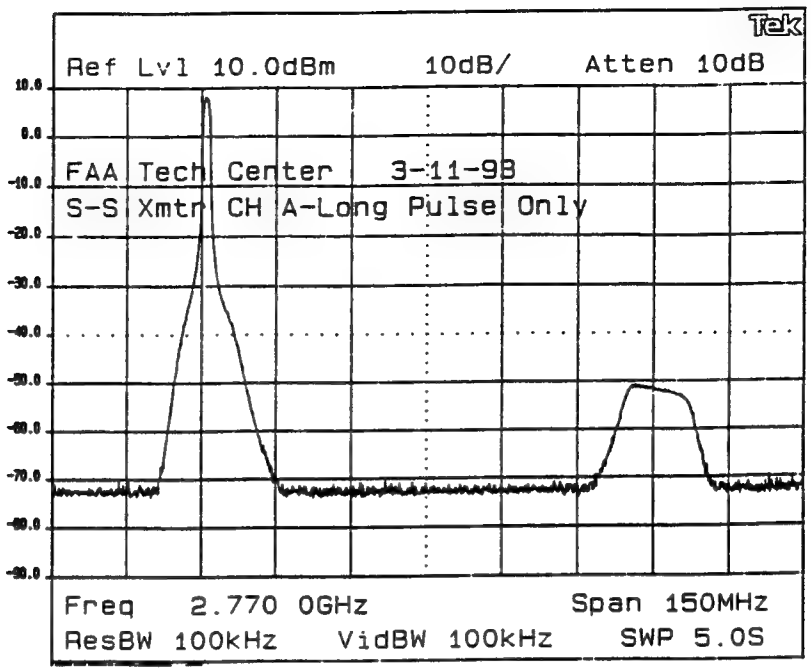

FIGURE 7.4-7. TRANSMITTED SPECTRUM - CHANNEL A - LONG PULSE ONLY

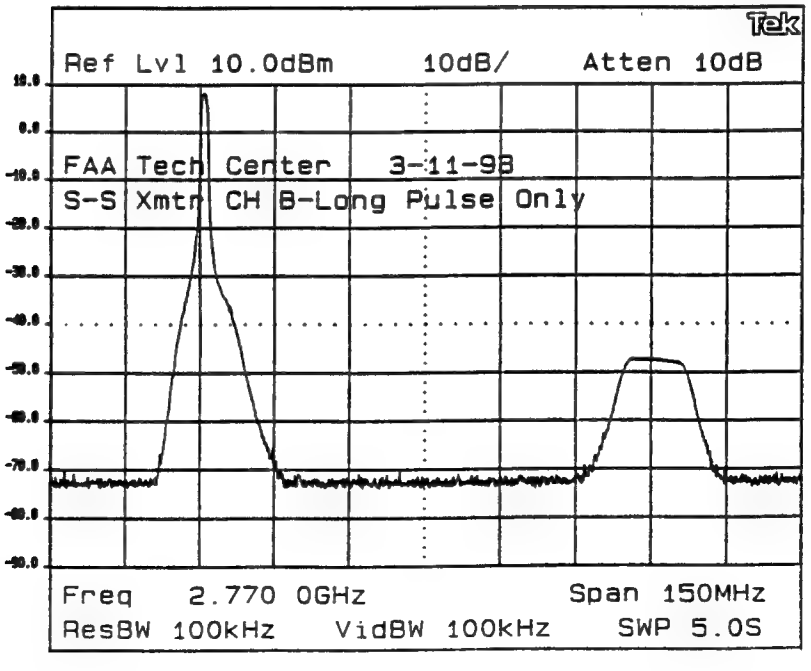

FIGURE 7.4-8. TRANSMITTED SPECTURM - CHANNEL B - LONG PULSE ONLY

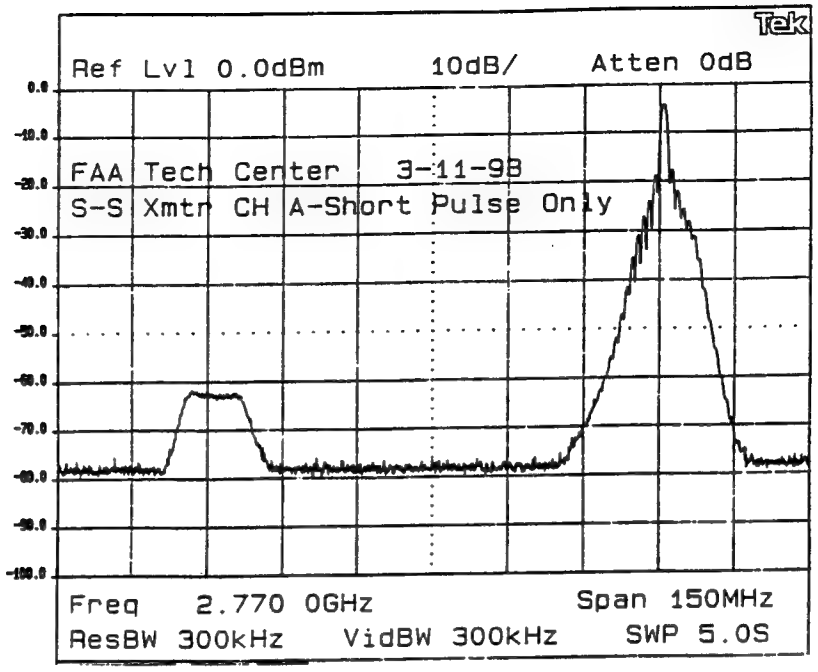

FIGURE 7.4-9. TRANSMITTED SPECTRUM - CHANNEL A - SHORT PULSE ONLY

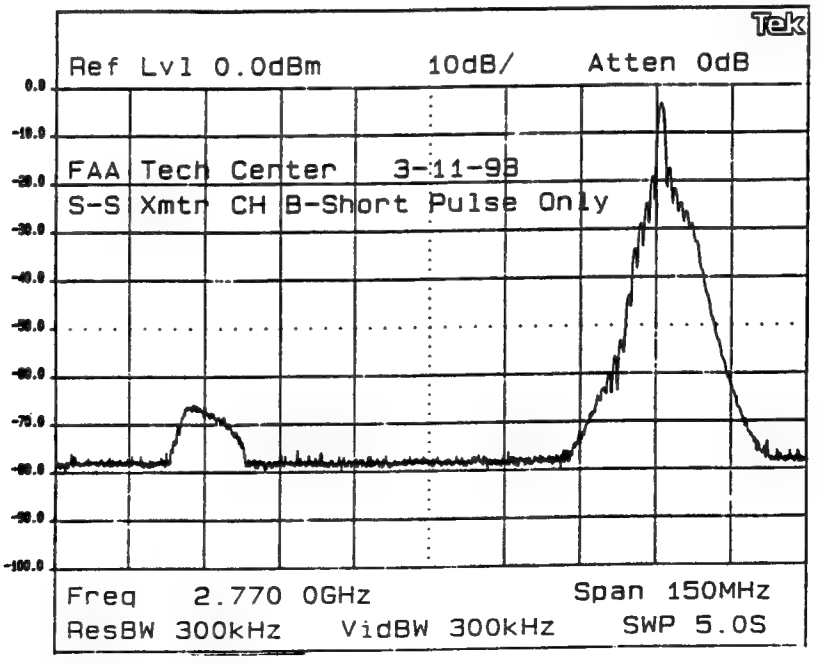

FIGURE 7.4-10. TRANSMITTED SPECTURM - CHANNEL B - SHORT PULSE ONLY

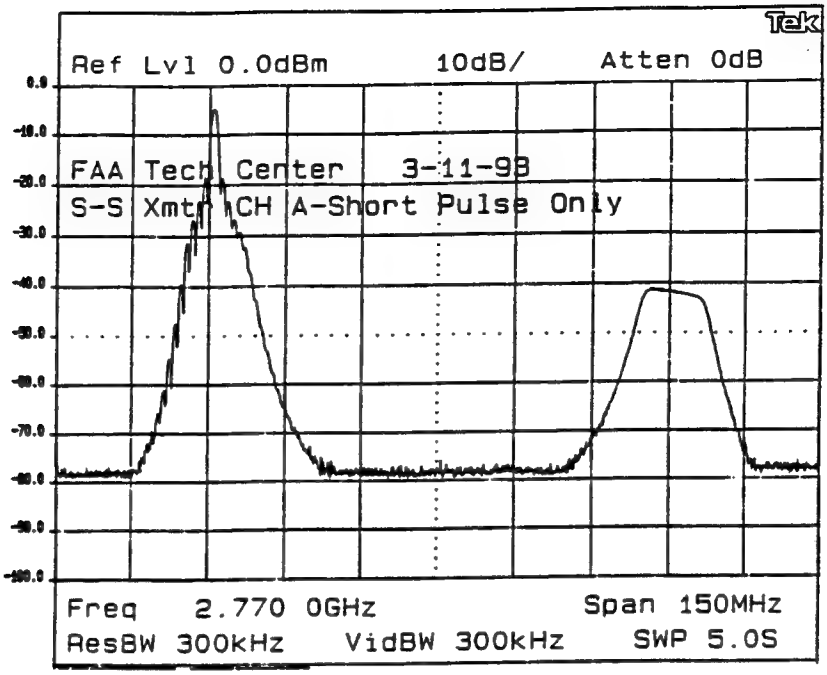

FIGURE 7.4-11. TRANSMITTED SPECTRUM - CHANNEL A - SHORT PULSE ONLY

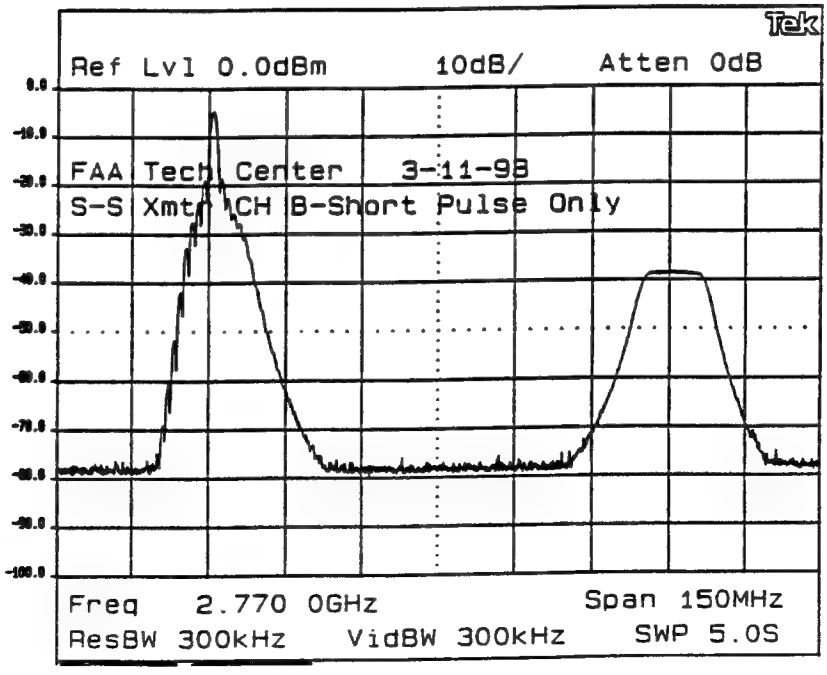

FIGURE 7.4-12. TRANSMITTED SPECTURM - CHANNEL B - SHORT PULSE ONLY

The energy leakage is not considered a problem operationally. Since the long pulse is modulated with nonlinear FM and the short pulse is a simple pulse, the leakage effects are not seen when the pulses are separately processed in the receiver.

Figures 7.4-13 and 7.4-14 show the spectra at a 150-MHz span with both pulses radiating. The relative amplitudes of the short pulses and long pulses are easily seen.

7.5 MAINTAINABILITY DEMONSTRATION.

7.5.1 BUILT-IN TEST (BIT).

The purpose of this test was to assess the BIT capabilities of the solid-state transmitter.

The transmitter contains BIT Light Emitting Diodes (LED) on its control/status panel and on each individual module (power supply, preamplifier, and driver and final stage rf amplifiers). Two LEDs on the status/control panel indicate the fault status; one for each of the transmitter channels. A channel fault is noted when the channel LED is lit. Green and red LEDs on each module indicate the status of the module. The green LED lights when the module is operational and red LED lights when the module is nonoperational.

The transmitter was operated in manual mode. Faults were introduced by turning off the preamplifier of each channel. The red LEDs were illuminated on the affected modules in the channel (i.e., the 2 RF amplifier drivers and the 40 final stage amplifiers). The fault LED of the affected channel was lit on the status/control panel. When the fault was removed, the green LEDs were lit on each module and the fault indication disappeared on the status/control panel.

7.5.2 FAIL-SOFT OPERATION.

The purpose of this test was to assess the "graceful degradation" feature of the solid-state transmitter. The transmitter was designed to operate with one or more failed rf amplifier final modules and with up to three failed power supply modules.

The solid-state transmitter was operated in automatic mode. The transmitter output power was monitored on a HP438A power meter (after appropriate attenuation) while module failures were simulated by turning off the power to randomly selected power supply and final stage rf output modules.

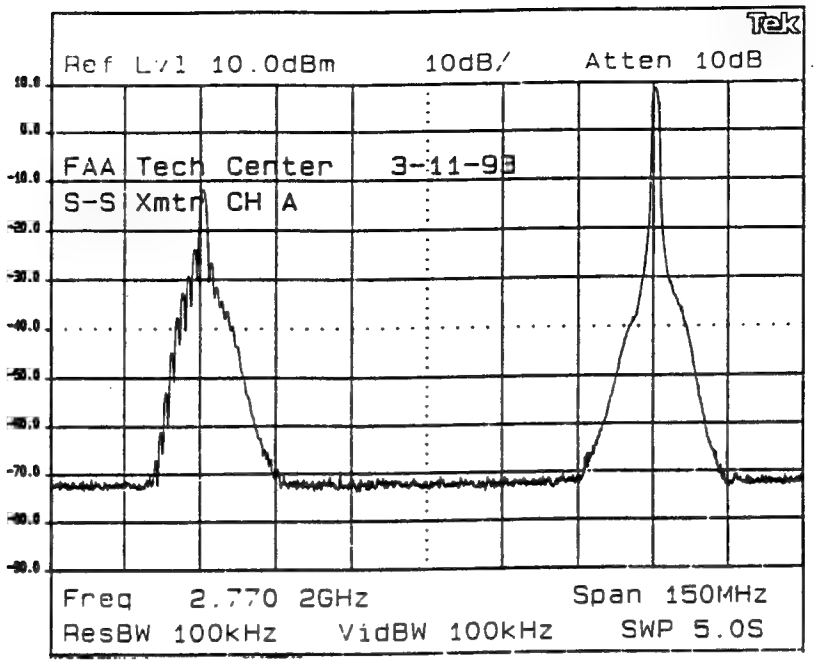

FIGURE 7.4-13. TRANSMITTED SPECTRUM - CHANNEL A - BOTH PULSES TRANSMITTED

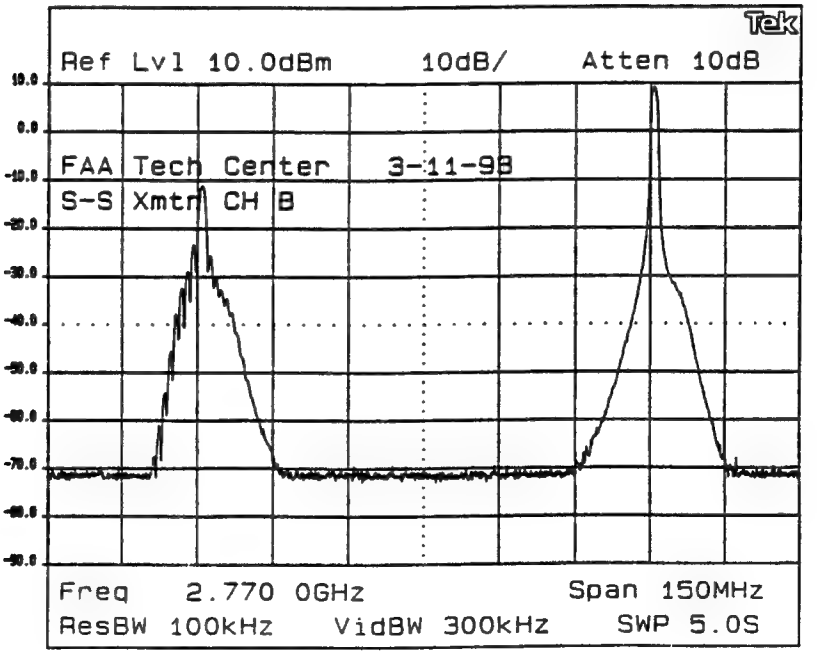

FIGURE 7.4-14. TRANSMITTED SPECTURM - CHANNEL B - BOTH PULSES TRANSMITTED

Power measurements were made when all modules were operational; when one or two of the 40 final stage RF amplifiers were turned off (with all power supply modules on); and with up to three power supply modules turned off (with all RF amplifiers on). The results are shown in table 7.5-1.

TABLE 7.5-1. TRANSMITTER FAIL-SOFT OPERATION

	Power (dBm)
All Modules on	-9.70
One failed RF module	-9.94
Two failed RF modules	-10.16
One failed power supply module	-9.72
Two failed power supply modules	-9.72
Three failed power supply modules	-9.72

The results show that transmitter output power gracefully degrades with failed modules. There is less than 0.5 dB drop in transmitted power with up to two failed RF modules and no change with up to three failed power supply modules.

7.5.3 Module Replacement.

The purpose of this demonstration was to show the "hot maintenance" feature of the transmitter. A power supply module and a rf amplifier module were selected at random. Each module was removed and replaced with a spare module. The replacement times were noted.

The replacement procedure consisted of turning off power to the module, disconnecting the dc power cable (for the rf amplifier module only), unscrewing two bolts, sliding the module out of the transmitter, sliding in the new module, tightening the two bolts, connecting the dc power cable, and turning on the module.

The time for replacement of a power supply module was 10 seconds. The time for replacement of an RF amplifier module was 50 seconds. The transmitter remained operational throughout the replacement period.

7.5.4 Remote Monitoring System.

The purpose of this test was to verify that the status of the transmitter is accurately monitored with a PC. The transmitter status was monitored as it operated in the automatic mode and faults were introduced manually.

The PC monitored the transmitter power out as read from a power meter. Power faults were introduced by turning off rf amplifier modules of the transmitter. The decrease in transmitter power was noted on the PC. The power reading on the PC was the same as that read on a power meter.

The PC monitored thermocouple probes in the transmitter and presented the temperature status. Temperature faults were introduced by turning off power to the blowers in the transmitter. The rise in transmitter temperature was noted on the PC.

The status of which channel was on-line and which modules were operational was also presented on the PC. The status was presented in a manner similar to the LED status on the transmitter modules (i.e., green is operational and red is faulted). Faults were introduced by turning off transmitter modules. The status of the affected modules immediately changed as seen on the PC.

The status of channel switching was also shown on the PC. When power of the preamplifier was turned off in one channel, the switch to the other transmitter channel was noted on the PC.

The PC accurately displayed the power, temperature, and configuration status of the transmitter. The use of a PC to monitor the status allows use of a PC-based modem to transmit the status to a remote location.

8. RECEIVER DEMONSTRATION.

8.1 NOISE FIGURE.

The purpose of this test was to measure the noise figure of both channels of the pulse compression receiver and compare the results to the noise figure of the ASR-9 receiver.

Noise from an excess noise diode was injected into the LNA of the ASR-9. The output of the LNA directly fed either the pulse compression receiver or the ASR-9 receiver. The value of the noise diode was 15 dB. The noise voltage at the IF output of the demonstration receiver and the ASR-9 receiver was measured on a true Route Mean Square (RMS) voltmeter as the noise diode was turned on and off.

The noise figure (in dB) is expressed as:

$$NF = 10 \log (Tex) - 10 \log ((V_2/V_1)^2 - 1)$$

where

Tex = the relative excess noise power available from the noise diode.

V_2 = the noise voltage at the IF output of the receiver with the noise diode ON.

V_1 = the noise voltage at the IF output of the receiver with the noise diode OFF.

Table 8.1-1 summarizes the results of the noise figure measurement for the long-pulse and short-pulse channels and for the ASR-9.

TABLE 8.1-1. RECEIVER NOISE FIGURE MEASUREMENTS

	V_2 (Volts)	V_1 (Volts)	Noise Figure (dB)
Demo Receiver			
Long Pulse	1.70	0.35	1.46
Short Pulse	1.70	0.35	1.46
ASR-9 Receiver	1.75	0.42	2.86

8.2 DYNAMIC RANGE AT I AND Q OUTPUTS.

The purpose of this test was to determine the dynamic range of each of the two channels of the pulse compression receiver. The dynamic range is defined as the difference between the maximum signal power that the receiver can handle (before a deviation from linearity) and the minimum detectable signal power.

The dynamic range measurement configuration is shown in figure 8.2-1. A synthesized signal (PRF = 1000 Hz) was injected into the ASR-9 directional coupler. The synthesizer trigger was delayed by approximately 30 nmi such that the signal was generated at the middle of the receiving period. A variable attenuator was used to adjust the power into the coupler. Eighteen-bit in-phase and quadrature (I and Q) data was collected at the output of the receiver.

The signal path for the measurement included the ASR-9 directional coupler (20-dB attenuation), STC, the low beam/high beam switch, and the LNA. The demonstration receiver signal path included the long-pulse and short-pulse channel RF/IF receivers, analog to digital converters, amplitude and phase detectors, and the long-pulse channel pulse compressor. The test was conducted without STC.

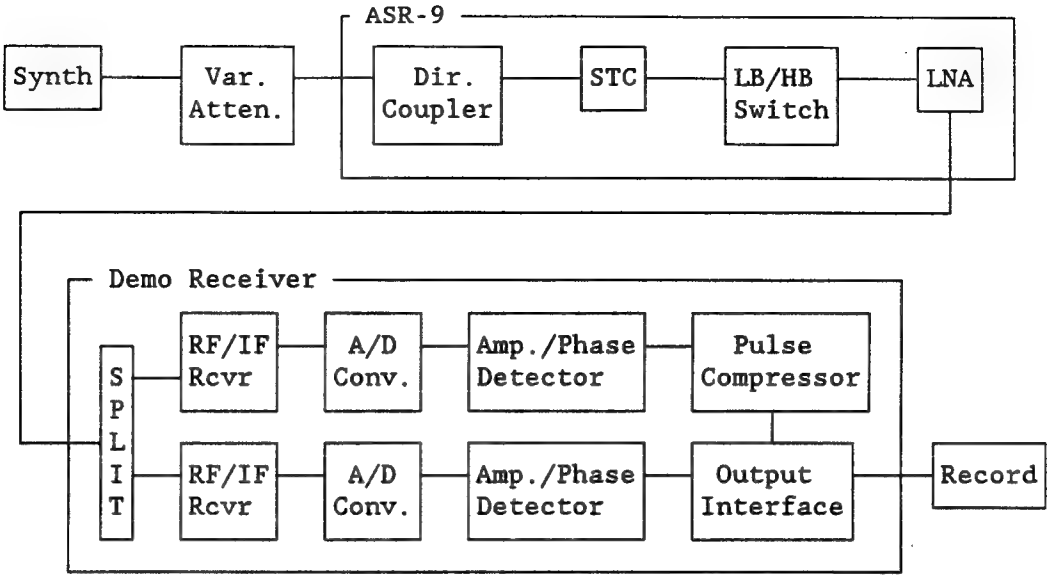

FIGURE 8.2-1. DYNAMIC RANGE MEASUREMENT CONFIGURATION

Data from the range cell of interest was recorded over N PRIs where N was 16384 for the noise power measurement and N was 1024 for the signal power measurement. The noise power at the receiver output was measured with no signal input to the system. The power of the synthesized signal at the input to the variable attenuator was 6.4 dBm for the long-pulse measurements and 5.44 dBm for the short-pulse measurements.

The results of the measurement are shown in table 8.2-1. The table shows the mean power and the standard deviation of the signal out of the receiver as the level of signal power into the system was varied. The values in the input power column of the table are the power levels input to the STC (i.e., after subtracting the variable attenuation and directional coupler attenuation (20 dB) from the synthesized power).

The mean power was calculated from the recorded I and Q data as shown.

$$\text{Mean Power} = 20 \log \left[1/N \, \Sigma(I^2 + Q^2)^{1/2}\right]$$

where N = 16384 (for noise) or N = 1024 (for signal)

The results of table 8.2-1 are plotted in figure 8.2-2 for the long-pulse and short-pulse channels. The 17-dB difference in gain between the two channels is evident in the figure.

The linear region of each curve is easily seen. The linear region is that part of the curve where the mean receiver output power changes by the same amount as the input power as the attenuation is increased. The dynamic range is the difference between the input power level at which the receiver enters the linear region and the input power level where the extrapolated linear curve intercepts the noise power level.

TABLE 8.2-1. RECEIVER DYNAMIC RANGE

	Long Pulse			Short Pulse		
Atten. (dB)	Input Power (dBm)	Mean (dBq)	STDV	Input Power (dBm)	Mean (dBq)	STDV
Noise	N/A	11.55	1.96	N/A	11.36	1.90
20	-33.6	94.57	5.08	-34.56	77.65	1.94
25	-38.6	94.08	5.88	-39.56	77.00	1.87
26	-39.6	93.97	4.96	-40.56	76.82	1.81
27	-40.6	93.85	5.00	-41.56	76.62	1.83
28	-41.6	93.70	4.75	-42.56	76.40	1.94
29	-42.6	93.54	4.75	-43.56	76.14	1.93
30	-43.6	93.34	4.97	-44.56	75.92	2.01
31	-44.6	93.16	5.42	-45.56	75.58	2.02
32	-45.6	92.87	4.95	-46.56	75.20	2.05
33	-46.6	92.50	5.42	-47.56	74.74	2.18
34	-47.6	92.02	6.27	-48.56	74.20	2.44
35	-48.6	91.42	5.72	-49.56	73.52	2.78
36	-49.6	90.63	6.80	-50.56	72.68	3.15
37	-50.6	89.70	8.19	-51.56	71.71	3.31
38	-51.6	88.72	7.45	-52.56	70.73	3.25
39	-52.6	87.74	6.05	-53.56	69.74	3.26
40	-53.6	86.76	5.82	-54.56	68.76	3.08
50	-63.6	76.71	3.99	-64.56	58.76	2.99
60	-73.6	66.92	4.48	-74.56	48.93	2.97
70	-83.6	56.74	3.96	-84.56	38.93	3.11
80	-93.6	46.67	3.72	-94.56	29.03	2.88
90	-103.6	36.16	3.48	-104.56	19.19	2.94
100	-113.6	27.80	3.67	-114.56	12.69	2.23
110	-123.6	27.14	4.45	-124.56	11.71	2.06

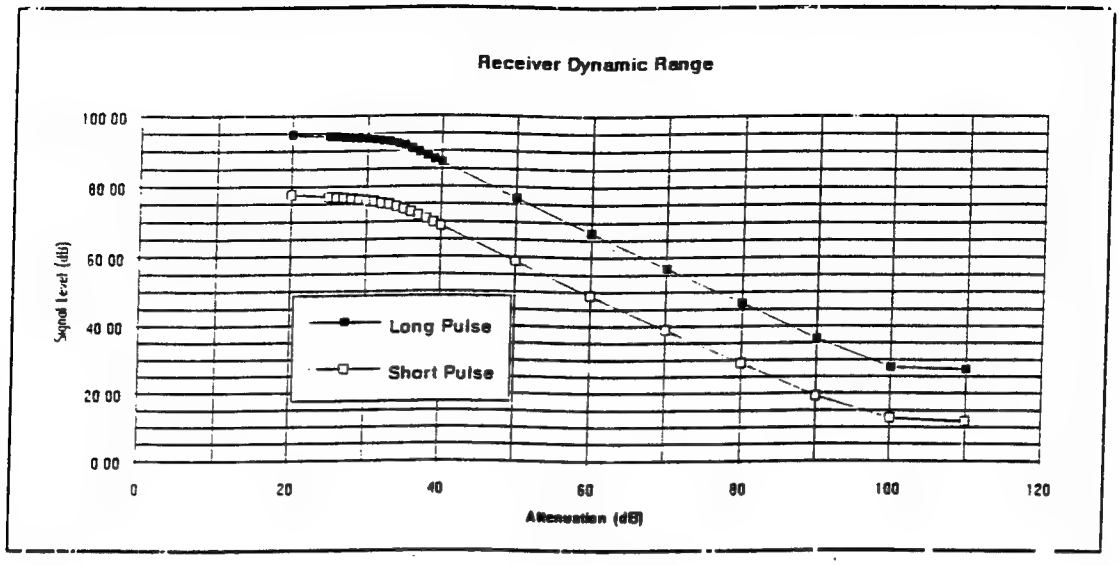

FIGURE 8.2-2. DYNAMIC RANGE

Refer to the measured values in table 8.2-1 for the dynamic range calculations. For the long pulse, as the attenuation is increased, the mean output power begins to decrease linearly when the input power is -49.6 decibel referenced to 1 milliwatt (dBm). With increased attenuation, the receiver departs the linear region when the input power is -103.6 dBm and the mean is 36.16 dB. The curve, when extrapolated, intercepts the noise level (11.55 dB) at -128.21 dB. This is the minimum detectable signal (MDS) of the long pulse. The dynamic range is:

$$\text{Dynamic Range}_{\text{Long Pulse}} = -49.6 \text{ dBm} + 128.21 \text{ dBm} = 78.61 \text{ dB}$$

For the short pulse, as the attenuation is increased, the mean output power begins to decrease linearly when the input power is -50.56 dBm. With increased attenuation, the receiver departs the linear region when the input power is -104.56 dBm and the mean is 19.19 dB. The curve, when extrapolated, intercepts the noise level (11.36 dB) at -112.39 dBm; the MDS of the short pulse. The dynamic range is:

$$\text{Dynamic Range}_{\text{Short Pulse}} = -50.56 \text{ dBm} + 112.39 \text{ dBm} = 61.83 \text{ dB}$$

8.3 BANDWIDTH AT I AND Q OUTPUTS.

The purpose of this test was to determine the bandwidth of each of the two channels of the receiver. The final stages of the channel primarily determine the bandwidth.

The bandwidth measurement configuration is shown in figure 8.3-1. A signal of constant amplitude from the synthesizer was injected into the receiver. The synthesizer trigger was delayed by approximately 30 nmi to generate the signal at the middle of the receiving period.

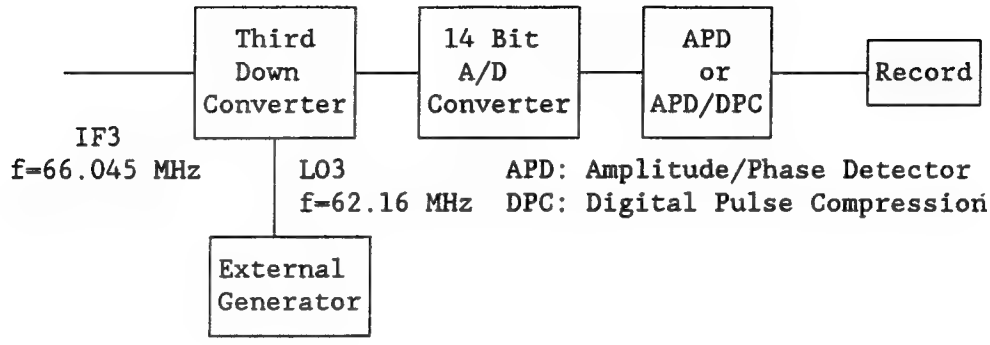

FIGURE 8.3-1. RECEIVER BANDWIDTH TEST CONFIGURATION

The local oscillator (LO3) was disconnected from the third down converter for this test. An external generator was then connected to the LO3 input. The frequency of the externally generated signal was adjusted on either side of 62.16 MHz (the LO3 frequency).

For each adjustment in frequency of the externally generated signal, 1024 PRIs of 18-bit I and Q data was recorded at the receiver output. Data was recorded for all of the range cells in each PRI. The peak power was then determined for each PRI. The peak power in the PRIs was then averaged over 1024 PRIs.

Table 8.3-1 shows the recorded power for each frequency offset of the generator for the short-pulse and long-pulse measurements.

The data is plotted in figure 8.3-2. The relative gain of the short-pulse and long-pulse channels can be seen (i.e., approximately 17 dB difference). The 3-dB bandwidth for the long-pulse channel is approximately 300 KHz and the 3-dB bandwidth for the short-pulse channel is approximately 600 KHz.

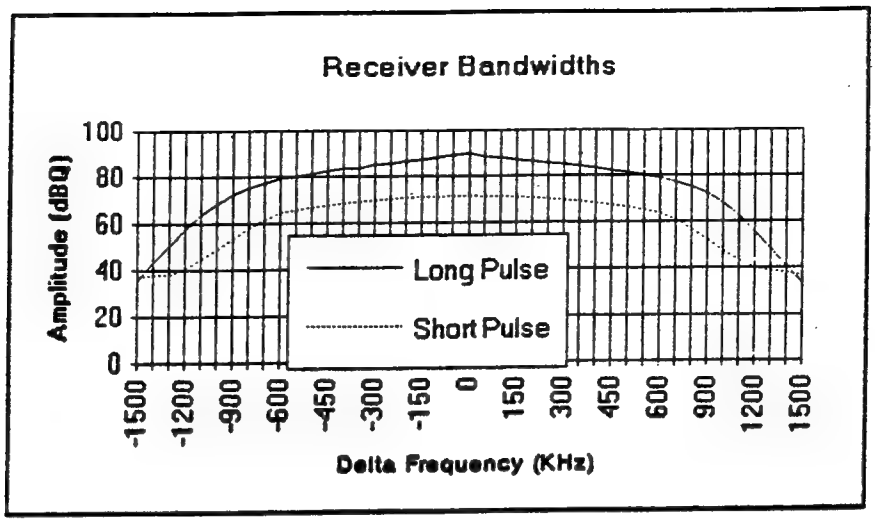

FIGURE 8.3-2. RECEIVER BANDWIDTHS

TABLE 8.3-1. RECEIVER BANDWIDTH MEASUREMENT

	Short Pulse		Long Pulse			Short Pulse		Long Pulse	
Offset (KHz)	Amp (dBQ)	STDV	Amp (dBQ)	STDV	Offset (KHz)	Amp (dBQ)	STDV	Amp (dBQ)	STDV
0	71.00	5.53	89.81	4.53					
50	70.92	5.57	88.16	5.55	-50	70.99	5.53	89.10	5.14
100	70.75	5.55	87.79	4.65	-100	70.87	5.53	88.13	4.26
150	70.48	5.56	86.65	4.10	-150	70.67	5.46	86.94	4.91
200	70.12	5.37	86.21	3.89	-200	70.37	5.51	86.56	4.33
250	69.67	5.14	85.40	3.39	-250	69.98	5.32	85.36	3.65
300	69.12	4.90	84.68	3.52	-300	69.49	4.99	84.96	3.36
350	68.47	4.68	83.79	3.27	-350	68.89	4.52	83.22	3.63
400	67.72	4.69	83.08	3.17	-400	68.19	3.88	83.28	3.02
450	66.85	4.39	82.04	2.84	-450	67.38	3.52	82.22	2.90
500	65.88	4.08	80.94	2.66	-500	66.45	2.10	81.02	2.72
550	64.77	3.70	79.84	2.41	-550	65.41	2.45	79.93	2.67
600	63.54	3.30	78.64	2.22	-600	64.23	2.21	78.90	2.19
700	60.63	2.71	76.85	1.85	-700	61.45	2.39	77.05	1.97
800	57.00	2.42	74.89	1.68	-800	57.98	3.39	75.00	1.65
900	52.38	2.41	71.84	1.43	-900	53.63	4.25	72.22	1.37
1000	47.57	5.97	67.54	1.28	-1000	48.83	9.56	68.38	1.31
1100	43.21	4.72	62.33	1.13	-1100	44.77	7.02	63.68	1.06
1200	40.01	3.52	55.50	0.10	-1200	40.81	5.51	57.69	1.17
1300	38.70	2.45	48.29	0.92	-1300	38.24	5.43	50.80	0.96
1400	37.97	1.71	40.48	0.87	-1400	38.13	2.33	43.47	1.01
1500	36.74	1.61	33.49	0.83	-1500	37.33	2.19	35.95	1.00

8.4 I AND Q PHASE AND AMPLITUDE ERRORS.

The purpose of this test was to determine the I and Q phase and amplitude errors within the frequency bandwidth for each of the two channels of the receiver. The test is a measure of the frequency image rejection which is a function of the I and Q phase and amplitude errors.

The configuration for the measurement is shown in figure 8.4-1. An external CW generator injected a signal into the IF3 input of the third down converter in the receiver. The generated signal power was -30 dBm for the short-pulse and long-pulse measurements. The test was repeated for the long-pulse channel with the generator output at -20 dBm. The frequency of the injected signal was adjusted around 66.045 MHz. Eighteen-bit I and Q data was collected at the output of the receiver.

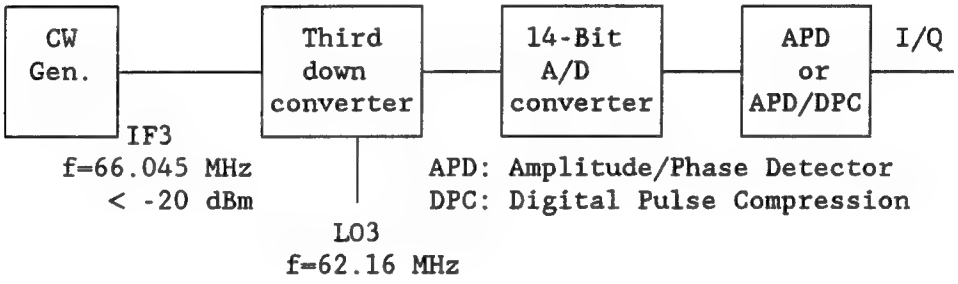

FIGURE 8.4-1. I AND Q PHASE AND AMPLITUDE ERRORS CONFIGURATION

A 512-point FFT was performed on the I and Q data. The resultant spectrum showed the spectral line at the IF3 frequency. When I and Q phase and amplitude errors are prevalent, an image of the spectral component at IF3 appears on the other side of the LO3 frequency symmetrical to IF3. The frequency image rejection is the ratio between the amplitude of the true IF3 signal and the amplitude of the image.

Tables 8.4-1 and 8.4-2 show the results for the short-pulse and long-pulse channels. The data shows that for both channels, the amplitudes of the image components are sufficiently low relative to the main components and, therefore, the I/Q phase and amplitude error levels are low.

TABLE 8.4-1. FREQUENCY IMAGE REJECTION - SHORT PULSE CHANNEL INPUT POWER = -30 dBm

Input Frequency (MHz)	Delta Frequency (MHz)	True Line Amplitude (dBq)	Image Line Amplitude (dBq)	Image Rejection (dBq)
66.245	0.20	111.87	62.95	48.92
66.145	0.10	114.68	57.17	57.51
66.135	0.09	114.87	56.68	58.19
66.125	0.08	115.02	55.12	59.90
66.115	0.07	115.15	54.41	60.74
66.105	0.06	115.24	53.15	62.09
66.095	0.05	115.30	51.28	64.02
66.085	0.04	115.33	49.82	65.52
66.075	0.03	115.34	49.02	66.31
66.065	0.02	115.31	45.93	69.38
66.055	0.01	115.24	38.29	76.95
66.045	0.00	115.15	xx.xx	xx.xx
66.035	-0.01	114.99	42.26	72.73
66.025	-0.02	114.83	38.39	76.44
66.015	-0.03	114.64	43.35	71.29
66.005	-0.04	114.42	46.07	68.34
65.995	-0.05	114.46	48.82	65.64
65.985	-0.06	114.57	50.85	63.72
65.975	-0.07	114.65	53.41	61.24
65.965	-0.08	114.69	54.10	60.60
65.955	-0.09	114.70	55.40	59.30
65.945	-0.10	114.69	56.18	58.50
65.845	-0.20	112.72	63.70	49.01

TABLE 8.4-2. FREQUENCY IMAGE REJECTION - LONG PULSE CHANNEL

	Input Power = -30 dBm				Input Power = -20 dBm			
Input Freq (MHz)	Delta Freq (MHz)	True Amp (dBq)	Image Amp (dBq)	Image Reject (dBq)	Delta Freq (MHz)	True Amp (dBq)	Image Amp (dBq)	Image Reject (dBq)
66.645	0.60	90.62	27.64	62.99	0.60	99.43	37.78	61.65
66.545	0.50	105.07	37.36	67.71	0.50	109.16	36.12	73.04
66.445	0.40	101.18	33.47	67.71	0.40	115.33	45.39	69.94
66.345	0.30	109.46	29.98	79.48	0.30	118.36	44.59	73.77
66.245	0.20	111.14	30.85	80.29	0.20	121.39	35.07	86.32
66.145	0.10	113.40	34.15	79.26	0.10	123.11	36.54	86.57
66.045	0.00	113.33	xx.xx	xx.xx	0.00	123.21	xx.xx	xx.xx
65.945	-0.10	113.23	22.33	90.90	-0.10	123.29	47.48	75.81
65.845	-0.20	111.51	31.90	79.62	-0.20	121.02	40.80	80.23
65.745	-0.30	108.48	36.75	71.74	-0.30	119.35	34.98	84.37
65.645	-0.40	105.45	35.98	69.47	-0.40	114.96	45.84	69.12
65.545	-0.50	99.29	28.39	70.90	-0.50	111.07	44.72	66.35
65.445	-0.60	89.55	25.09	64.46	-0.60	100.52	34.56	65.96

8.5 PULSE COMPRESSION MEASUREMENTS.

The purpose of these tests was to determine the effects on the pulse widths and sidelobes at the I and Q output of the long-pulse channel when the received signal was varied in doppler, in range, and in power level.

The measurement configuration is shown in figure 8.5-1. The coupled transmitter output was attenuated and injected into the ASR-9 directional coupler. A variable attenuator was used to adjust the power into the coupler. Eighteen-bit in-phase and quadrature (I and Q) data was collected at the output of the receiver.

The signal path for the measurement included the ASR-9 directional coupler, STC, the low-beam/high-beam switch, and the LNA. The demonstration receiver signal path included the long-pulse channel RF/IF receivers, analog to digital converters, amplitude/phase detectors, and the pulse compressor.

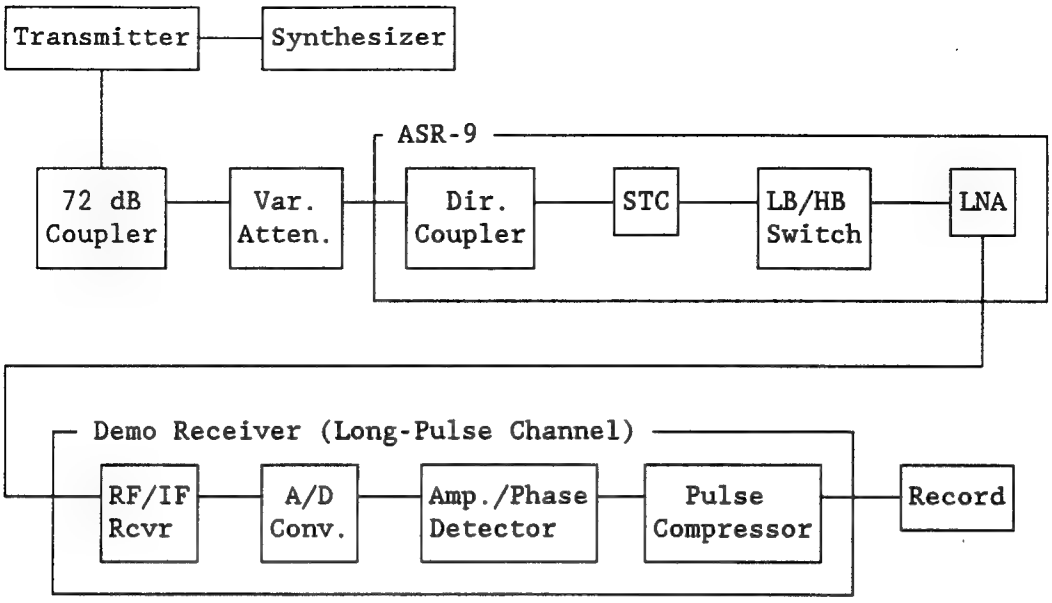

FIGURE 8.5-1. PULSE COMPRESSION MEASUREMENT CONFIGURATION

The tests were conducted without STC. The synthesizer generated signal was constant at 1000 Hz. The power measured after the 72-dB coupler was 1.55 dBm. The attenuation due to the directional coupler was 20 dB and the gain of the LNA was 25 dB.

8.5.1 Waveform Characterisitcs at Pulse Compression Output Versus Doppler.

The signal range and signal level into the receiver were kept constant throughout this test. The synthesizer trigger was delayed by approximately 30 nmi such that the signal was generated at the middle of the receiving period. The transmitter output signal was injected into the ASR-9 directional coupler through an adjustable attenuator (Attl). The value of Attl was kept constant at 23 dB for this test.

The test was conducted for five doppler values: 0, 30, 50, 90, and 130 meters per second (m/s).

The doppler frequency was simulated by modifying the phase of the generated pulse. For a radial velocity V, the phase of the generated pulse was:

$$\phi(t) = \phi_0(t) + \frac{4nV}{c} f_0 t$$

where : $\phi_0(t)$ = the nominal phase (with no doppler)
V = radial velocity in m/s
c = speed of light in m/s
f_0 = radar frequency in Hz (2725 MHz)

Eighteen-bit I and Q data was recorded at the output of the receiver for all the range cells in a pulse repetition period. The power was calculated for each range cell and plotted as a function of the range. The difference between the peak and the maximum sidelobe was recorded.

The results of the test are summarized in table 8.5-1. The data is plotted in figure 8.5-2. It is evident that the sidelobe levels are affected by the doppler of the received pulse but for the five doppler values shown, the difference between the peak and sidelobe levels is greater than 51 dB. The doppler effects on the pulse width were minimal.

TABLE 8.5-1. SIDELOBE LEVELS AND PULSE WIDTHS VERSUS DOPPLER

Doppler		Peak Level	Maximum Sidelobes	Difference	Pulse Width
(m/s)	(nm/hr)	(dBq)	(dBq)	(dB)	(μs)
0	0	90.02	33.94	56.08	1.04
30	58.3	90.52	33.88	56.65	1.03
50	97.1	90.09	34.30	55.79	1.03
90	174.8	90.87	37.33	53.54	1.03
130	252.5	90.64	39.27	51.37	1.02

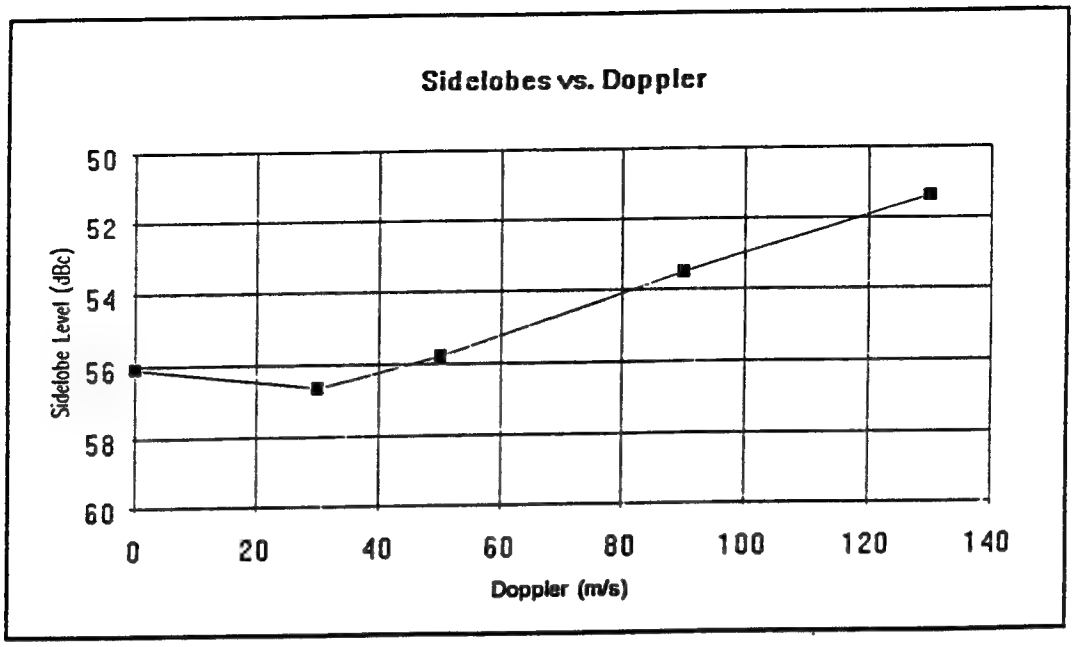

FIGURE 8.5-2. SIDELOBE LEVELS VERSUS DOPPLER

8.5.2 Waveform Characteristics at Pulse Compression Output Versus Range Position.

The signal level and doppler velocity were kept constant throughout this test. The value of Att1 was kept constant at 23 dB. No doppler velocity was introduced to the generated pulse.

Measurements were made at five different ranges: 8 nmi (128 range cells (RC)), 16.125 nmi (258 RC), 32.125 nmi (514 RC), 48.125 nmi (770 RC), and 60.75 nmi (972 RC). The short-pulse/long-pulse transition was set at 7.94 nmi (127 RC). The different range positions were achieved by delaying the synthesizer trigger by the appropriate amount.

Eighteen-bit I and Q data was recorded at the output of the receiver for all the range cells in a pulse repetition period. The power was calculated for each range cell and plotted as a function range. The difference between the peak and the maximum sidelobe was recorded.

The results of the test are summarized in table 8.5-2. The range cell size is 1/16 nmi. The data is plotted in figure 8.5-3. For the five-range positions, all sidelobe levels were greater than 55 dB. There were no significant edge effects due to not receiving the entire pulse (i.e., at minimum and maximum range). There was no significant effect on the pulse width due to range position.

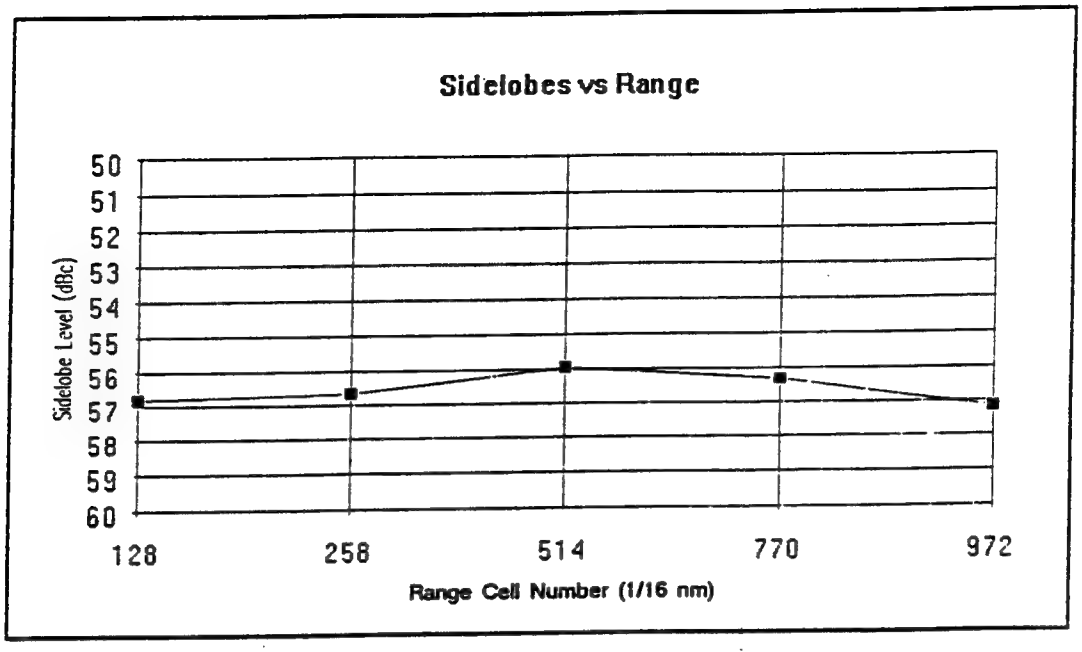

FIGURE 8.5-3. SIDELOBES LEVELS VERSUS RANGE POSITION

TABLE 8.5-2. SIDELOBE LEVELS AND PULSE WIDTHS VERSUS RANGE

Range Cell	Peak Level (dBq)	Max Sidelobes (dBq)	Difference (dB)	Pulse Width (μs)
128	90.03	33.22	56.82	0.93
258	90.16	34.49	56.67	1.03
514	90.29	34.35	55.93	1.03
770	90.24	33.92	56.32	1.03
972	89.92	32.75	57.17	X.XX

8.5.3 Waveform Characteristics at Pulse Compression Output Versus Input Level.

The doppler velocity of the received pulse was set to zero for the test. The signal range was kept constant at approximately 30 nmi. The transmitter output signal was injected into the ASR-9 directional coupler through an adjustable attenuator (Attl). The value of Attl was adjusted from 4 dB to 65 dB. The power of the signal in the waveguide was:

Power = (Power out of 72 dB coupler) - Attl - (directional coupler value)
= 1.55 - Attl - 20 = - 18.45 dBm - Attl.

For each value of Attl, eighteen-bit I and Q data was recorded at the output of the receiver for all the range cells in a pulse repetition period. The power was calculated for each range cell and plotted as a function of range. The difference between the peak and the maximum sidelobe was recorded.

The results of the test are summarized in table 8.5-3. Those values marked with an asterisk were values measured when the sidelobes were in the noise. The difference between the peak level and the peak sidelobe level was greater than 55 dB for all values of Attl. The effects on the pulse width were minimal.

TABLE 8.5-3. SIDELOBE AND PULSE WIDTHS VERSUS INPUT LEVEL

	868 Point Filter				1008 Point Filter			
Attl (dB)	Peak Level (dBq)	Max. Side-lobe (dBq)	Diff. (dB)	Pulse Width (μs)	Peak Level (dBq)	Max. Side-lobe (dBq)	Diff. (dB)	Pulse Width (μs)
4	94.96	39.20	55.76	1.06	95.73	38.02	57.71	1.02
5	94.87	38.86	56.01	1.06	95.63	38.02	57.61	1.02
6	94.77	38.95	55.82	1.06	95.54	38.21	57.33	1.02
7	94.67	38.70	55.96	1.06	95.42	37.91	57.51	1.02
8	94.57	38.76	55.80	1.06	95.32	37.91	57.41	1.02
9	94.44	38.53	55.91	1.06	95.19	37.41	57.78	1.02
10	94.32	38.45	55.87	1.06	95.06	37.52	57.54	1.02
11	94.18	38.23	55.95	1.06	94.92	37.33	57.58	1.02
12	94.02	38.05	55.97	1.06	94.74	36.93	57.81	1.02
13	93.82	37.57	56.26	1.06	94.51	36.33	58.18	1.01
14	93.59	37.21	56.37	1.06	94.24	35.94	58.30	1.01
15	93.29	36.50	56.79	1.06	93.90	35.48	58.43	1.01
16	92.92	36.12	56.80	1.05	93.48	34.51	58.97	1.00
17	92.43	35.76	56.67	1.05	93.37	33.37	59.55	X.XX
18	91.82	35.19	56.63	1.04	92.23	32.15	60.08	0.99
19	91.01	34.77	56.24	1.04	91.35	31.61	59.74	0.99
20	90.01	34.10	55.92	1.04	90.44	31.29	59.15	0.99
30	80.26	24.15	56.11	1.04	80.70	20.97	59.73	0.99
40	70.43	15.31	55.12	1.04	70.43	15.31	57.88	0.99
50	60.88	12.30	48.57*	1.03	61.40	10.00	51.40*	0.99
60	51.73	9.03	42.70*	1.02	52.22	10.00	42.22*	0.98
65	47.82	9.54	37.82*	1.02	48.14	12.30	35.84*	0.96

The data is plotted in figure 8.5-4. The data was collected with the receiver using a 868-point filter and a 1008-point filter. The curves for both filters are shown in the figure. The sidelobe levels were lower when the 1008-point filter was used. Those data points reflecting increased sidelobe levels when the attenuation is 50 dB and above are actually the results of the sidelobes being obscured by the noise level.

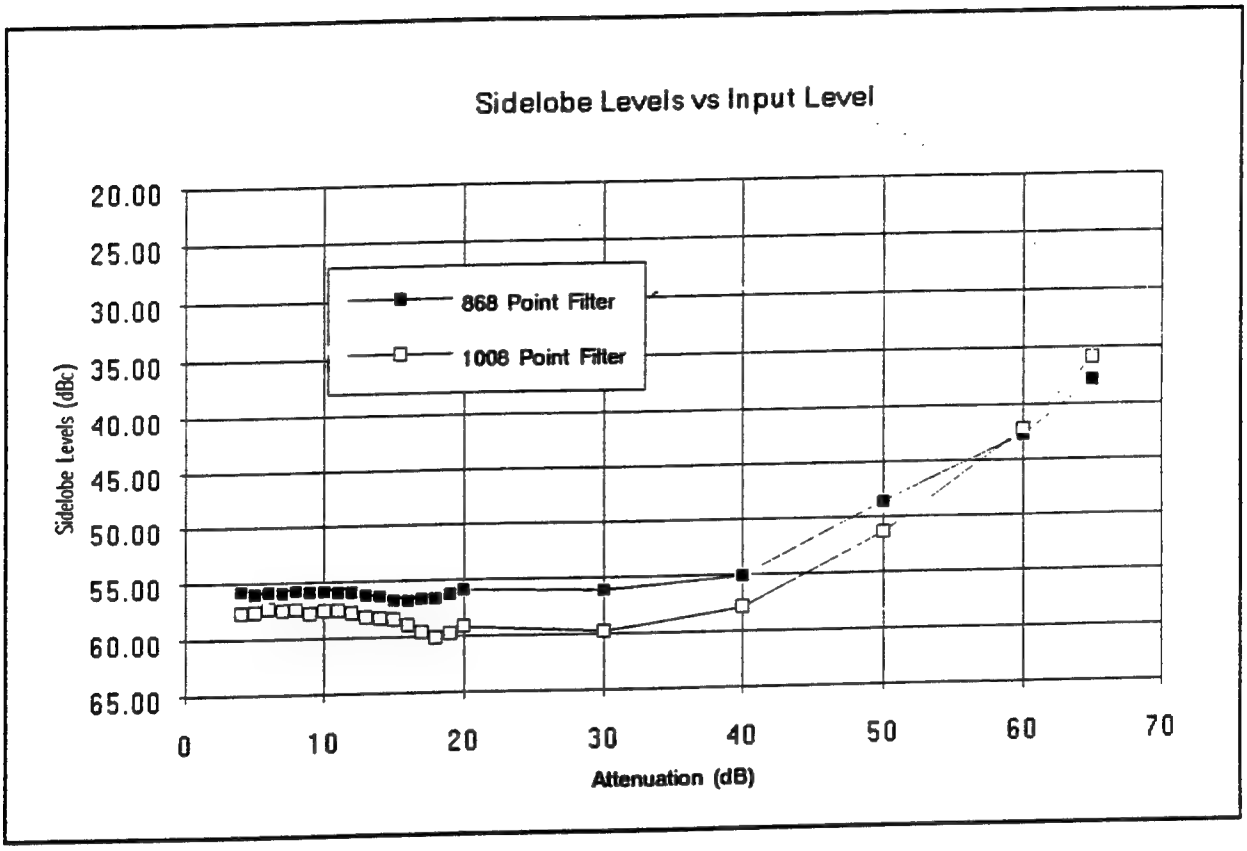

FIGURE 8.5-4. SIDELOBES VERSUS INPUT LEVELS

9. SYSTEM TESTS.

In addition to the transmitter and receiver demonstration tests described above, system level tests were performed to assess the capabilities of the demonstration equipment in a field environment. The system tests included measurements of stability, time sidelobe performance, detection, resolution, and false alarms. The stability, time sidelobe performance, and short-pulse/long-pulse transition detection analyses were performed at Lincoln Laboratory. Further assessment of detection, resolution, and false alarm analyses were performed at the FAA Technical Center.

9.1 STABILITY MEASUREMENTS.

The purpose of the following set of measurements was to assess the overall system stability as measured by local loop tests and in the field. The measurement of radar system stability is a challenging task. Stability should always be measured with a relatively long-time delay inserted between the transmitter and the receiver, because otherwise the radar's phase noise sources will be correlated and the measurement will significantly underestimate the instability residue. Long delays are difficult to obtain at microwave frequencies, and up/down conversion to a lower frequency convenient for bulk delay devices can contaminate the measurement with local oscillator phase noise from the test set. The best way to obtain long delays is to use a radar repeater located several miles from the system under test. In this case, the repeater must be stable enough not to corrupt the measurement (for modern high-stability radars, this means that the repeater must not use frequency conversion). The repeater must also have sufficient power to drive the radar receiver to near saturation and significantly overcome returns from the surrounding ground clutter, and interference must be minimized both in the repeater design and in the subsequent data processing.

The radar stability measurement comprises recording complex samples of the repeated radar return, processing the data in the time and frequency domains to reject interference, and computing the ratio of the power of deterministic component of the repeated signal to the power of its noise components.

The radar repeater used for stability assessment of the ITT Gilfillan/Thomson-CSF solid-state radar was designed to provide very clean, high-level signals at ranges of approximately 10 to 20 miles from the radar. It has two modes of operation; one is as a straight-through amplifier (yielding a return that appears to be a strong stationary point clutter source), and the other is as a MTS. When in the MTS mode, the repeated signal appears as a strong target moving at the maximum unambiguous velocity of the radar. It accomplishes this effect by applying a 180° phase reversal to every other repeated pulse. This feature is useful for stability measurements in the presence of strong local ground clutter, as the signal appears in the part of the radar's doppler space farthest from the clutter return.

Straight-through amplification in the repeater is implemented by a low-noise amplifier with an approximately 2-dB noise figure driving a 1-watt power amplifier. The repeater front end is protected from nearby radar interference by a multipole cavity filter and a limiter. Radar signals are received and transmitted through stacked multielement Yagi antennas with about 22 referenced to an isotropic source (dBi) of gain. Yagi antennas were chosen because of their compact size and light weight; horn antennas with the same gain and beamwidth would have been prohibitively heavy and large.

When employed as a moving target simulator, the repeater samples the received pulses from the host radar and triggers a digital delay circuit. After about 100 μs (well past the time when the 75 μs radar pulse has been repeated), the delayed trigger inverts the polarity of a current driving a mixer placed in the repeater signal path. The mixer, acting as a biphase modulator, changes the phase of the next received pulse by 180°. Since the radar's pulse repetition interval is about 1 ms, the phase modulator has ample time to settle before the next pulse is received. The process repeats for each subsequent pulse, accomplishing the desired alternating pulse phase inversion. The advantages of this system are that no local oscillators are used in the repeater, spurious modulation is minimized because the modulator changes state between pulses, and amplitude/phase imbalances between the two modulator states affect only the carrier balance (zero doppler or clutter line) of the received signal.

It is important that the repeater's trigger circuit not be tripped by interference from other (short pulse) radars; to discriminate against short pulses, the trigger circuit was designed with long time constants. The narrowband front-end filter also minimizes false triggering.

One of the keys to a successful field experiment is to give the field crew as much situational awareness as possible, such as a direct means of knowing that the field equipment is adjusted, oriented, and operating properly. In the MTS, the square-wave current drive to the biphase modulator is loosely coupled to an outboard battery-powered audio amplifier. When the repeater is operating properly, a pure tone at half the radar's PRF is heard. The tone will sound broken if the repeater is not reliably triggering on the radar signal because, for example, the receive antenna is not pointed right at the radar. The audio amplifier can also be unplugged from the MTS and a simple dipole/Schottky diode video radar detector substituted at the amplifier's input jack. By swinging this "repeater detector" in front of the transmit antenna, the operator can hear detected radar pulses and ascertain that rf energy is indeed being transmitted, confirming that the radar repeater is operating properly.

Two main types of measurements were made. These were the following:

a. Loop tests (radar exciter output coupled to receiver input), with and without the repeater placed in the loop. This measurement confirms that the repeater's added phase noise is sufficiently low to allow a meaningful stability measurement. It also shows which power line-related spurious or other coherent signals can be attributed to the radar system and which are due to the repeater. Both constant PRF and staggered PRF data were taken.

b. Field tests. The radar repeater was located approximately 10 miles away from the radar under test, at the site of an Air Route Surveillance Radar, Model 2 (ARSR-2) enroute facility. The repeater operated from local power and was placed on a tower approximately 50 feet above ground level, inside the ARSR-2 radome. The ARSR-2 antenna was not rotating during the measurements. Measurements were made with the ASR-9 antenna halted and staring at the repeater, using fixed and staggered PRFs. No data were taken while the ASR-9 antenna was scanning since the repeater could not be located with the limited data acquisition/display capabilities of the Thomson-CSF demonstration computer.

The objective of this series of measurements was to assess the inherent amplitude and phase instability of the radar transmitter/receiver system. As in any measurement, and in particular for a field measurement, the data can be corrupted by a number of sources. These include power-line related spurious signals, interference from nearby emitters, imbalances and spurious modulation imposed by the radar repeater, and deterministic amplitude and/or phase modulations imposed by the transmitter. Each of these undesired signals will be removed by the following data processing techniques.

The first data processing procedure is to remove line-type spectral components due to prime-power harmonics or subharmonics. The procedure is applied to constant PRF data; staggered PRF data requires different processing described below. The 1024-pulse constant PRF data is first transformed to the frequency domain, where spurious lines are identified and excised. The excision replaces the amplitude/phase data associated with the particular line with an averaged value based on the noise level of the adjacent frequency bins. The data is then inverse transformed back to the time domain, and again transformed to the frequency domain to check that the spectrum has not been corrupted by the editing procedure.

Depending on the particular data, other spurious components are removed from the power spectrum. These components may include moving targets in the range cell (even at 3 a.m. when the field data was taken), or low-level spurious noise from the doppler modulator in the MTS. In general, these components were removed in the frequency domain, with an inverse transform and then another transform back into the frequency domain to ensure that the underlying noise and zero-doppler clutter data have not been affected.

A final source of interference is pulse-type noise either from a neighboring radar (such as the magnetron-based Weather Surveillance Radar (WSR)-57 weather radar a few hundred feet from the ASR-9), or from stuck bits in the Thomson-CSF analog-to-digital converter. These outliers are easily found in the time domain data, and are edited to an average level corresponding to the data points in the vicinity. Very few such bad data points (about 2) are present in a 1024 point data set, however, they act like time-domain impulse functions and can noticeable raise the average noise level of the spectrum, particularly when that noise level is already 90 dB below the carrier. A typical before/after power spectrum for constant PRF (1000 Hz) data from the repeater is shown in figure 9.1-1. Frequency domain data from an MTS test are shown in figure 9.1-2 (the plus or minus 1/2 PRF lines from the MTS modulator are moved to zero doppler by the processing).

For staggered PRF data, frequency domain editing is not appropriate because of the limited resolution of the 8/10 pulse transforms. Time domain data processing is required, and is complicated by the deterministic amplitude and/or phase modulations imposed by the transmitter. The modulation source is due to the thermal time constants of the transistors in the ITT Gilfillan transmitter. There are short-term and long-term effects from this thermally-induced modulation. During the 75 μs pulse, the transmitter output droops in amplitude and imposes a nonlinear phase change on the transmitted signal. The Thomson-CSF pulse compression system compensates for this effect.

A constant PRF waveform needs no further compensation; however, the staggered ASR-9 PRFs introduce different duty cycles and therefore different long-term thermal effects. The primary effect is an exponential-like amplitude rise and fall during the 8- and 10- pulse sequences. A secondary effect is a step phase change during each pulse group. Since both these effects are deterministic and could be removed by the signal processor (as Thomson-CSF did for the short-term thermal effects), the stability measurement calculation for the staggered PRF waveforms considers only random phase and amplitude variations. The data processing procedure to remove the staggered PRF thermal effects is to fit a function of the form

$$A_0 + A_1*\mathrm{Cos}((\mathrm{pi}*(n-1)) + Bn + Cn^2 + Dn^3$$

to the amplitude and phase of each of n pulses in a 8- or 10-pulse group. The first term corrects for DC offsets (due to amplitude imbalance in the repeater's biphase modulator), the cosine term removes the biphase modulation from MTS data, and the linear, quadratic, and cubic terms perform an approximately exponential fit to the average value of the n data points. For the nondoppler data, the amplitude of the time series is corrected with a cubic fit with the A_1 term set to zero; phase correction is performed with a linear fit only (A_1, C, and D are set to zero). For doppler data, amplitudes were corrected with a quadratic fit and phase with a linear fit, with A_1 set to unity to remove the doppler modulation. An example of pre- and post-data processing for staggered PRF amplitudes is shown in figure 9.1-3. Note that the data processing removes the long-term modulations due to interference sources (clutter movement, etc.) while preserving the noise-like pulse-to-pulse variations associated with the radar's instability residue.

In all cases, stability was calculated in both the time and frequency domains. Time domain results were obtained by comparing the average dc power of the data to its varying alternating current (ac) power. Frequency domain results are calculated by comparing the power in the DC line (or 1/2 PRF line when the repeater is used as an MTS) to the sum of the powers in all other frequency bins. The results are expressed as a power ratio in dB.

Results for all the field measurements, whether at fixed or staggered PRFs, and whether or not the repeater was operated in doppler mode, were very consistent. Stability measurements for the fixed PRF mode (as indicated on figure 9.1-1) were 61 dB. The average stability for the staggered PRF mode was 62 dB. A plot of the stability estimates for a typical run of staggered pulse groups is shown in figure 9.1-4. Three 1024-point data runs each were taken for fixed and staggered PRFs, with and without the doppler modulator enabled in the repeater.

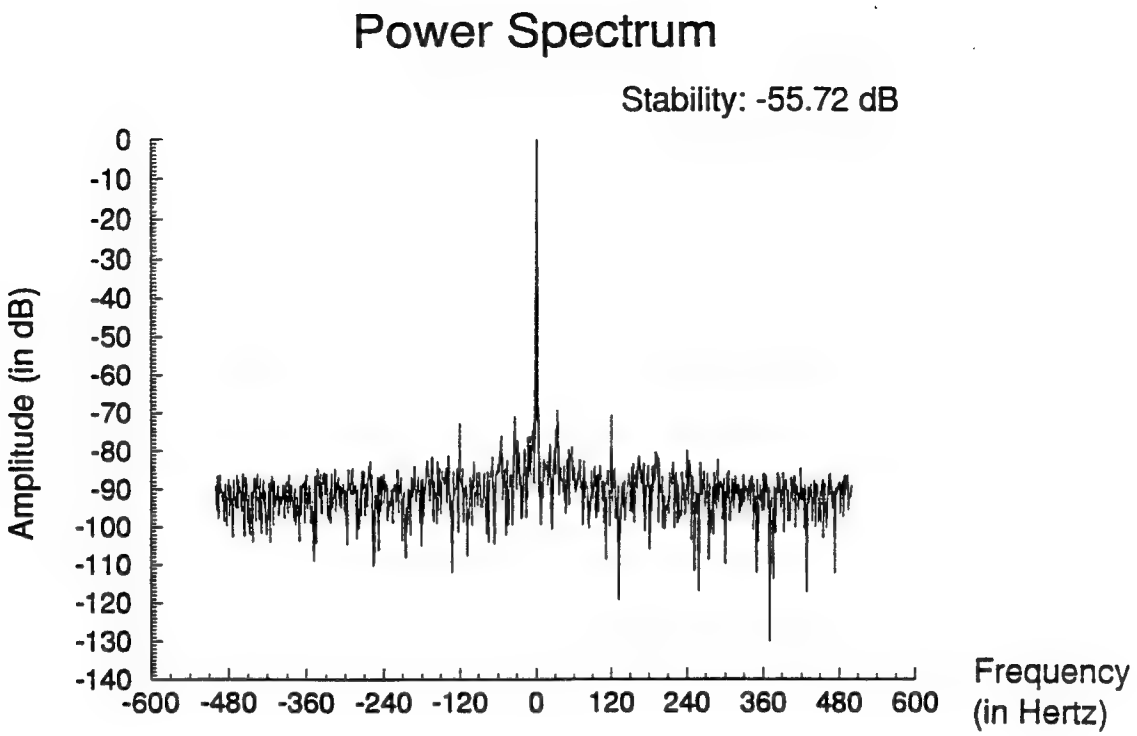

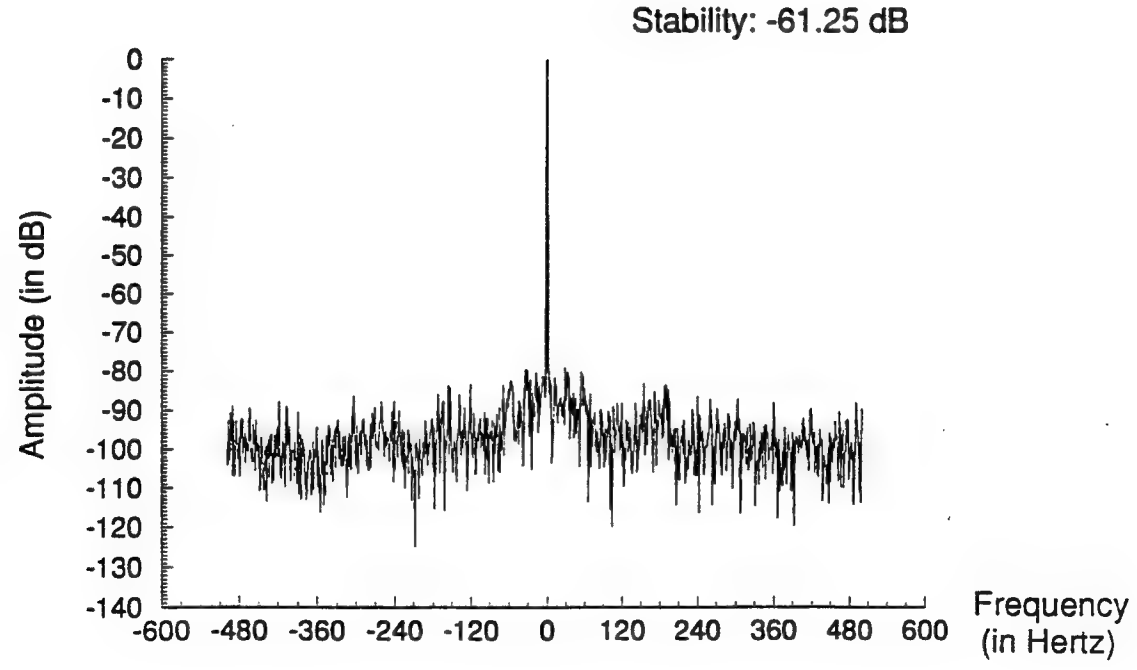

FIGURE 9.1-1. FIELD TESTS; RAW/EDITED MTS DATA

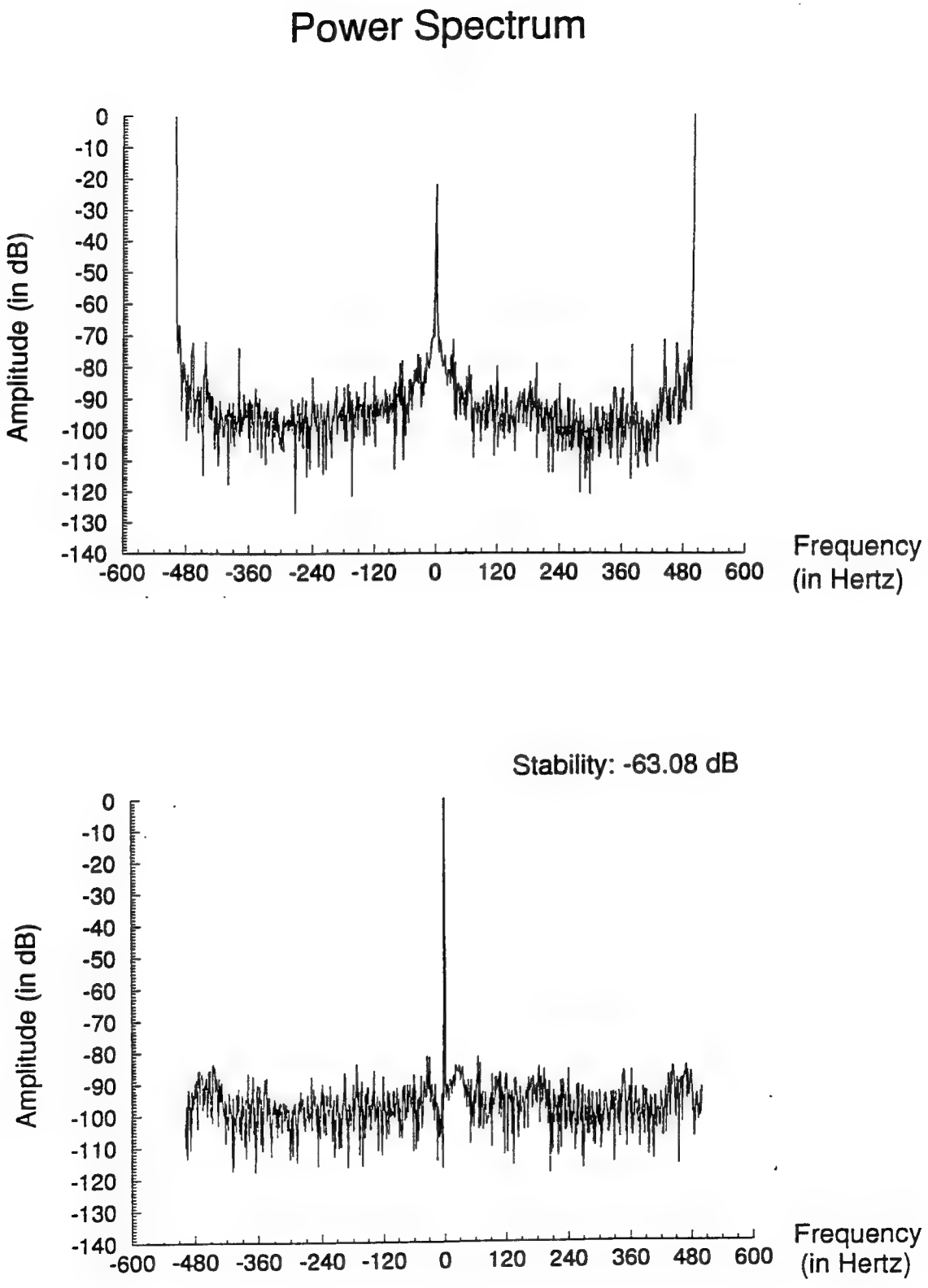

FIGURE 9.1-2. FIELD TESTS; RAW/EDITED MTS DOPPLER DATA

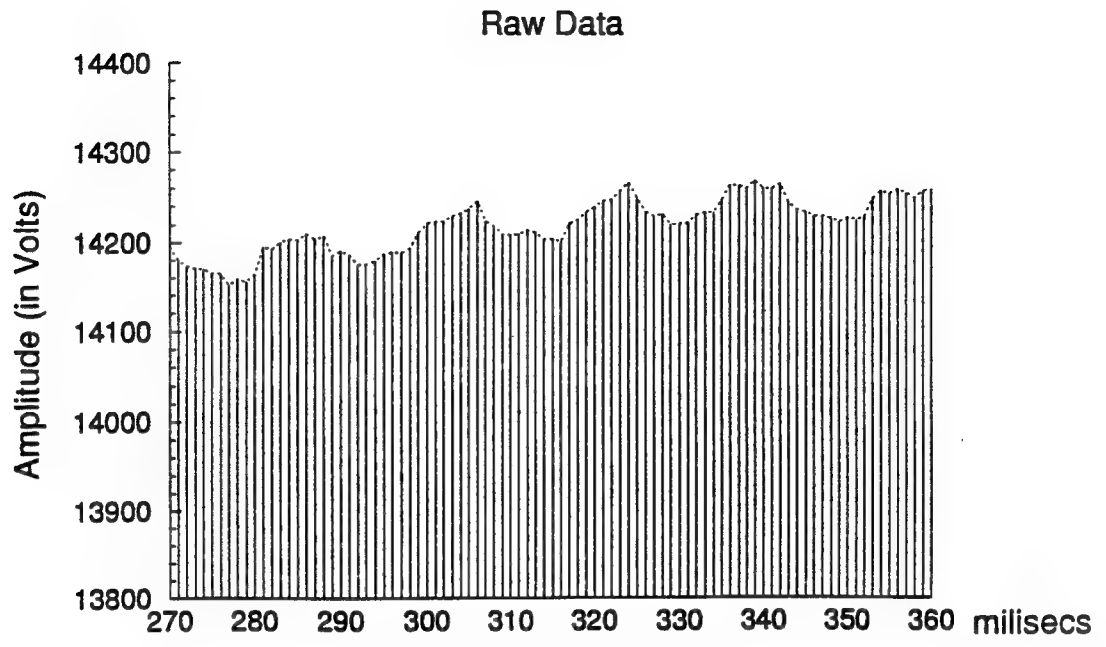

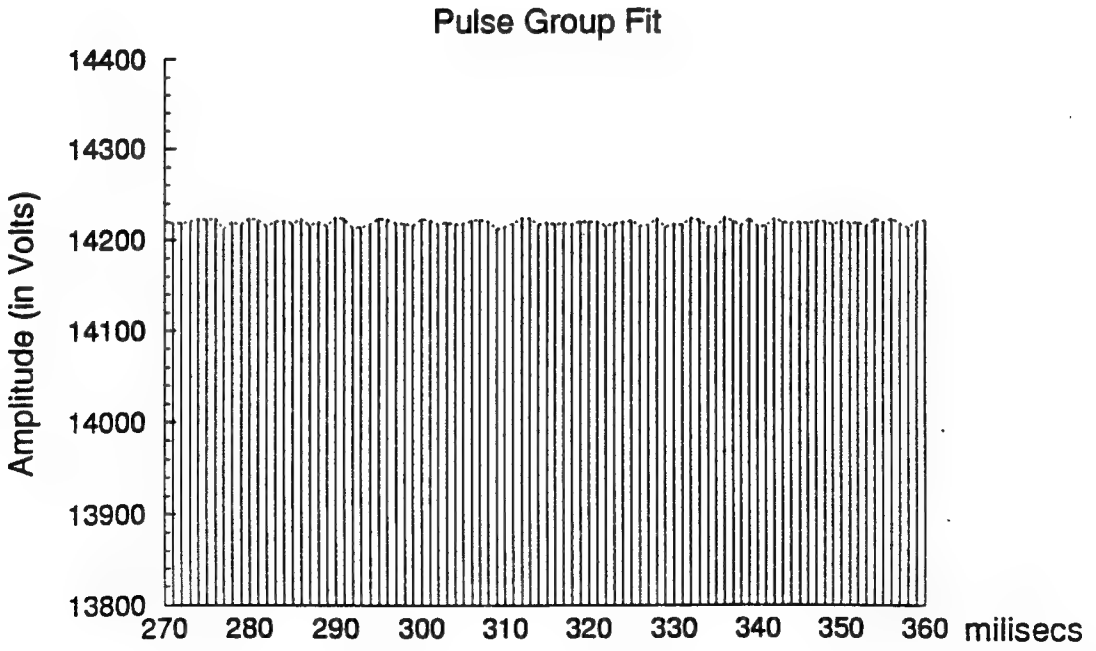

FIGURE 9.1-3. AMPLITUDE VERSUS TIME FOR STAGGERED PRF MTS RAW/EDITED

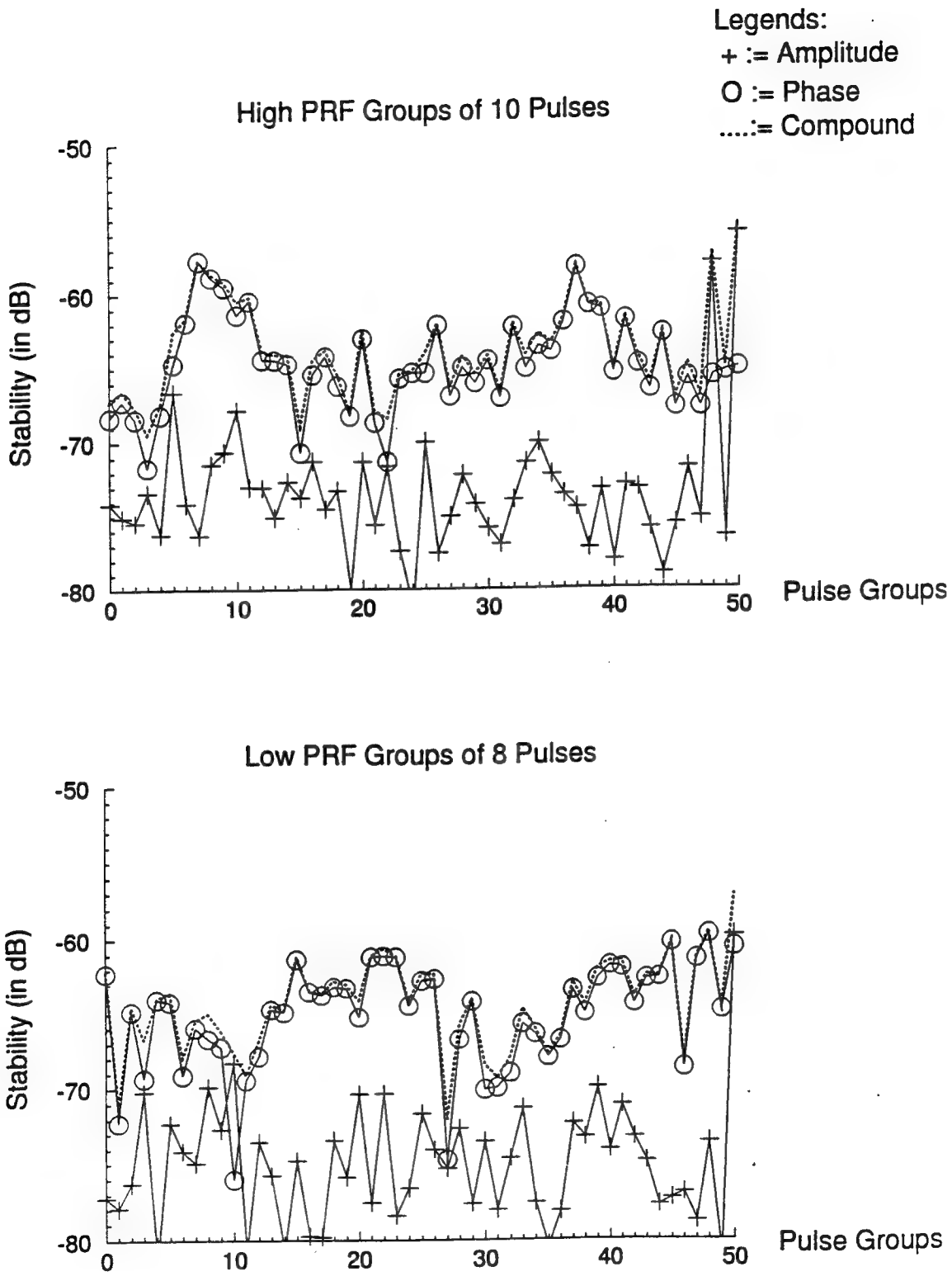

FIGURE 9.1-4. STABILITY VERSUS PULSE GROUP (HIGH/LOW PRF)

Local loop tests revealed that the repeater had a stability floor of about 71 dB. This is 9 dB better than the field measurement results, so the repeater did not compromise the stability measurement. It was interesting to note that power-line related spurious (such as seen in figure 9.1-1) were present without the repeater in the loop, so the repeater's power supply was very clean. The radar's power line components are, however, at a very low level.

The pulse stagger data reveals an interesting phenomenon relevant to the application of the ITT Gilfillan transmitter to windshear/microburst detection. The windshear channel uses 27 pulses sampled across a 10-8-10 pulse stagger group. The signal processor interpolates the data to obtain higher resolution doppler spectra across these pulse groups. In figure 9.1-5, we see that for the solid-state transmitter, the average phases of each 8- or 10-pulse group changes in a step fashion, that is, the 8-pulse group has an average phase approximately .3° different from the 10-pulse group. Unless this effect is compensated in the windshear channel signal processor, the stability of the 27-pulse transform will be affected by the step phase change. If we take this .3° phase shift to be a typical value, and apply a simple FM sideband calculation, then the resultant 27-pulse stability degrades to 52 dB. However, since the pulse group phase change is deterministic and appears to be quite stable, it can be easily compensated.

9.2 TIME SIDELOBE PERFORMANCE.

The purpose of the following set of measurements was to assess the time sidelobe performance as a function of doppler shift and in the presence of short-pulse interference. Because solid-state radar power amplifiers have limited peak output power, they use pulse compression techniques to increase the energy on target to that comparable to a conventional short-pulse high peak power klystron-based transmitter. However, pulse compression results in undesired time (range) sidelobes, and if means are taken to suppress their amplitude at any one doppler, the range sidelobe levels generally increase for other dopplers. As in any matched filter process, time sidelobes extend from the target return to the range equivalent of the uncompressed pulse length in front of the target, to the range equivalent of the uncompressed pulse length behind the target.

The Thomson-CSF pulse compression system uses a proprietary nonlinear FM waveform with time sidelobes that remain at very low levels over a wide range of doppler shifts. The uncompressed pulse is 75 μs long, so the range sidelobes extend approximately 6 nmi in range and out range from the compressed target return.

Time sidelobes were measured using loop test methods, that is, by coupling the transmitter/exciter directly back to the receiver through a cable or with various test items interposed. No time sidelobes were observed during target detections (no target signal had sufficient signal-to-clutter level), except when the radar repeater was employed. (As mentioned above, the repeater was designed to provide a near-saturation level signal into the radar. Time sidelobes were at the same level with the fielded radar repeater as were observed during the loop tests.)

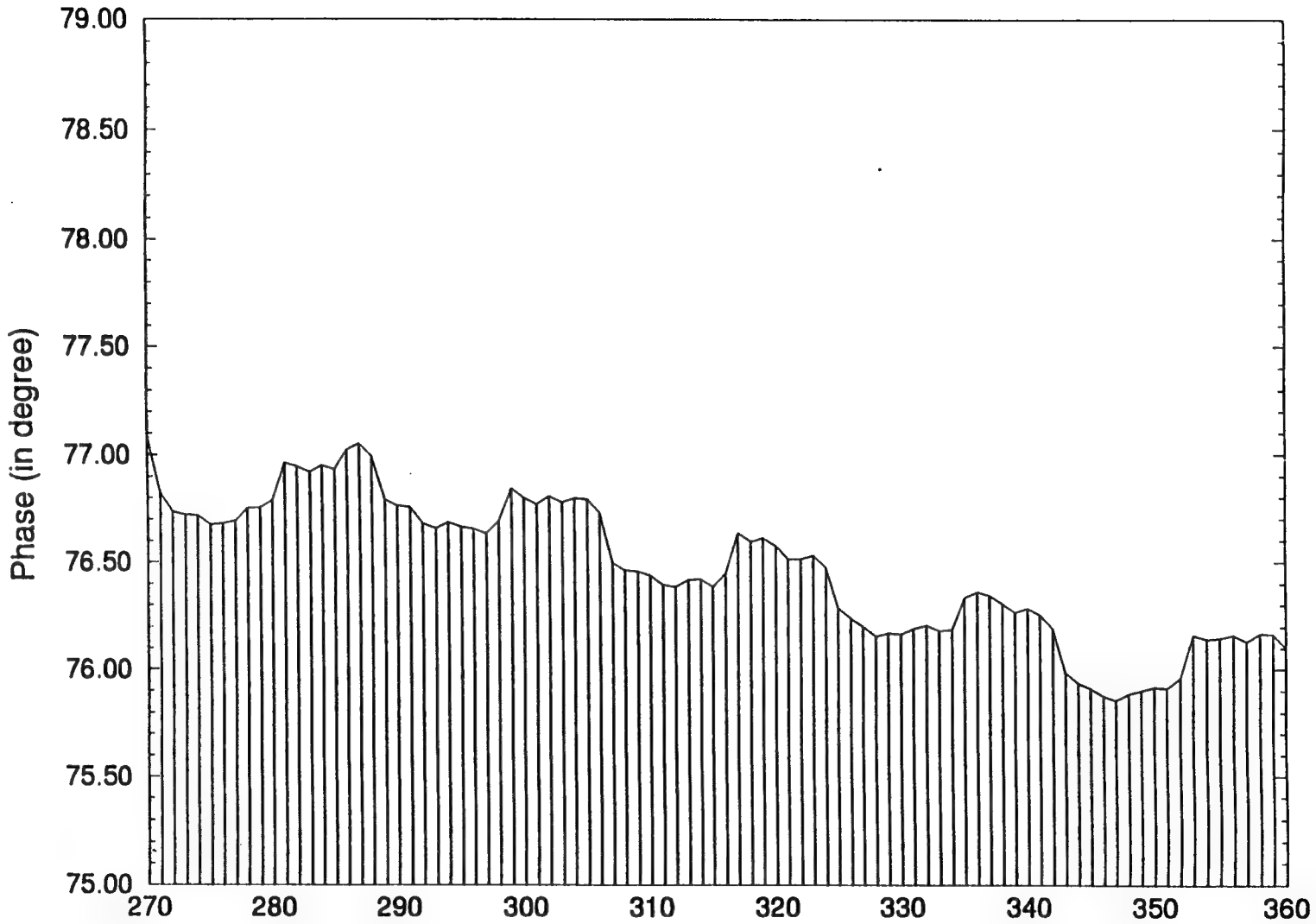

FIGURE 9.1-5. PHASE VERSUS PULSE GROUP (NO DOPPLER)

Loop tests were conducted with and without the repeater in line, with and without the doppler modulator engaged, with and without the transmitter in the loop, and at varying doppler shifts imposed by the waveform generator in the Thomson-CSF exciter. In addition, time sidelobe levels were checked with a Lincoln-designed 100-μs delay line in the loop, to see if the levels were range dependent.

A final measurement was to substitute three spare "cold" transmitter power amplifier modules for three randomly chosen "hot" modules operating in the transmitter. The intent was to see if the time sidelobes were degraded by the random substitution of cold spares for operating modules. We also compared the sidelobe levels measured when the entire transmitter had been operating for several hours to the levels measured when the transmitter had been operating for about 5 minutes from a cold start.

The pulse compression time sidelobes were approximately 55 dB down at all the doppler shifts available in the exciter (and looped repeater), whether or not the 100-μs delay line was added to the loop. Figures 9.2-1 to 9.2-5 show the time sidelobe level as a function of doppler shift; -51 dB worst case peak time sidelobes occurred at a doppler corresponding to a 130-meter/second target. Note that although the detailed structure of the time sidelobes changes at differing dopplers, the average value changes little at different shifts. There were negligible time sidelobe differences between cold/hot transmitter module swaps or between a transmitter that had been operating for several hours and a transmitter that had been operating for about 5 minutes from a cold start.

Figure 9.2-6 illustrates the system time sidelobe performance without the transmitter in the loop, that is, the exciter only was looped into the receiver. No doppler shift was imposed on the exciter signal. Peak sidelobes are 55 dB down, but the average sidelobe levels are nearly 70 dB down. Compared to figures 9.2-1 to 9.2-5, which are loop tests that include the ITT Gilfillan power amplifier, we note that the amplifier's nonlinear phase runout and amplitude droop contribute significantly to the average sidelobe level, even though the pulse compressor uses a transmitter compensation algorithm. The comparison underscores the sensitivity of these very low time sidelobe levels to minor mismatches in transmitter phase runout and amplitude droop compensation algorithm.

Although the peak sidelobes remain low, the increased average time sidelobes from unwanted transmitter effects and from doppler shifts will correspondingly increase the integrated time sidelobe level. The integrated time sidelobe level is simply the ratio of the energy in the main target response to the total energy in the time sidelobes. Low integrated time sidelobes are important to minimize range smearing near extended targets with high reflectivity gradients and complex doppler signatures, like thunderstorms. The integrated time sidelobes for the ITT Gilfillan/Thomson-CSF radar range from about -43 to -35 dB, depending on the transmitter compensation and doppler. These levels may be adequate, but no demonstration data were taken to confirm weather detection performance. Additional field data and detailed simulations would be required to properly address this issue.

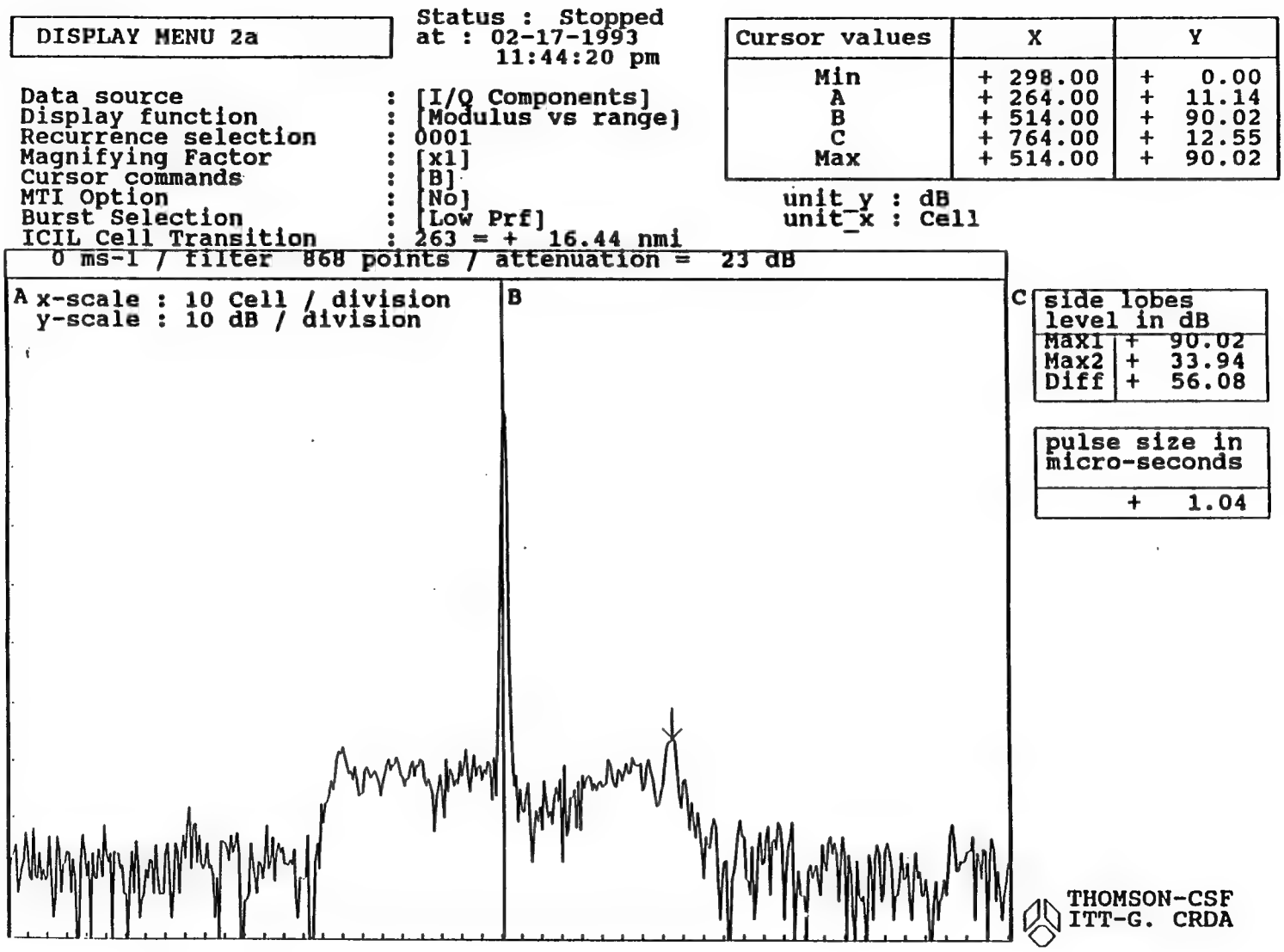

FIGURE 9.2-1. RADAR TIME SIDELOBES, 0 M/SEC DOPPLER

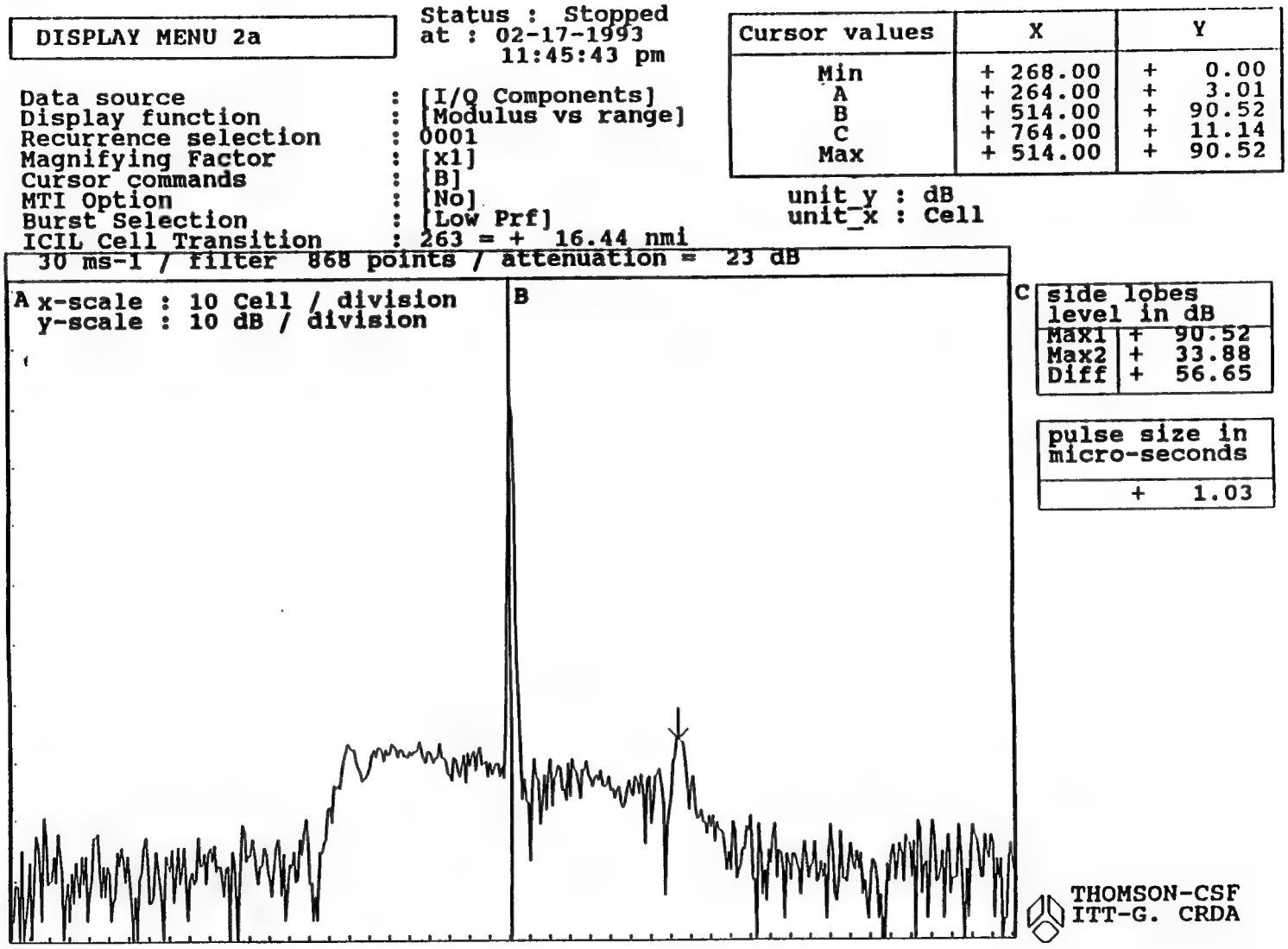

FIGURE 9.2-2. RADAR TIME SIDELOBES, 30 M/SEC DOPPLER

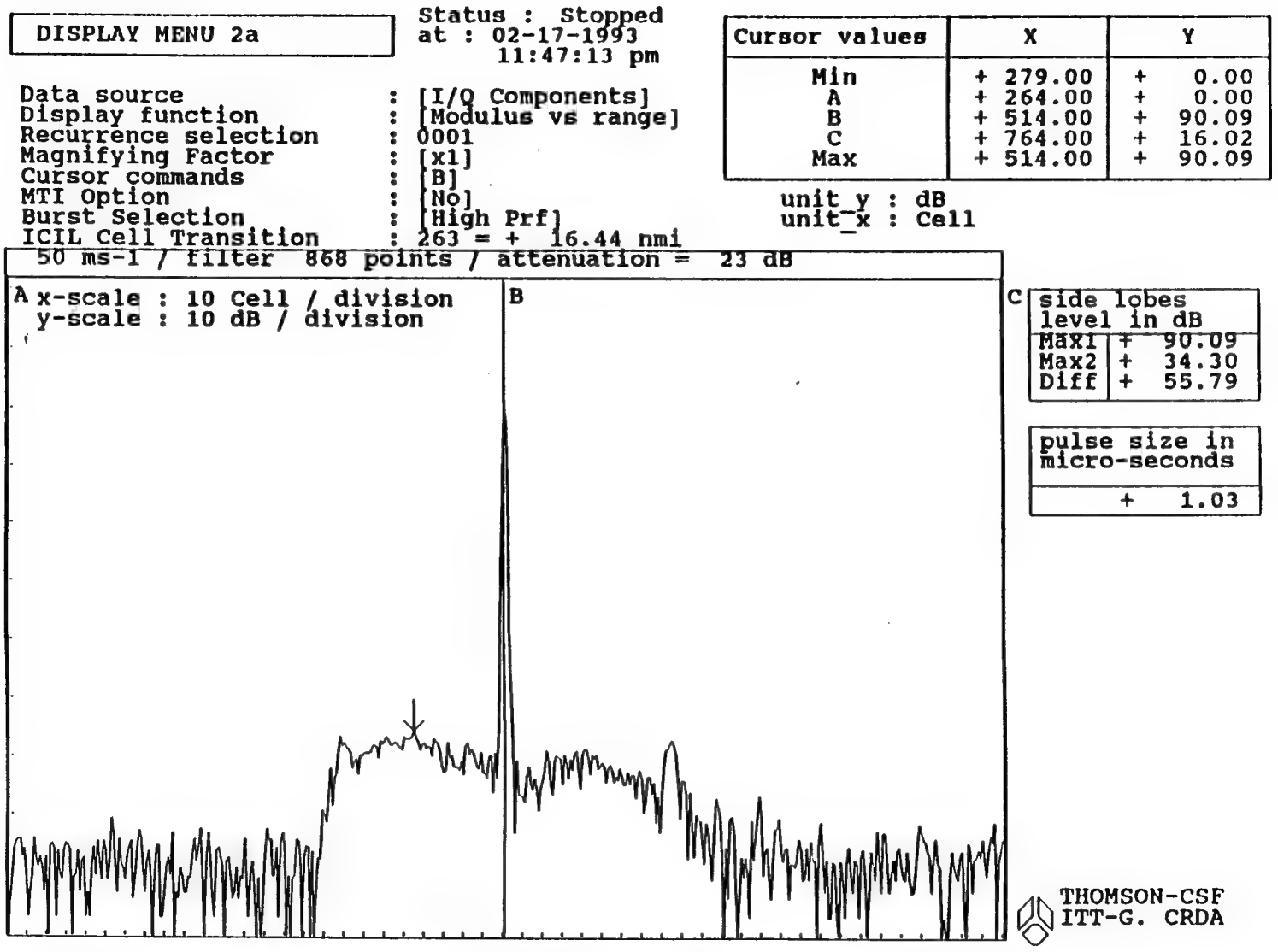

FIGURE 9.2-3. RADAR TIME SIDELOBES, 50 M/SEC DOPPLER

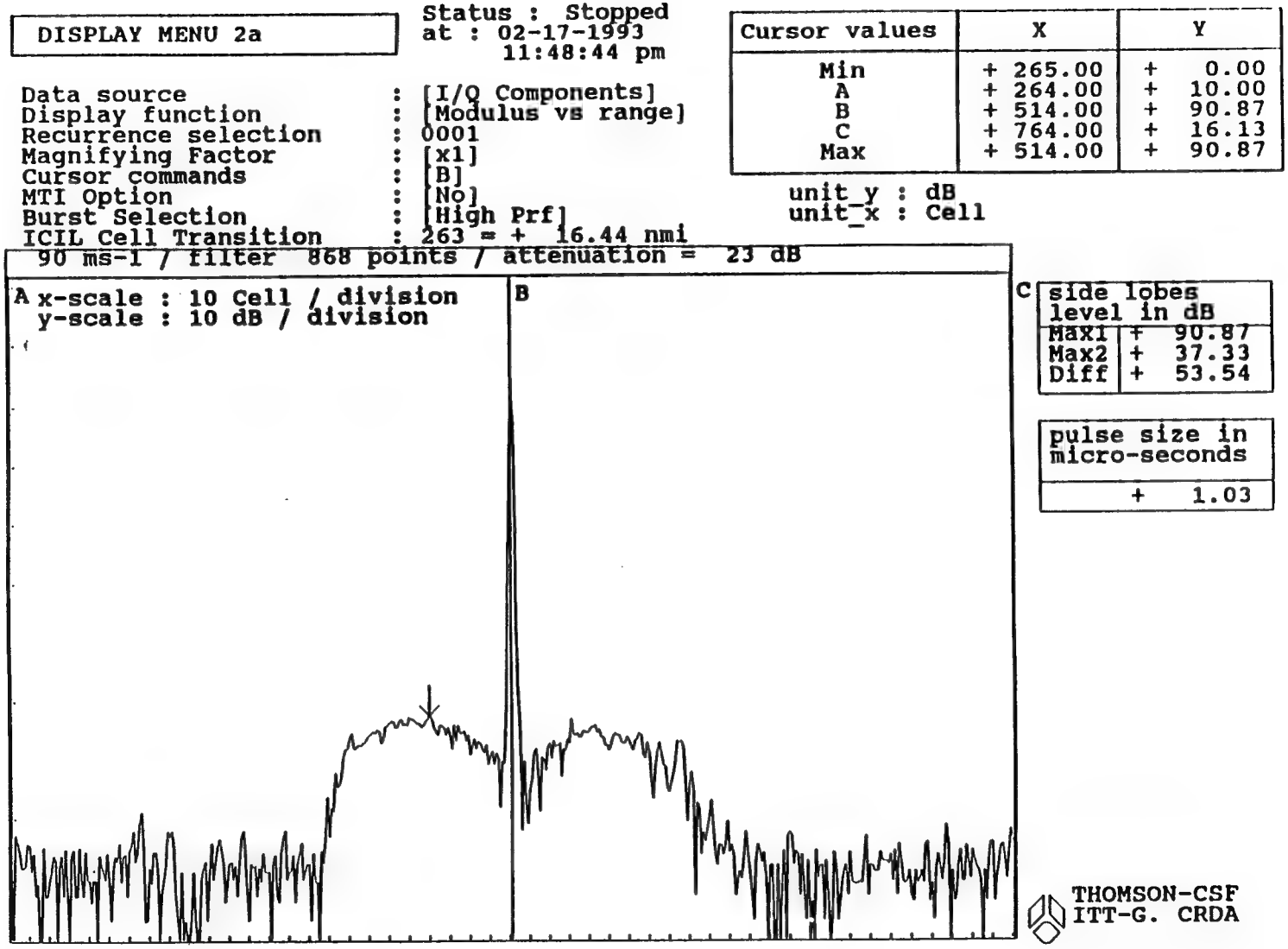

FIGURE 9.2-4. RADAR TIME SIDELOBES, 90 M/SEC DOPPLER

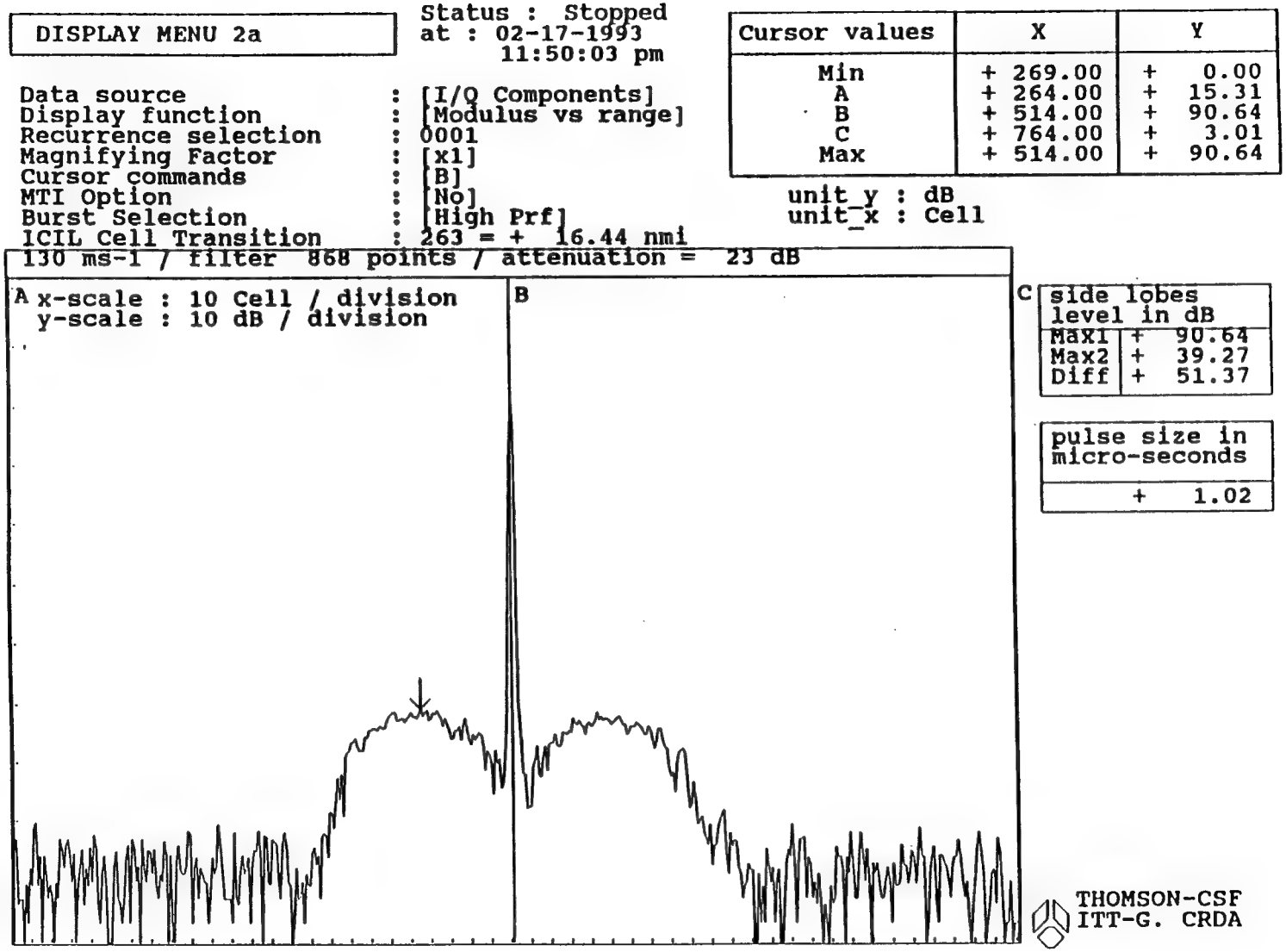

FIGURE 9.2-5. RADAR TIME SIDELOBES, 130 M/SEC DOPPLER

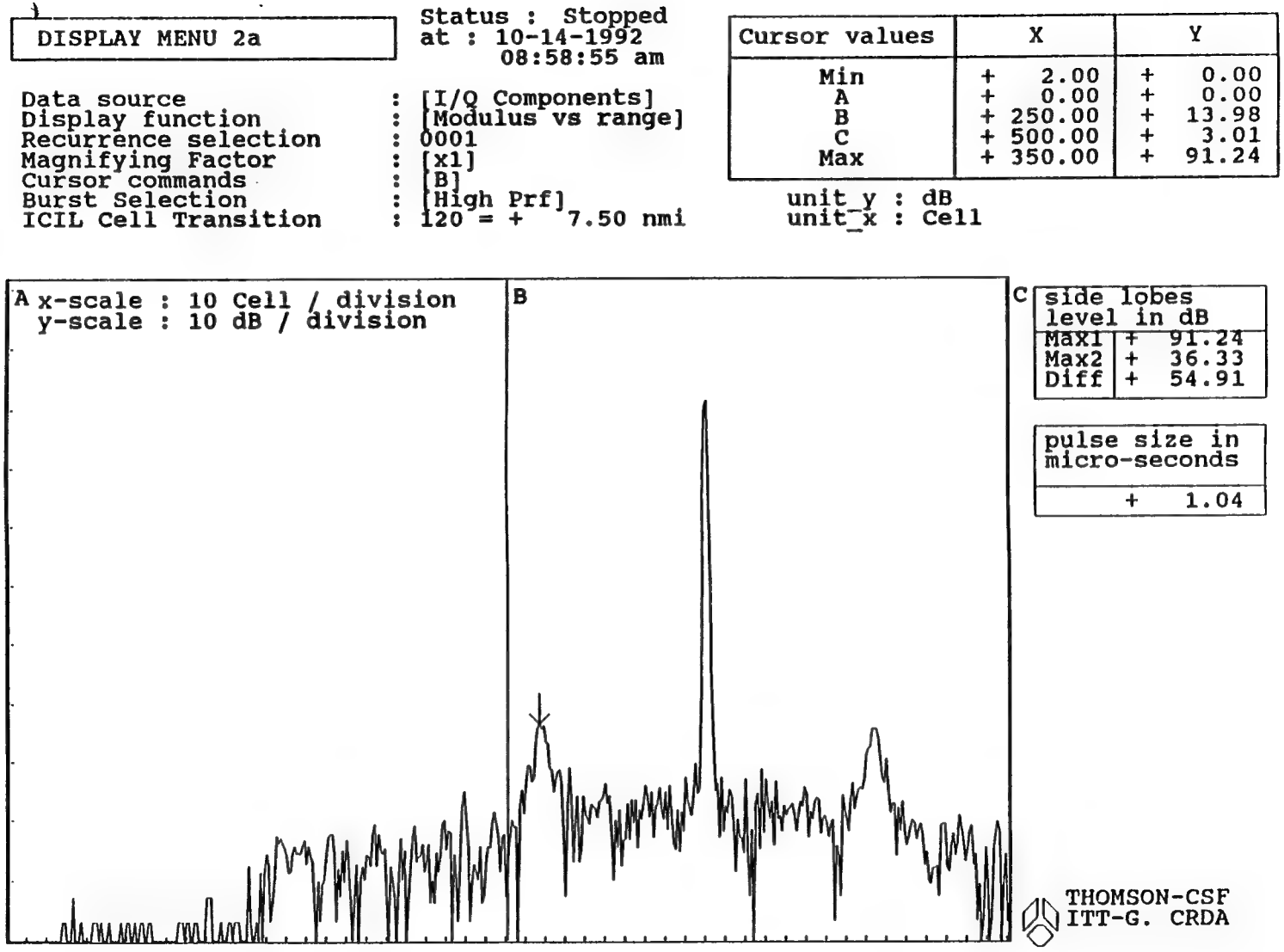

FIGURE 9.2-6. RADAR TIME SIDELOBES (EXCITER ONLY, NO DOPPLER)

During the demonstration at the FAA Technical Center, interference from the nearby WSR-57 weather radar was often observed on test equipment connected to the solid-state radar receiver. The WSR-57 is a 35-year old magnetron-based radar, operating at S-band (the same frequency range as the ASR-9). It is a high peak-power, short-pulse radar.

Figure 9.2-7 shows a typical range profile (amplitude versus range) along a single radial taken with the ITT Gilfillan/Thomson-CSF radar. This range profile covers a range of 16 nmi, with the short-pulse/long-pulse transition occurring at 7.8 nmi, about half way across the plot. The range profile of the very next PRI, taken along essentially the same radial, is shown in figure 9.2-8. Note that the amplitude of the "clutter" from the short-pulse/long-pulse transition to about 6 nmi outrange has increased by about 20 dB. The range profile of the next PRI appears again (see figure 9.2-7).

The briefly increased clutter amplitude over that 6 nmi range extent is due to the effects of short-pulse interference from the WSR-57. The interfering short pulse (approximately 1 μs long) acts as an impulse-like excitation for the 75 μs pulse compression filter. The filter rings for 75 μs (5 nmi in range), just as an analog pulse expander forms long pulses from an impulse excitation.

Short-pulse interference to pulse compression radars is a potentially serious concern, since many dozens of range cells and all doppler filters are affected. The interference will degrade or render ineffective the radar's dynamic thresholding and doppler estimates made on real targets present in the affected range cells. In addition, short-pulse interference can be present at many azimuths, depending on the antenna sidelobe performance of the two radars, the spectral purity of the interfering radar, and the selectivity of the pulse compression radar receiver. A modern (short pulse) air traffic control (ATC) radar such as the ASR-9 has a short-pulse interference detection and limiting scheme which will not work properly in a pulse compression receiver. Short-pulse interference to pulse compression receivers is not an insoluble problem, but it must be addressed in the radar receiver and processor design if pulse compression is to be successfully fielded in ATC applications.

9.3 DETECTION PERFORMANCE.

The purpose of the following set of measurements was to assess inner and outer range target detection and detection performance as an aircraft passes through the short-pulse/long-pulse transition. Independent analyses of different data sets were performed at Lincoln Laboratory and at the Technical Center. Although some of the information presented is common to both analyses, the results from each assessment are presented.

Lincoln Laboratory Assessment

As indicated above, the limited peak power of the ITT Gilfillan solid-state power amplifier requires that a long pulse be used to obtain sufficient energy on target at long ranges. This pulse is 75 μs long, which masks close-in targets up to about 6 nmi from the radar. A short (1 μs long) pulse is also transmitted after the long pulse, and at a different frequency, to fill in the 6 nmi range swath blanked during long-pulse transmission.

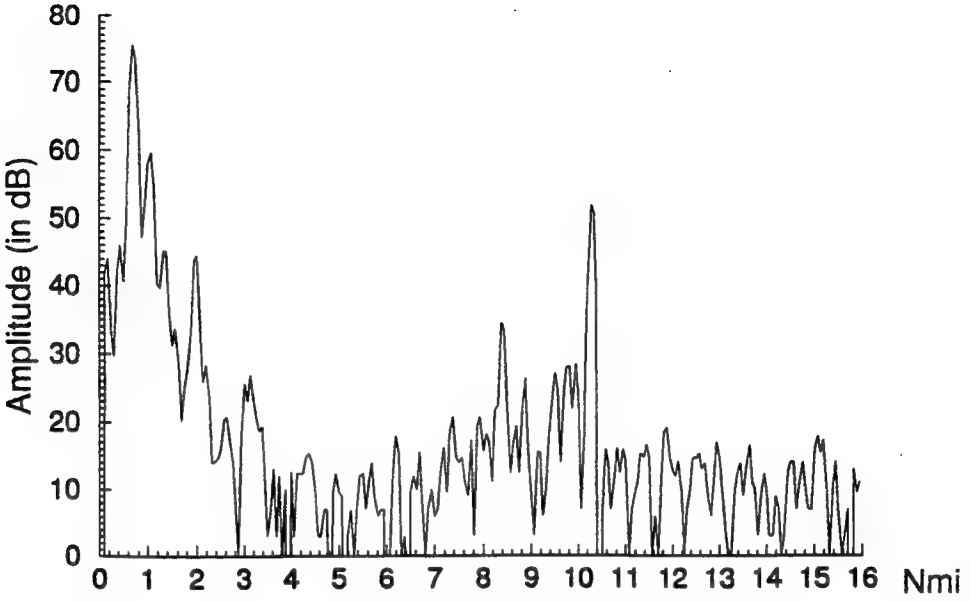

FIGURE 9.2-7. RANGE PROFILE - NO INTERFERENCE

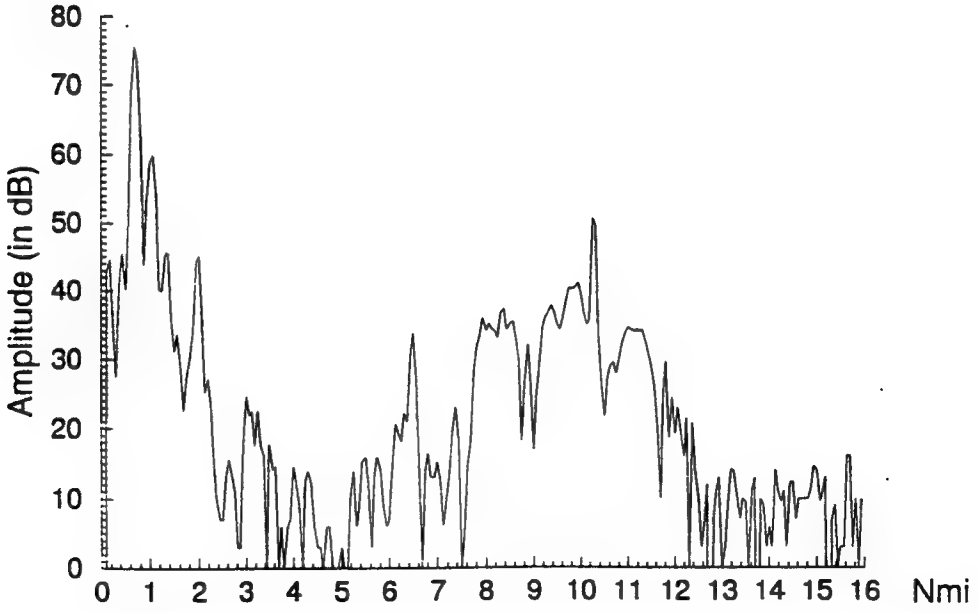

FIGURE 9.2-8. RANGE PROFILE WITH SHORT PULSE INTERFERENCE

Enough energy is in the long pulse to yield target detection capabilities identical or slightly better than that of an ASR-9. A simple calculation shows that if the short-pulse/long-pulse transition is set to occur at 7 or 8 nmi, the short-pulse energy is also sufficient to ensure ASR-9 like target detection for the first 7 or 8 nmi.

The solid-state demonstration radar fed I and Q data into the ASR-9 MTD processor. Two limitations arise because of the use of the ASR-9 MTD: (1) the 18-bit I and Q data from the Thomson-CSF receiver was truncated to 12 bits to accommodate the ASR-9; and (2) the ASR-9 MTD processor was not designed for dual pulsewidth waveforms. The latter limitation means that ASR-9 range-averaging constant false alarm rate (CFAR) will be biased by the 19-dB energy discontinuity in the vicinity of the short-pulse/long-pulse transition. This effect, which will tend to set the CFAR threshold too high for the outer range of the short pulse, results in biased target detection statistics as reported at the ASR-9 MTD output.

Limited data was collected to investigate how a MTD processor optimized for dual pulse waveforms might report unbiased target detection. Data was taken on a single flight of a small aircraft at a 4500-foot altitude, flying inbound along a radar radial and crossing over the long-pulse/short-pulse transition. The transition occurred at 7.8 nmi. For the short pulse, the radar received on the high beam for the first 3 nmi; for the long pulse, the radar received on the high beam from 7.8 to 9 nmi, then from the low beam. STC was applied to the high beam only with a $1/R^3$ characteristic, up to 3 nmi from the radar.

The data was processed by performing a discrete Fourier transform on each of the 8- and 10-pulse complex data samples produced by the Thomson-CSF pulse compressor. The processed data are shown in figures 9.3-1 to 9.3-6. Each figure plots the doppler filter amplitudes, normalized to the largest return, for the target range gate when the target is present (solid line) and when the target is absent (dotted line). Target absent data is taken from a scan when the aircraft is in another range cell. The target crosses the short-pulse/long-pulse transition between scans 4 and 5.

Note that in every figure the fourth pulse group shows very little evidence of target presence; this is because the Thomson-CSF demonstration recorder could not be set up to center the aircraft radial in the recording wedge. The aircraft is just within the beam for the first three PRIs, and by the fourth PRI, the antenna has scanned away.

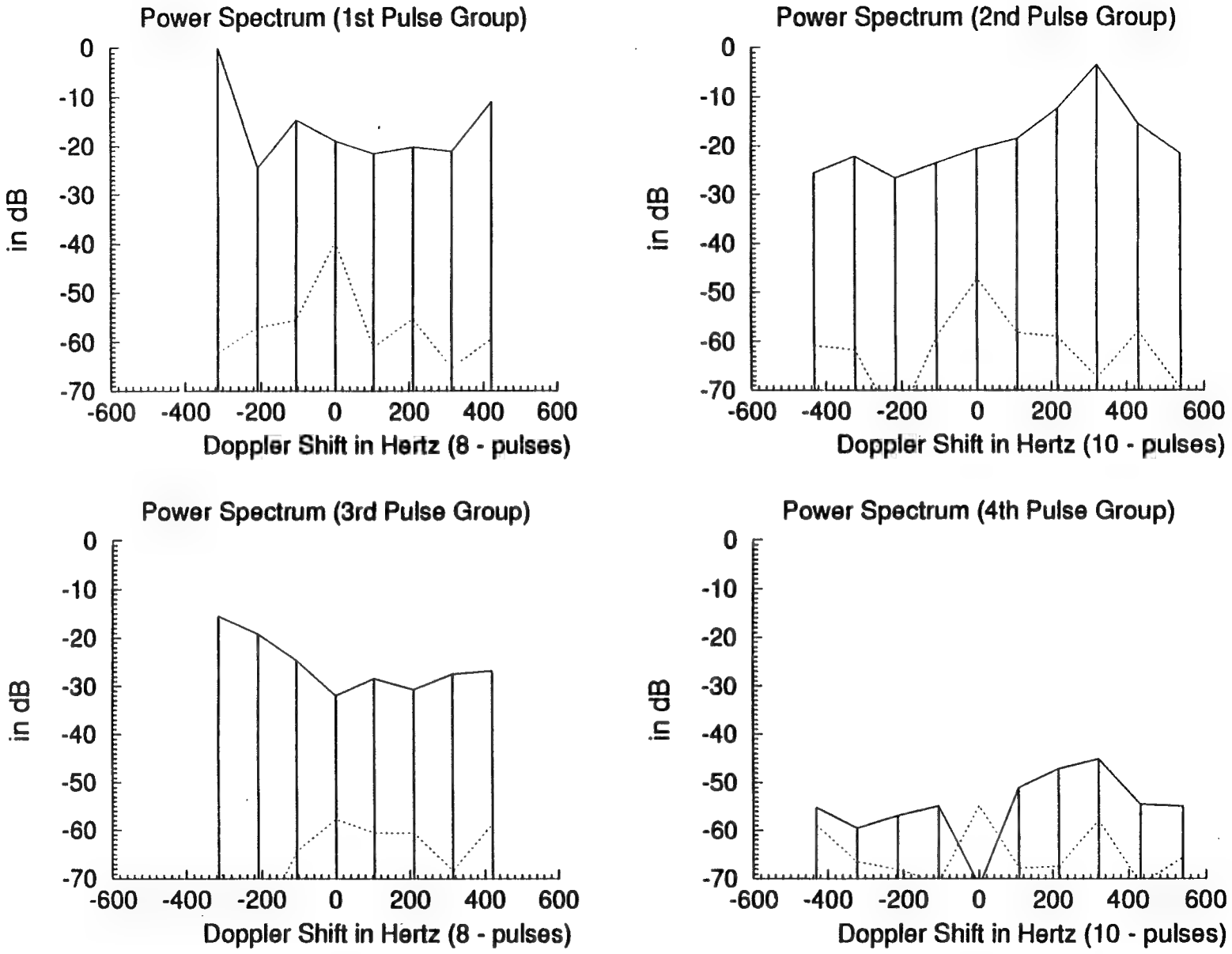

FIGURE 9.3-1. DOPPLER FILTER AMPLITUDES, SCAN 1 (TARGET) AND 3 (NOISE) RANGE CELL #156

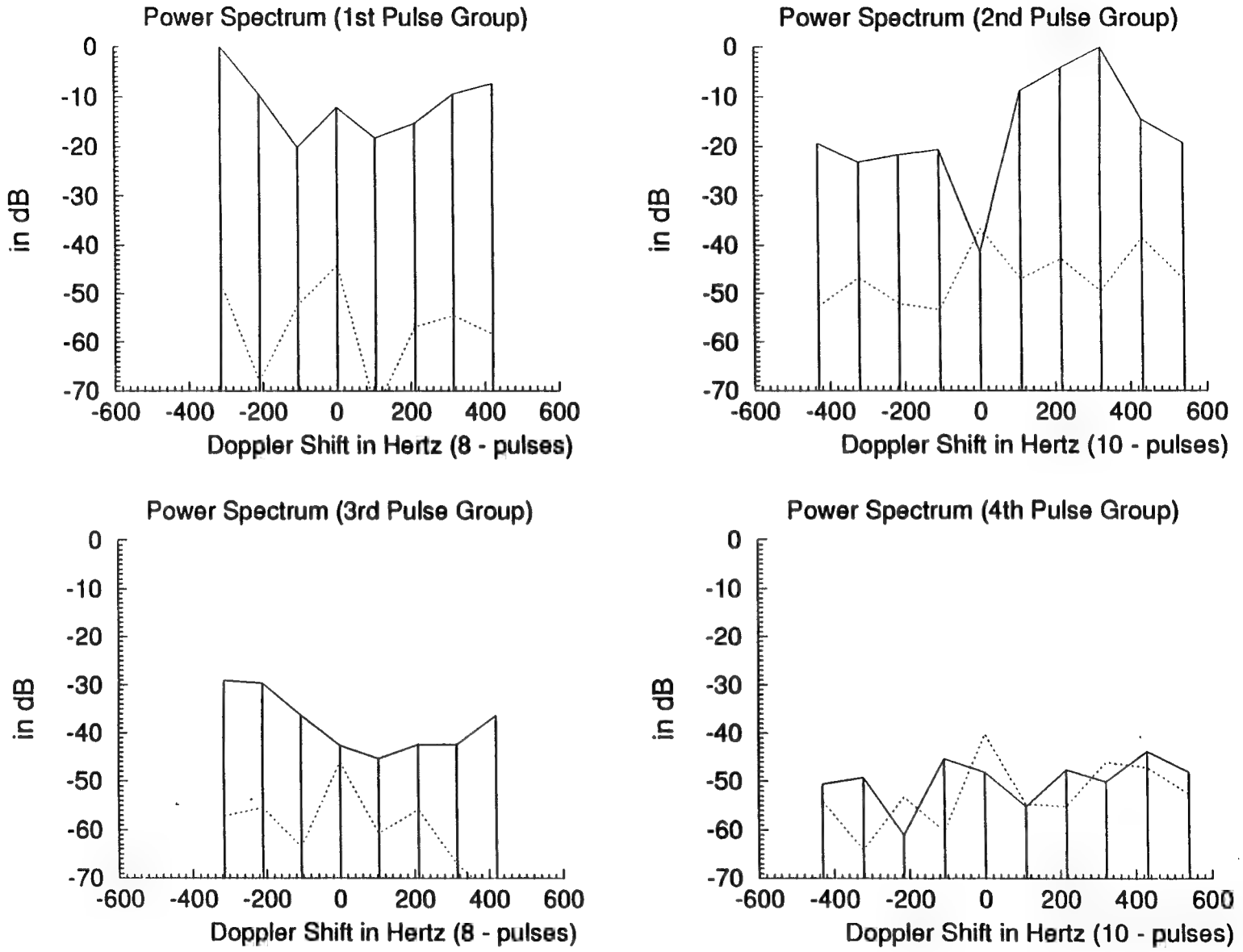

FIGURE 9.3-2. DOPPLER FILTER AMPLITUDES, SCAN 3 (TARGET) AND 1 (NOISE) RANGE CELL #137

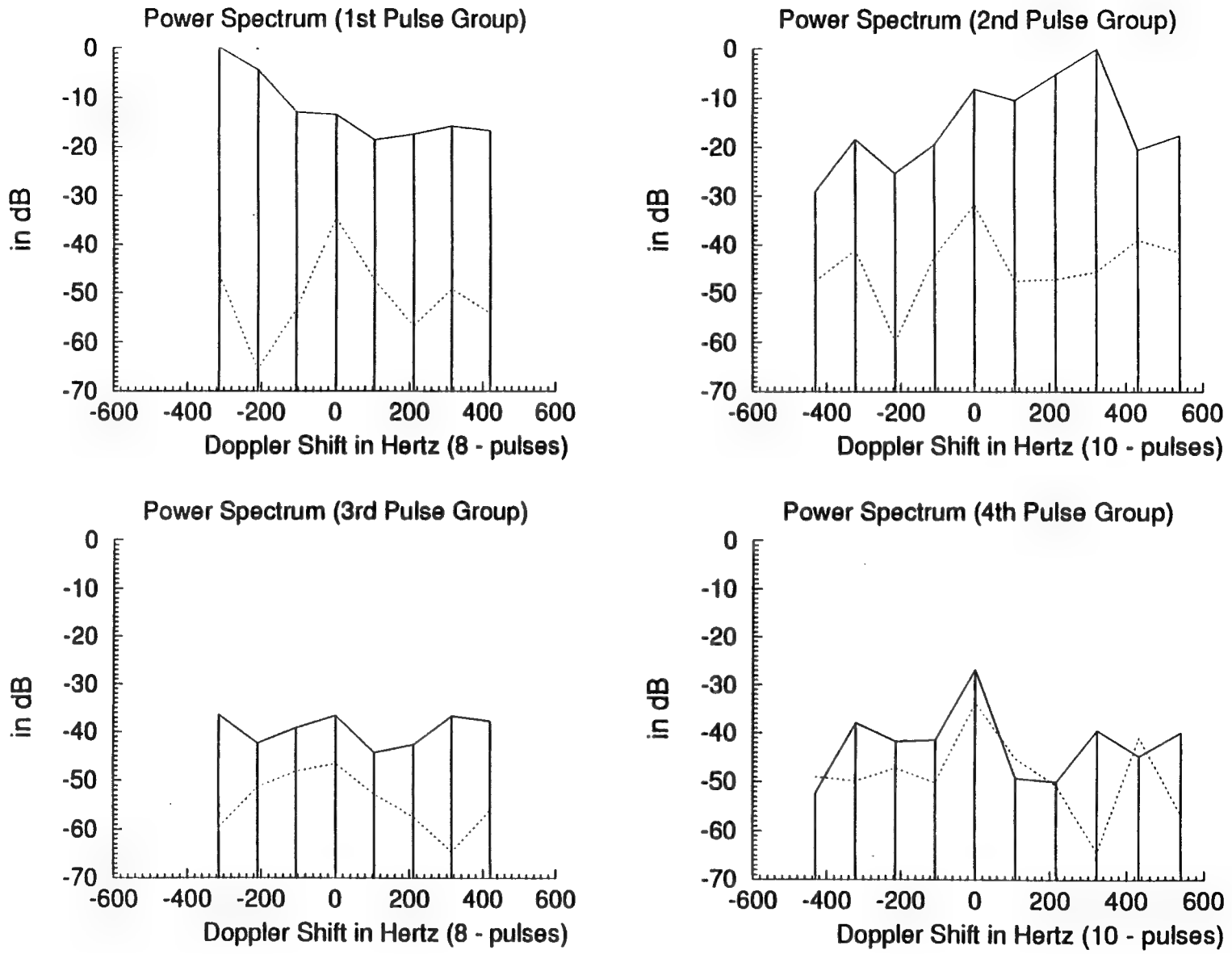

FIGURE 9.3-3. DOPPLER FILTER AMPLITUDES, SCAN 4 (TARGET) AND 1 (NOISE) RANGE CELL #127

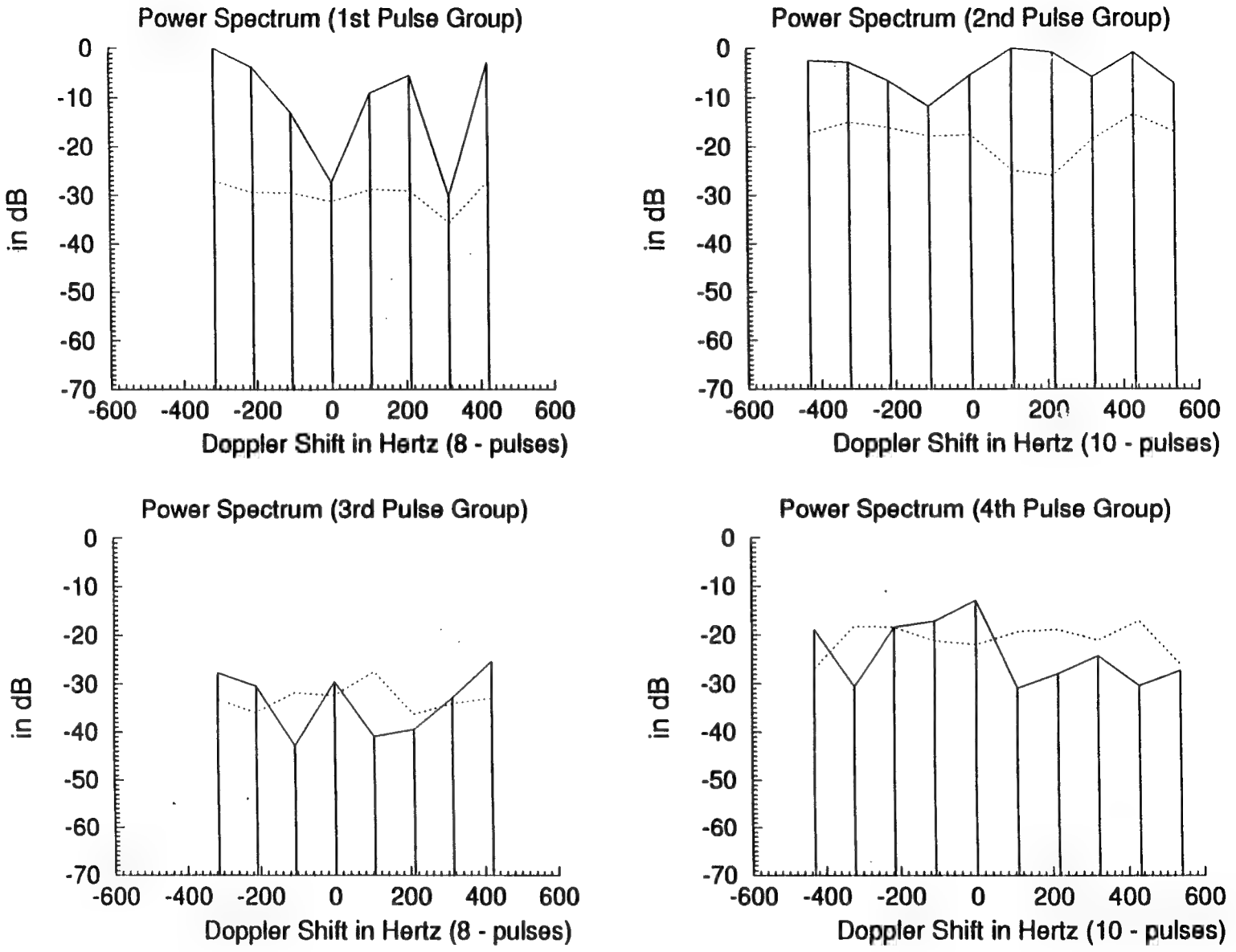

FIGURE 9.3-4. DOPPLER FILTER AMPLITUDES, SCAN 5 (TARGET) AND 7 (NOISE) RANGE CELL #118

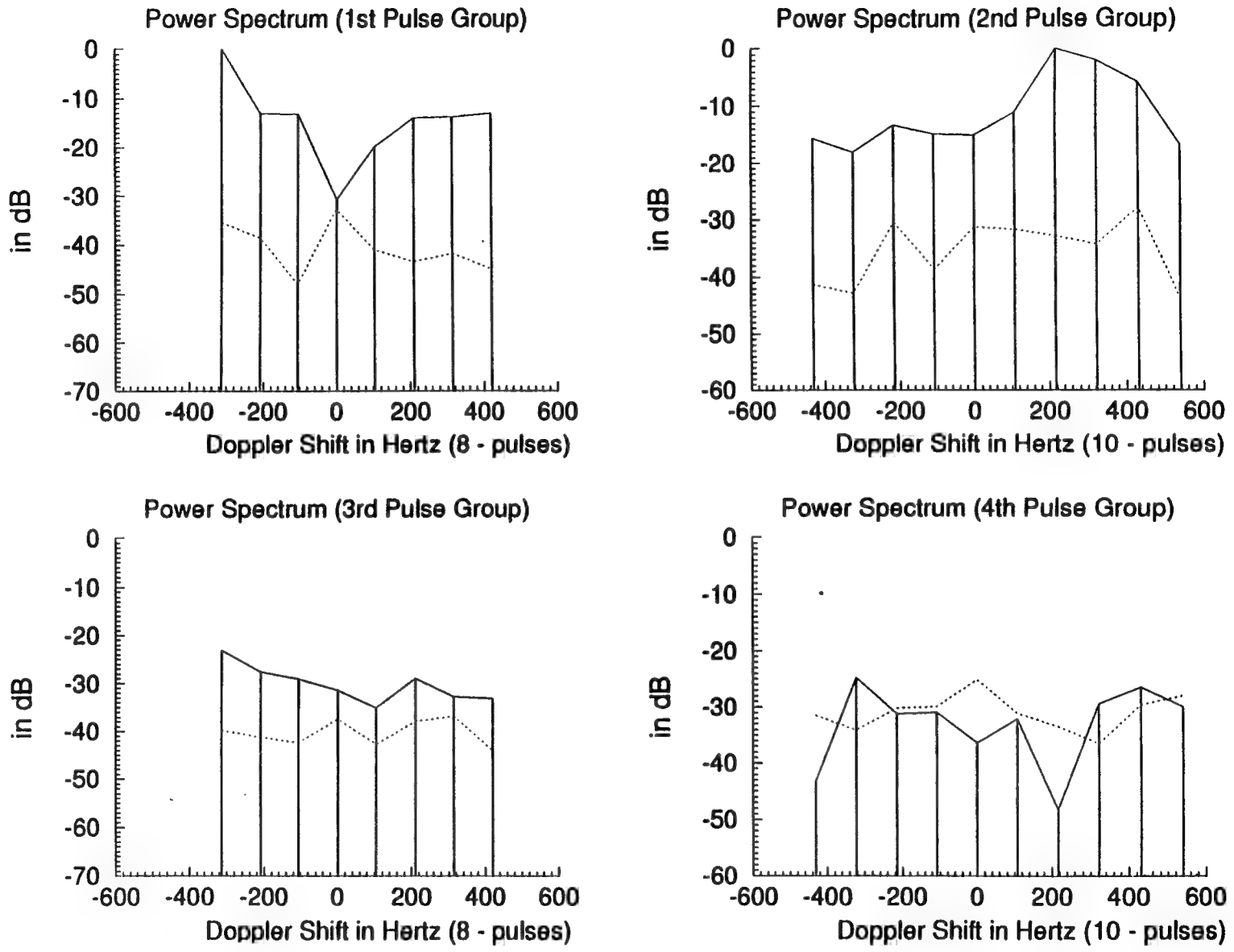

FIGURE 9.3-5. DOPPLER FILTER AMPLITUDES, SCAN 6 (TARGET) AND 8 (NOISE) RANGE CELL #108

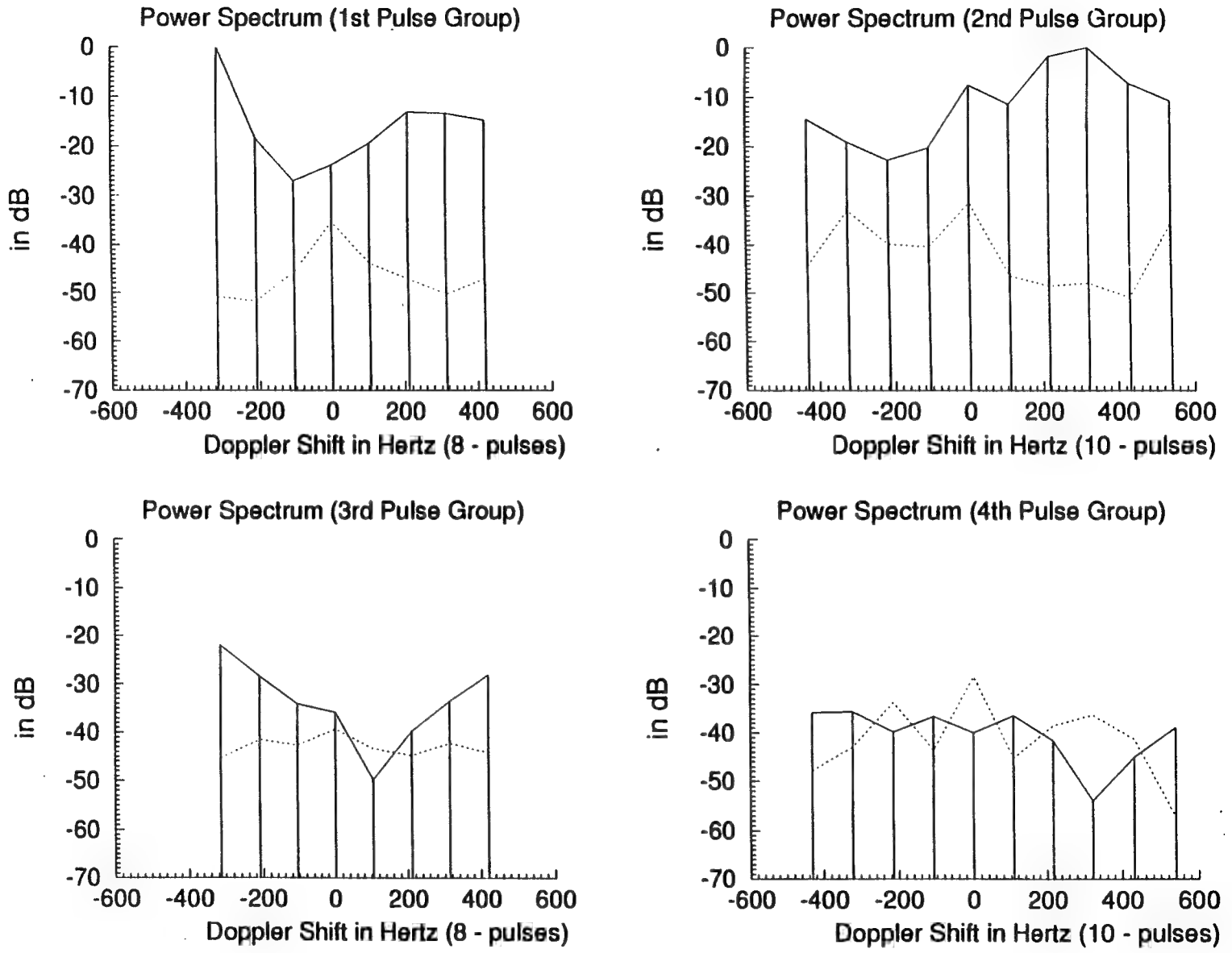

FIGURE 9.3-6. DOPPLER FILTER AMPLITUDES, SCAN 8 (TARGET) AND 6 (NOISE) RANGE CELL #88

Examining the first three pulse groups (an 8/10/8 staggered PRF sequence when the aircraft is in the beam) for several scans as the aircraft proceeds inbound yields:

Scan Number	Range nmi	Peak SIR Pulse Group 1	Peak SIR Pulse Group 1	Peak SIR Pulse Group 1
1	9.75	62 dB	62 dB	55+ dB
3	8.56	48 dB	50 dB	31 dB
4	7.93	46 dB	45 dB	27 dB
5	7.38	27 dB	25 dB	7 dB
6	6.75	35 dB	33 dB	13 dB
8	5.50	51 dB	47 dB	23 dB

where the Peak SIR denotes the signal to interference ratio measured in the target's doppler bin with the target present and absent. The target crosses the short-pulse/long-pulse transition between scans 4 and 5.

Two observations can be made about this limited data set: (1) target energy drops by 19 to 20 dB when the aircraft crosses the short-pulse/long-pulse transition, precisely as would be predicted from the pulse energy difference and the slight range difference, (2) when the target is plainly in the beam (that is, for pulse groups 1 and 2), signal to interference levels for the outer range of the short-pulse region (scan 5) yield adequate detection performance. The 25 dB or greater SIR shown will yield a greater than 0.95 probability of detection and a 10^{-12} probability of false alarm against a Swerling I target.

This single data set, with its low altitude target appearing at the edge of the recording wedge, does not address other issues related to target detection with dual pulse lengths. These issues include optimization of the radar's STC, the high/low-beam switchover points, and the MTD processor's limited dynamic range and CFAR. The data does demonstrate that the solid-state radar energy is sufficient for adequate target detection at the outer range of the short-pulse waveform, and that the design of a CFAR optimized for dual pulse operation should begin by taking into account the fundamental energy differences between the two pulsewidths.

Technical Center Assessment

For those flights where the demonstration equipment was installed, the ASR-9 STC and high/low-beam switch was controlled from the demonstration receiver. The STC in the low beam was set at 0 dB. In the high beam, the initial value of STC was set at 20 dB and followed a $1/r^3$ curve out to 3 nmi. The short-pulse/long-pulse transition was set at 7.84 nmi. The high/low beam transition for the short pulse was 3 nmi and for the long pulse was 9.5 nmi.

Six detection flight tests were performed. Three flight tests (RUN011, RUN012, and RUN015) were executed on the 230° radial of the radar from 0 to 60 nmi at 9500 feet above ground level (AGL) (close to the peak of the beam of the ASR-9 at maximum range). A range-azimuth plot of the flight scenario is shown in figure 9.3-7. The data in the figure is IRES radar and beacon flight test data which was filtered by range and azimuth to show only the test aircraft.

The radial flight tests were designed to measure detection at the full instrumented range of the radar. The demonstration equipment was installed for RUN011 and RUN015. RUN015 was a repeat of RUN011 after an apparent interface problem between the demonstration receiver and the ASR-9 processor was discovered and corrected. RUN012 was performed with the standard ASR-9 klystron transmitter and receiver installed.

In addition to the radial flights, three flight tests of figure eight patterns were performed. Filtered IRES radar and beacon reports in figure 9.3-8 illustrate the figure eight pattern. The center of the figure eight was positioned above the radar and the maximum range achieved on either side of the radar was approximately 15 nmi. These tests were designed to measure the inner coverage and detection at the short-pulse/long-pulse boundary with the demonstration equipment installed. RUN016 was performed at 17500 feet above ground level (AGL); RUN018 was performed at 9500 feet AGL; and RUN019 was performed at 4500 feet AGL.

Data was recorded using IRES, the demonstration I/Q recorder and the ASR-9 DRI. However, data was not collected with all systems for all runs. Table 9.3-1 lists the filenames of the data collected with each system for each test. IRES data was collected for each test. Data was collected for each test using the demonstration 18-bit I and Q data recorder. However, the recorder could collect data in only a small range; azimuth window and oftentimes the aircraft was not in the record window. Radar primitive data was collected with the ASR-9 digital recorder interface for runs 15, 16, 18, and 19.

RUN011 was flown on March 2, 1993, with the demonstration equipment installed. RUN011 was a radial detection flight test performed between 0 and 60 nmi at 9500 feet AGL. The test aircraft was a Aero Commander AC680E. The radar cross section (RCS) of the Aero Commander is approximately 1.8 to 2 square meters. The absolute cross section is unknown; however, for comparison with ASR-9 detection performance, the RCS is not needed.

ASR-9 reports were recorded at the output of the radar using IRES. The output reports were sorted in range/azimuth order, filtered by range and azimuth, and tracked using a selective tracker in IRES which tracks the aircraft of interest when the beacon code is known. The percentage of detection was then calculated for the tracked data at each range along the flight path.

In addition to the range and azimuth filtering, Quality 0 reports (those reports with returns on one coherent processing interval (CPI) only) were eliminated from the file since these were almost always false reports. Interference from other radars in the vicinity of the Atlantic City ASR-9 contributed to many of the quality 0 false reports recorded at the radar output. The ASR-4 operates at 2760 and 2850 MHz; the ASR-8 operates at 2710 and 2790 MHz; and the WSR-57 weather radar operates at 2885 MHz.

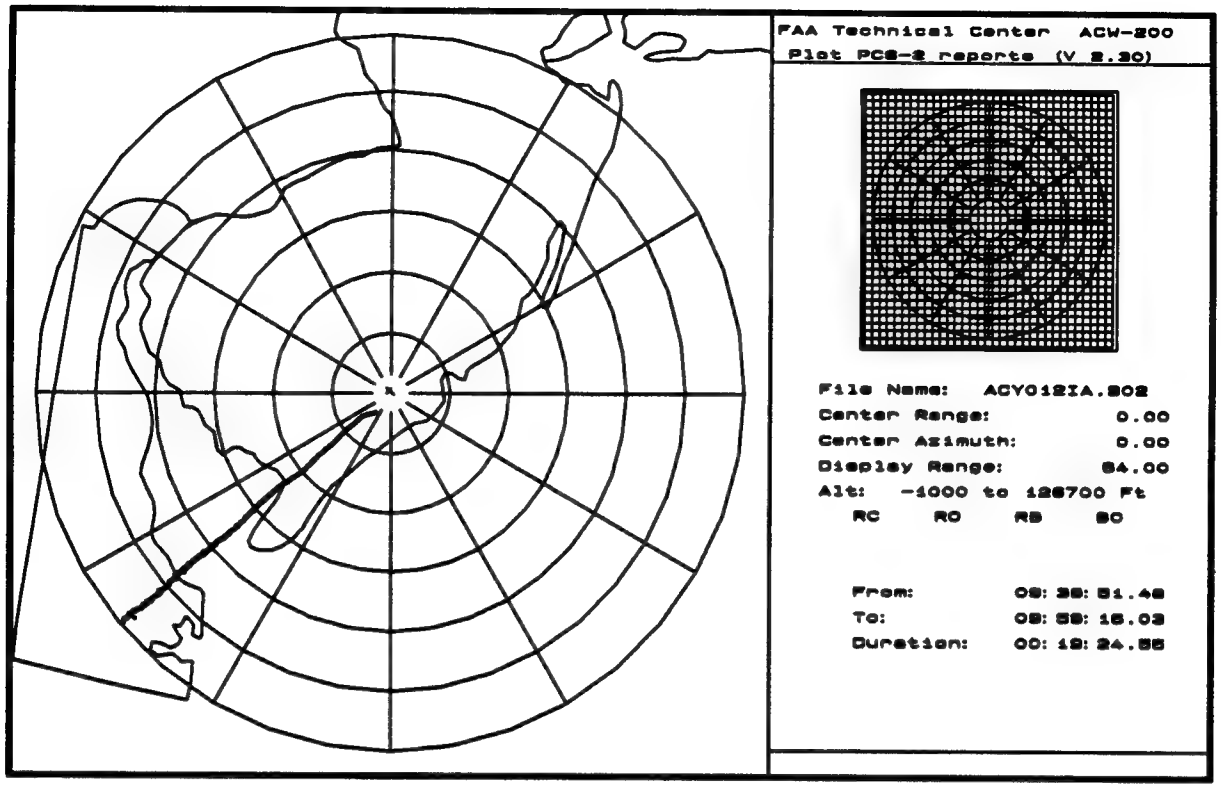

FIGURE 9.3-7. RADIAL FLIGHT TEST SCENARIO

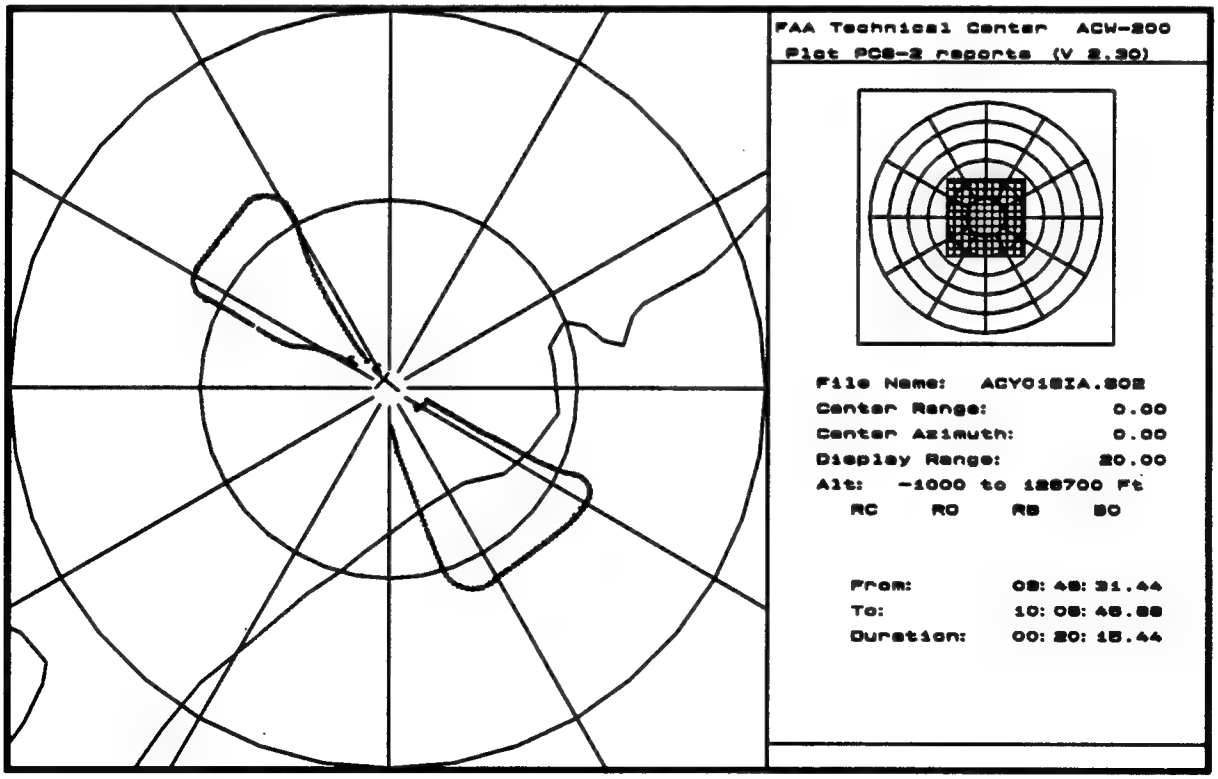

FIGURE 9.3-8. FIGURE EIGHT FLIGHT TEST SCENARIO

TABLE 9.3-1. DETECTION FLIGHT TEST DATA COLLECTED

	IRES	Demonstration 18 bit I/Q	ASR-9 DRI
RUN011	ACY011IA.REC	FLTEST1 FLTEST2	
RUN012	ACY012IA.REC		
RUN015	ACY015IA.REC	FLTEST6 FLTEST7	RUN015X.RAP
RUN016	ACY016IA.REC		RUN016X.RAP
RUN018	ACY018IA.REC		
RUN019	ACY019IA.REC		RUN019X.RAP

A percent detection histogram for RUN011 IRES data is shown in figure 9.3-9. Each bar in the chart shows the percent detection in a 1-mile range bin. The 80 percent detection line on the chart represents the specified ASR-9 detection performance (for a one square meter target). The shading of each bar in the chart indicates that more than eight samples were collected in that range bin. The data presented in the histogram was smoothed by averaging the percent detection over three range bins (i.e., the smoothed detection for range bin N is the average of the raw percent detections for range bins N-1, N, and N+1).

A tabular representation of the IRES data for RUN011 is shown in table A-1 in appendix A. The table shows the number of opportunities and hits. The raw and smoothed percent detections are also shown.

Analysis of IRES data from RUN011 shows poor detection. The percent detection crosses the 80 percent detection level at 47 nmi for the inbound legs and at a lesser range for the outbound legs. Later investigation into the poor detection revealed an interface problem between the demonstration receiver and the ASR-9 processor. The voltage levels of the I and Q data measured at the input to the processor were between logical 0 and logical 1 states. The problem was corrected and the flight test was repeated in RUN015.

It should be noted that data collected with the CRO recorder is 18-bit data whereas the ASR-9 MTD processor is a 12-bit processor. The interface of the demonstration receiver to the ASR-9 processor was accomplished by eliminating the most significant six bits of I and Q data in order to preserve system linearity. This introduced a limit to the dynamic range of the demonstration system. Therefore, the full capabilities of the demonstration system may not be seen in data collected at the output of the ASR-9. Poor performance as measured at the output of the radar during some of the tests may be due to the dynamic range reduction and should not be attributed solely to the demonstration equipment.

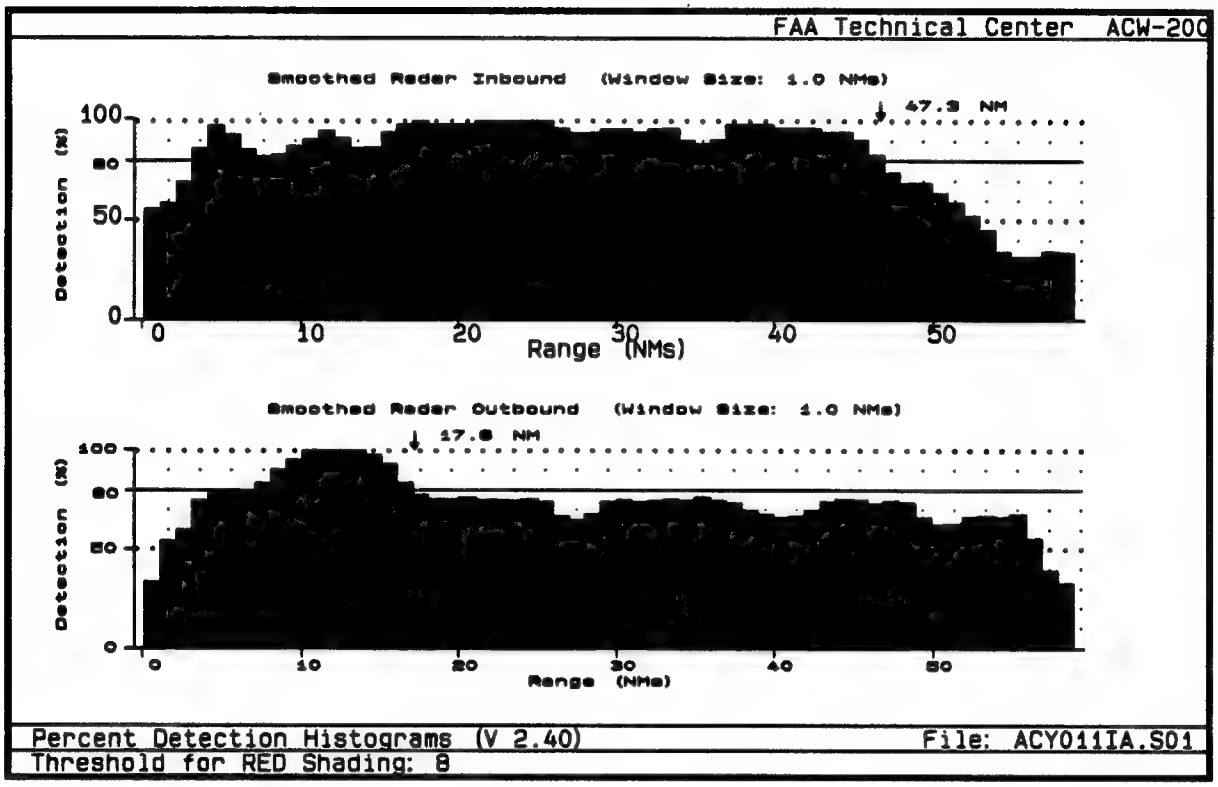

FIGURE 9.3-9. RUN011 - IRES PERCENT DETECTION

Eighteen-bit I and Q data were collected at the output of the demonstration receiver using the CRO data recorder. The power at each range cell was calculated and plotted as a function of range on the CRO computer. A peak detection process isolated the data that was above noise along each PRI. The signal amplitudes and range cell numbers were recorded. The data for the aircraft was then manually extracted by comparing the time of the recorded scan and the range of the return with the time and range of the beacon reports recorded with IRES.

The data collected for RUN011 with the demonstration recorder is contained in two files; FLTEST1 and FLTEST2. FLTEST1 contained 22 scans of data and FLTEST2 contained 42 scans of data. For each of the files, the record window range extended from range cells 300 to 900 and the azimuth window extended 32 PRIs centered on the 230° radial.

Filtered FLTEST1 and FLTEST2 data isolating the aircraft is shown in tables A-7 and A-8 in appendix A. The data shows the signal amplitudes and the range cell number for the test aircraft returns in each PRI. The reported beacon range and azimuth are included for each scan as a source of truth.

Those PRIs (of the 32 recorded PRIs in each scan) absent from the tables either contained returns from aircraft other than the test aircraft or had signal amplitudes in the noise. The noise level was approximately 12 dB. Due to the small azimuth extent of the record window, the aircraft often flew on the "edge" of the window. Therefore, some scans contained more data than others.

Each CRO recorded file began with scan 1. Data was collected on every other radar scan. Of the 22 scans of data in FLTEST1 and 42 scans of data in FLTEST2, the aircraft was in the record window (as compared to the beacon reports) for only those scans presented in the table.

RUN012 was flown on March 3, 1993, with the standard ASR-9 configuration. The Aero Commander flew the radial pattern shown in figure 9.3-7.

Data was recorded with IRES only for this test. The percent detection histogram for RUN012 is shown in figure 9.3-10. The outer range at which 80 percent detection is achieved is 59 nmi for the inbound legs and 56.7 nmi for the outbound legs. Figure 9.3-10 shows solid detection of the test aircraft beyond 55 nmi. A tabular form of the data is shown in table A-2.

RUN015 was flown on March 9, 1993, with the demonstration equipment installed. The Aero Commander flew the same radial pattern as in RUN011.

IRES percent detection data for RUN015 is shown in figure 9.3-11 and table A-3. Comparison of detection data in figure 9.3-11 with the data in figure 9.3-9 (RUN011) shows a marked improvement in outer range detection for RUN015; indicating that there was an interface problem during RUN011.

The detection data in figure 9.3-11 shows good outer range detection. There is, however, a drop in detection in the vicinity of the short-pulse/long-pulse transition. There are several possibilities for the lower detection rate as seen in data recorded at the output of the radar.

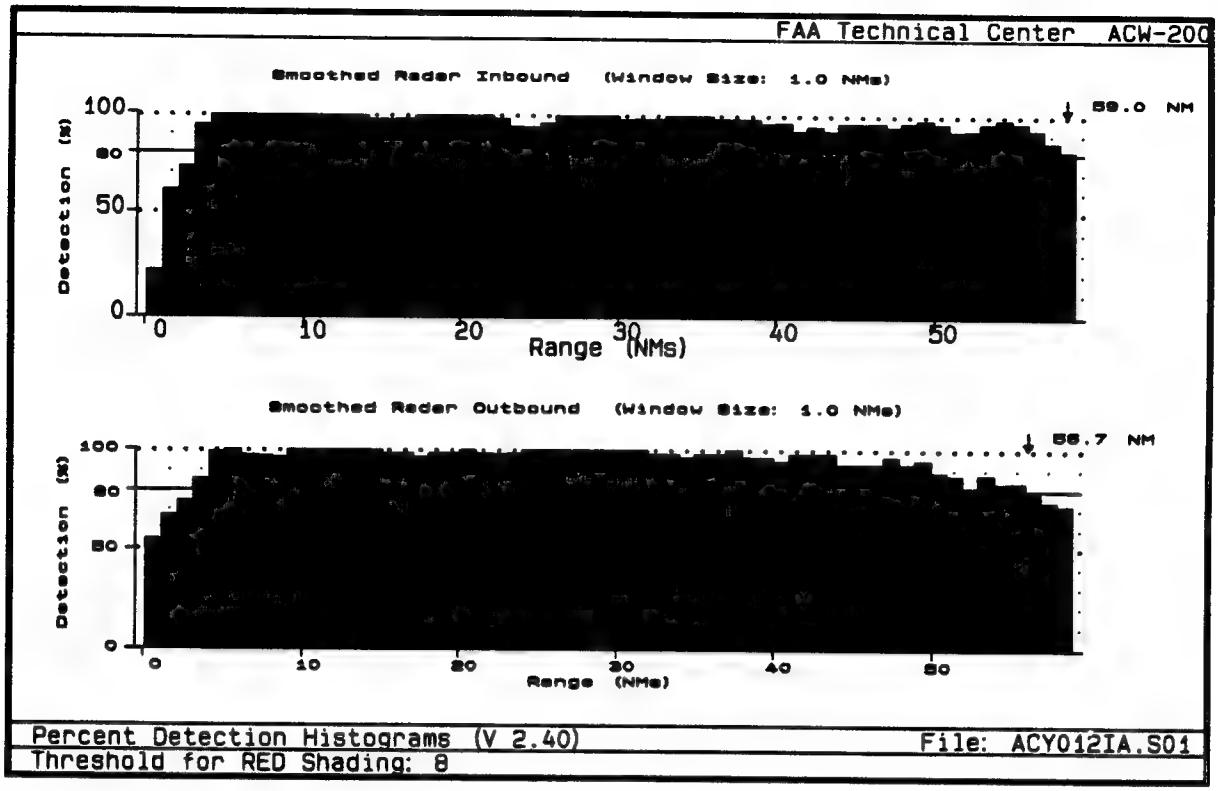

FIGURE 9.3-10. RUN012 - IRES PERCENT DETECTION

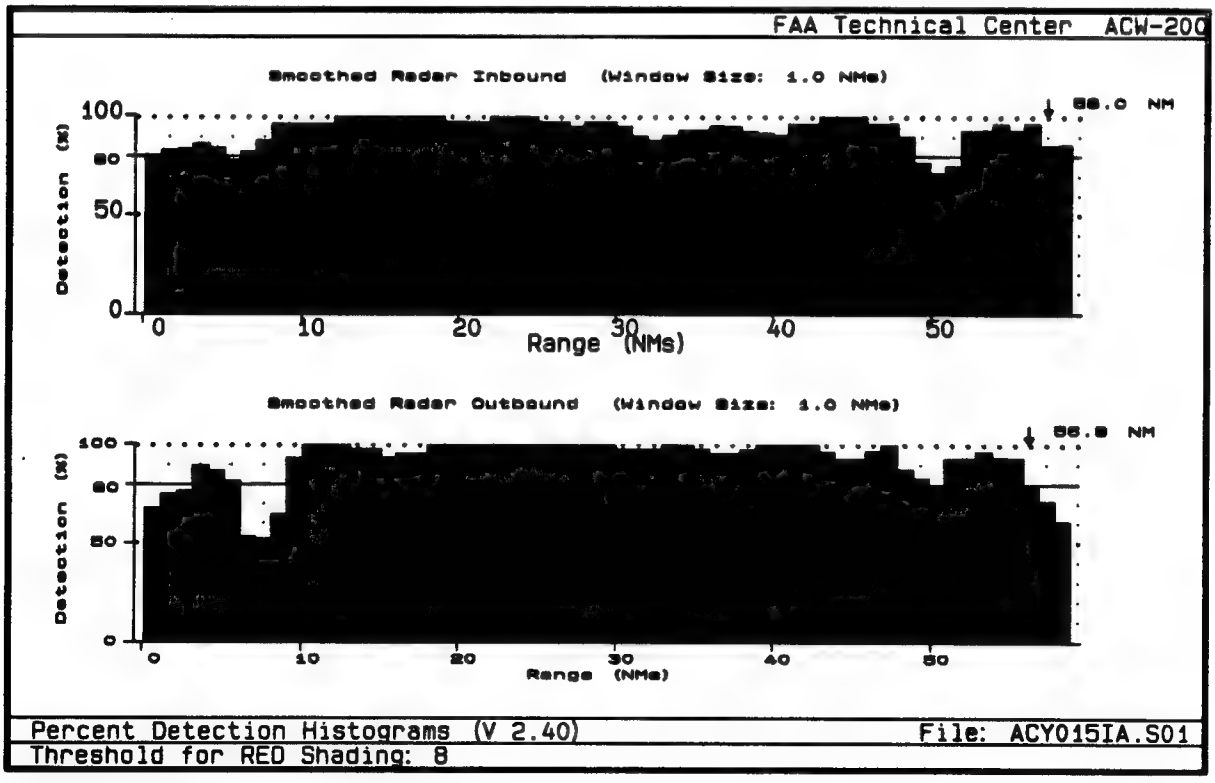

FIGURE 9.3-11. RUN015 - IRES PERCENT DETECTION

First, the ASR-9 CFAR process determines the mean level threshold for each range cell using the signal levels at neighboring range cells. The twelve range cells above (far range window) and below (near range window) the target cell in range are used to determine the threshold of the target cell. The two cells adjacent to the target cell are not used in the threshold determination. The range cell with the maximum signal in each range window, along with the two cells closest to it (neighbors) are eliminated from the threshold determination process. The threshold is taken from the greater of the average of the remaining nine far range window cells and the average of the nine near range window cells.

Since the long pulse has much more energy than the short pulse, the mean level thresholds for those cells close to the transition are set higher than needed for the short pulse and the returns from the short pulse are thresholded out. Since the CFAR windows extend 13 range cells on both sides of the target cell, the effects of the CFAR process on the loss of detection at the transition extend 13/16 nmi from the short-pulse/long-pulse transition range (7.94 nmi).

Another possibility for the drop in detection at the short-pulse/long-pulse transition shown in figure 9.3-11 is an artifact of the dynamic range limitation introduced when the 18-bit demonstration receiver is interfaced to the 12-bit ASR-9 processor. Figure 9.3-12 shows the percentage of all primitive reports recorded with the DRI for RUN015 which were flagged as saturated as a function of range. The data show peaks in the percent of saturated reports at the short-pulse/long-pulse transition range and at the beam crossover point (where differences in the low and high beam STC are noticed).

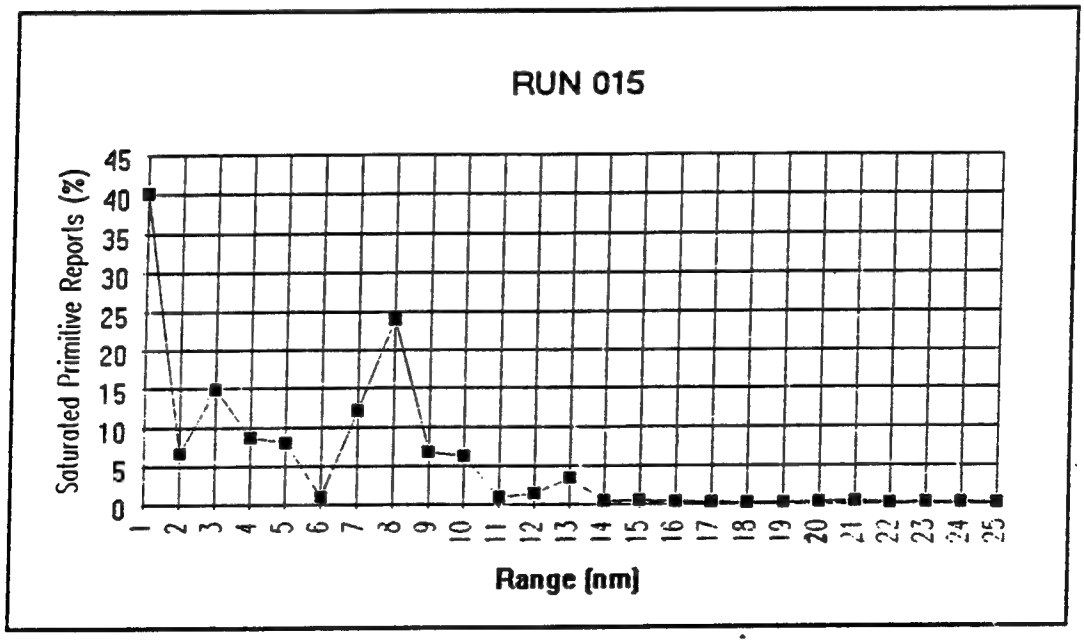

FIGURE 9.3-12. RUN015 - PERCENT SATURATED REPORTS VERSUS RANGE

The ASR-9 centroid algorithm used for these saturated returns may report the position of the target outside the IRES tracking window causing an apparent missed detection. Investigation of this possibility using raw, untracked IRES data showed no evidence of this centroiding effect.

Data was recorded at the digital recorder interface of the ASR-9 for RUN015 using the XRAP/personal computer interface. The data was converted to IRES format for analysis. The data for the aircraft was filtered and tracked as before. The report peak amplitudes versus the range for the test aircraft are plotted in figure 9.3-13. A theoretical $1/r^4$ shows the expected attenuation effects as a function of range. The curve is normalized at 60 nmi to the average of the reported amplitudes. The difference in the amplitudes of the short-pulse and long-pulse returns are evident in the figure.

The quality of the reports for the track are plotted versus the amplitude in figure 9.3-14. The ASR-9 defines quality as follows:

Quality 0 - CPI (almost always false alarms)
Quality 1 - two CPI reports of different types (both PRFs)
Quality 2 - two or more CPI reports (same PRFs)
Quality 3 - three of more CPIs and both PRFs

Quality 0 reports were filtered out of the file and are not included in figure 9.3-14. The plots show that the majority of the reports were quality 1 and 3; indicating detection on both PRFs.

Eighteen-bit I and Q data was collected for RUN015 at the output of the demonstration receiver using the CRO data recorder and is contained in files FLTEST6 and FLTEST7. FLTEST6 contained 166 scans of data and FLTEST7 contained 111 scans of data. For FLTEST6, the record window range extended from range cells 700 to 915 and the azimuth window extent was 76 PRIs centered on the 230° radial. For FLTEST7, the record window range extended from range cells 400 to 912 and the azimuth window extent was 32 PRIs centered on the 230° radial.

Filtered FLTEST6 and FLTEST7 data isolating the aircraft is shown in tables A9 and A10. The data shows the signal amplitudes and the range cell number for the test aircraft returns in each PRI. The reported beacon range and azimuth are included for each scan as a source of truth.

Those PRIs absent from the tables either contained returns from aircraft other than the test aircraft or had signal amplitudes in the noise. The noise level was approximately 12 dB. Due to the small azimuth extent of the record window, the aircraft often flew on the "edge" of the window. Therefore, some scans contained more data than others.

Each CRO recorded file began with scan 1. For the most part, data was collected on every other radar scan. Of the 166 scans of data in FLTEST6 and 111 scans of data in FLTEST7, the aircraft was in the record window (as compared to the beacon reports) for only those scans presented in the table.

RUN016 was flown on March 15, 1993, with the demonstration equipment installed. The figure eight pattern shown in figure 9.3-8 was flown at 17500 feet AGL. The test aircraft was a Beechcraft BE-200.

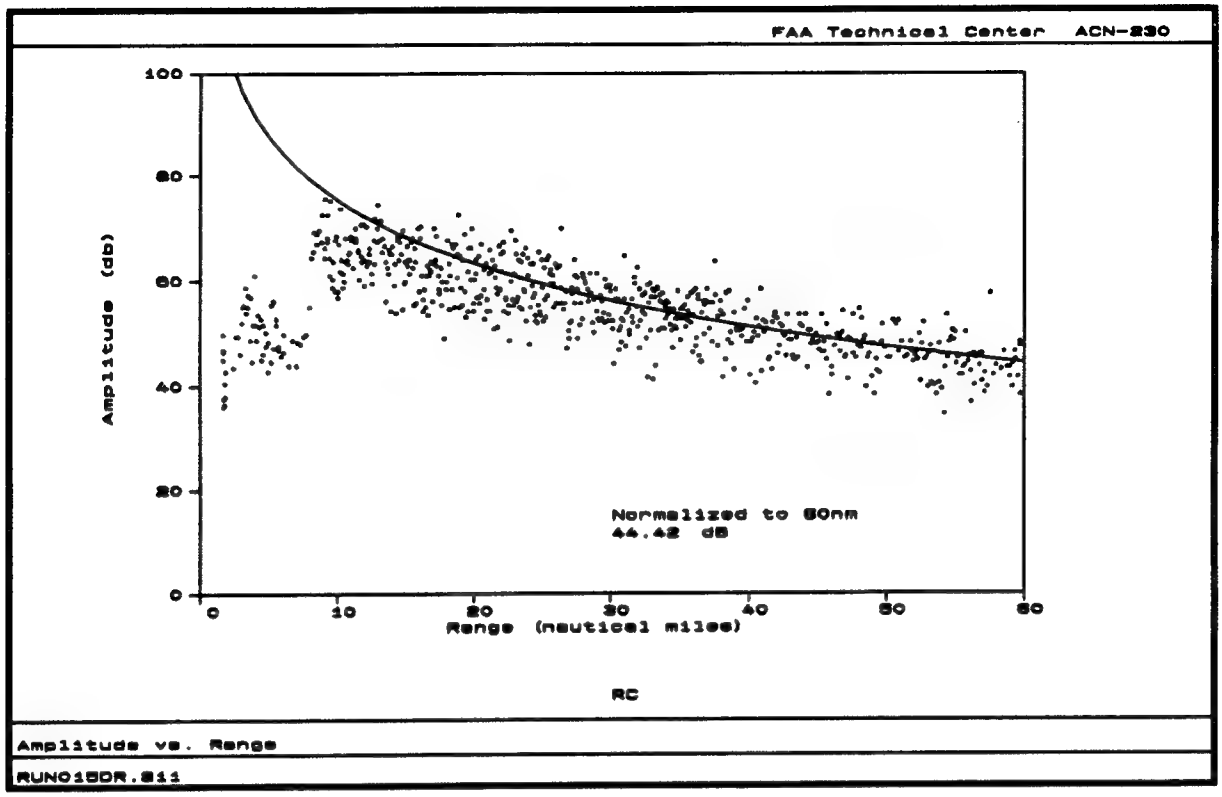

FIGURE 9.3-13. RUN015 - REPORT AMPLITUDES VERSUS RANGE

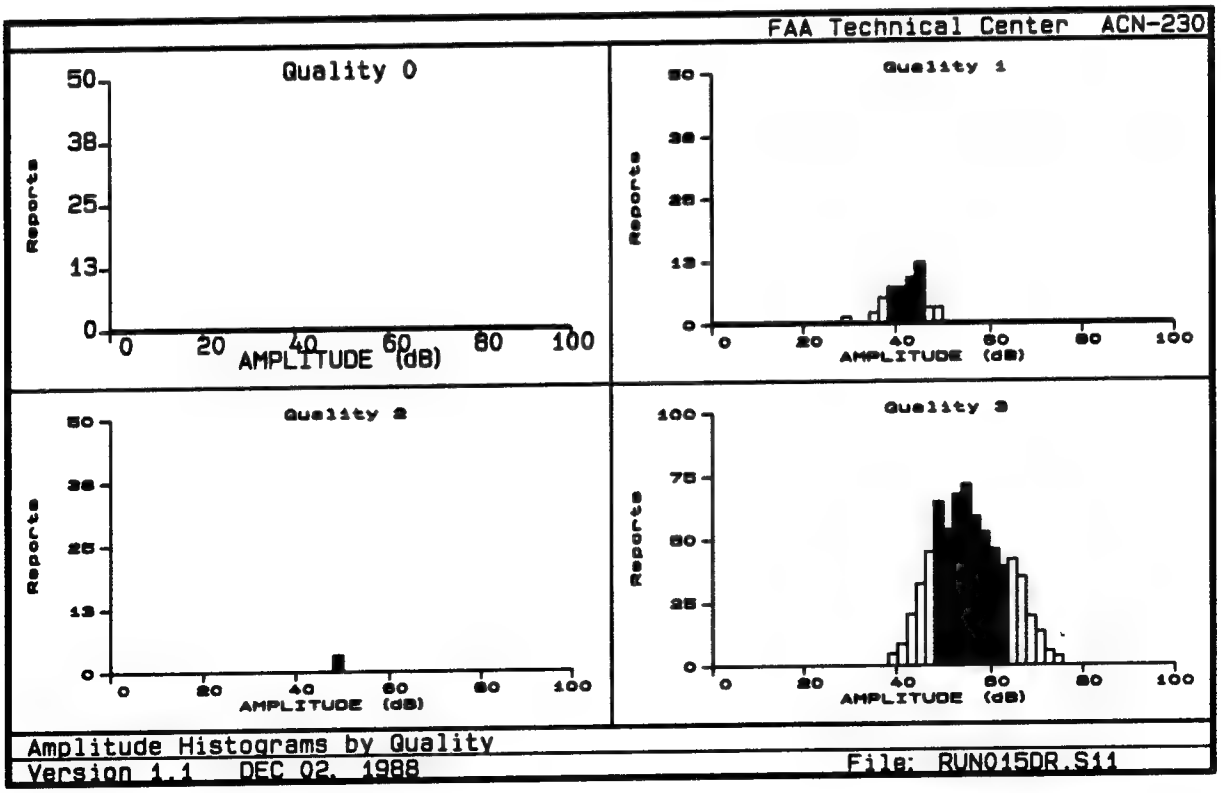

FIGURE 9.3-14. RUN015 - REPORT QUALITY DISTRIBUTION

IRES analysis of data recorded at the output of the ASR-9 is shown in figure 9.3-15. The poor detection shown in the figure appears to be the result of incompatibility of the demonstration system with the ASR-9 cosecant square antenna pattern.

Figure 9.3-16 shows the amplitude versus range plot for the test aircraft for RUN016. The $1/r^4$ curve is normalized to a lower value than for RUN015. This appears to be caused by a combination of two effects; (1) lower amplitude returns from the higher elevation flight test, and (2) a decrease in the average return amplitude due to differences in the flight scenarios (i.e., RUN015 contains more returns from the long pulse which would increase the normalization level).

Figure 9.3-17 again shows that the majority of reports were quality 1 and 3 reports, although there is an increase in the number of quality 2 reports when compared to RUN015 results.

The figure eight pattern was repeated for RUN018 at 9500 feet AGL with the Beechcraft BE-200. IRES data recorded at the radar output is shown in figure 9.3-18 and table A-5.

Figure 9.3-18 shows improved detection when compared with IRES data in RUN015 at the same altitude. The improved detection is most likely the result of the use of a larger cross section test aircraft coupled with an increased number of data samples due to flight pattern differences.

Comparison of the detection shown in figure 9.3-18 with that shown in figure 9.3-15 again shows the decrease in detection with increase in elevation.

The figure eight pattern was flown for RUN019 at 4500 ft AGL. IRES data recorded at the radar output is shown in figure 9.3-19 and table A-6. The percent detection shown in the figure is much improved compared to the data from higher elevations.

Figure 9.3-20 shows the report amplitude versus range plot for RUN019. The $1/r^4$ curve is normalized to 45.04 dB. Comparison of figure 9.3-20 with figure 9.3-16 shows the differences in report amplitudes with differences in the elevation of the flight scenarios. These differences in report amplitude are reflected in the percent detection differences between figure 9.3-19 and figure 9.3-15. Figure 9.3-21 shows that the majority of reports collected during RUN019 are quality 3 reports.

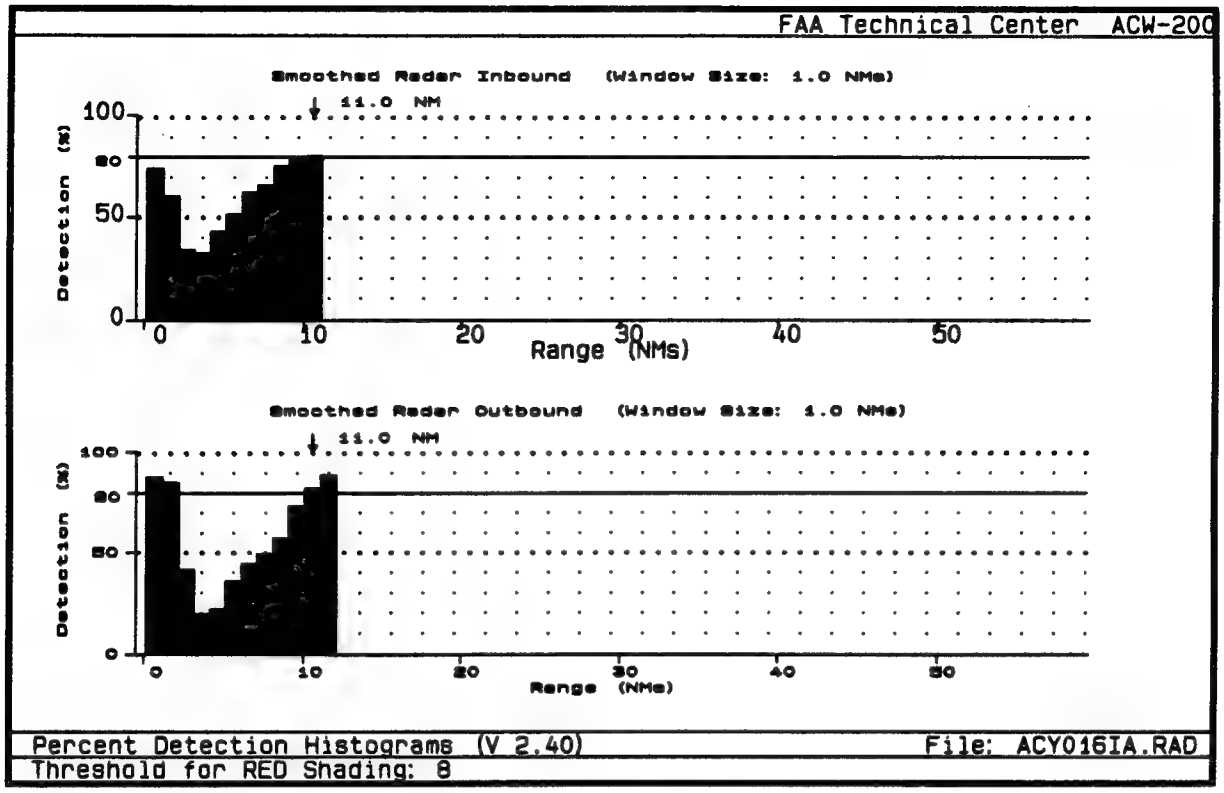

FIGURE 9.3-15. RUN016 - IRES PERCENT DETECTION

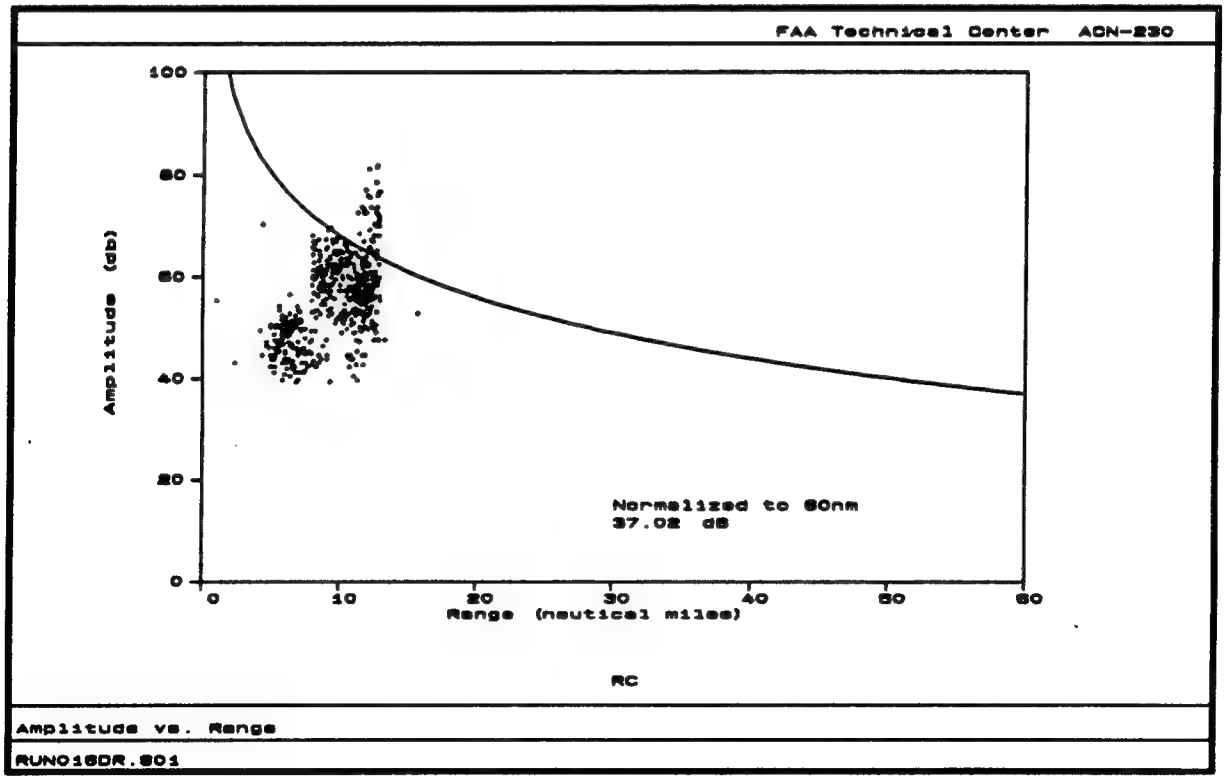

FIGURE 9.3-16. RUN016 - REPORT AMPLITUDES VERSUS RANGE

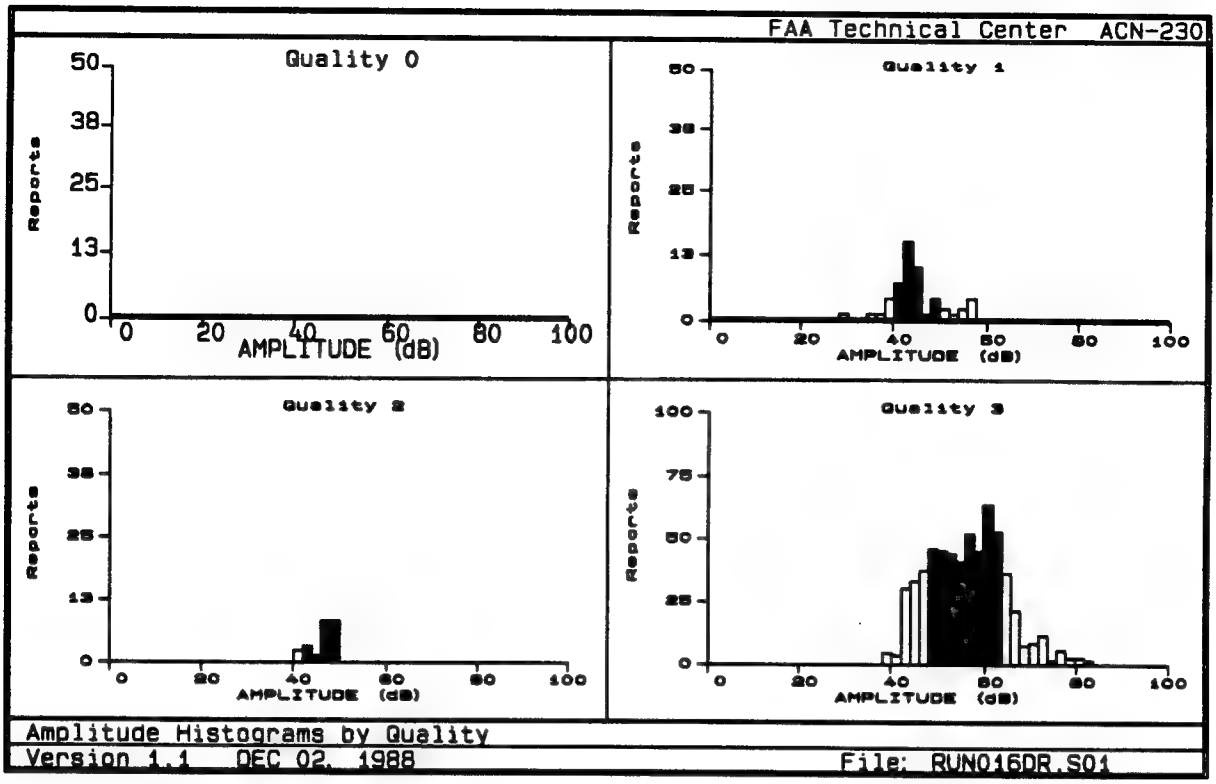

FIGURE 9.3-17. RUN016 - REPORT QUALITY DISTRIBUTION

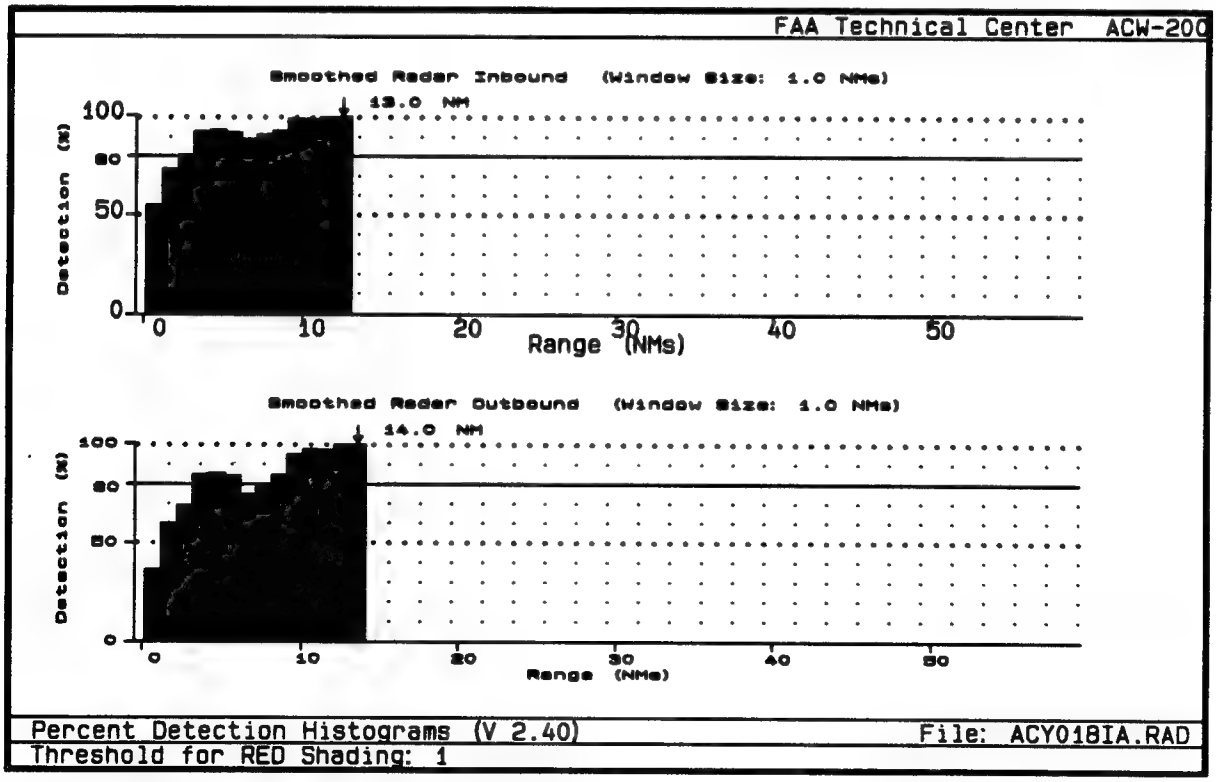

FIGURE 9.3-18. RUN018 - IRES PERCENT DETECTION

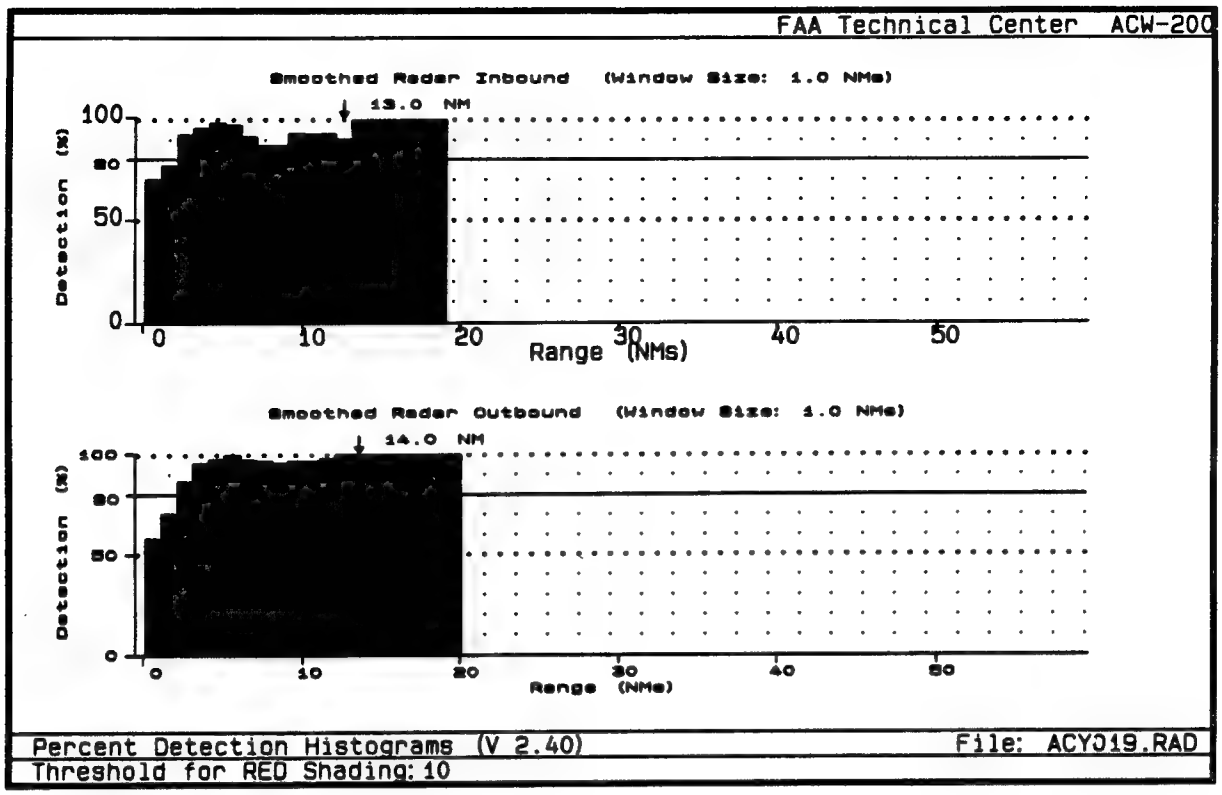

FIGURE 9.3-19. RUN019 - IRES PERCENT DETECTION

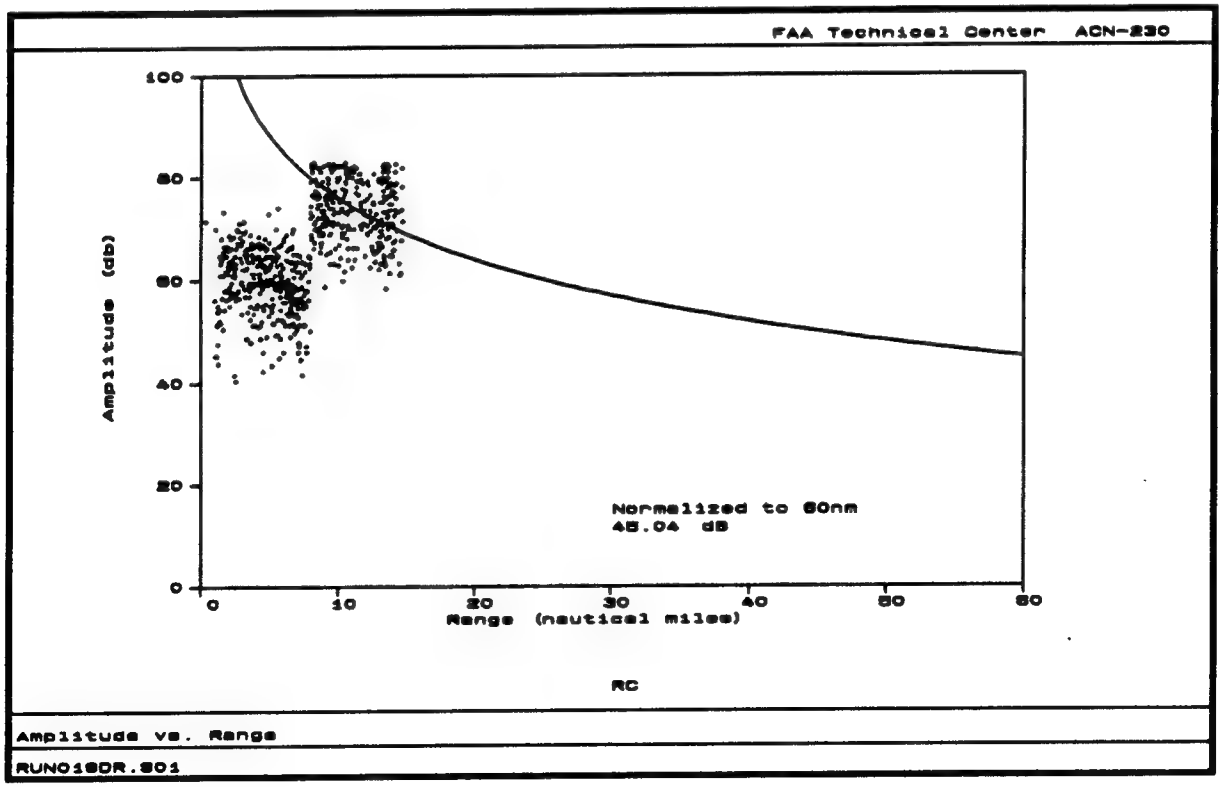

FIGURE 9.3-20. RUN019 - REPORT AMPLITUDES VERSUS RANGE

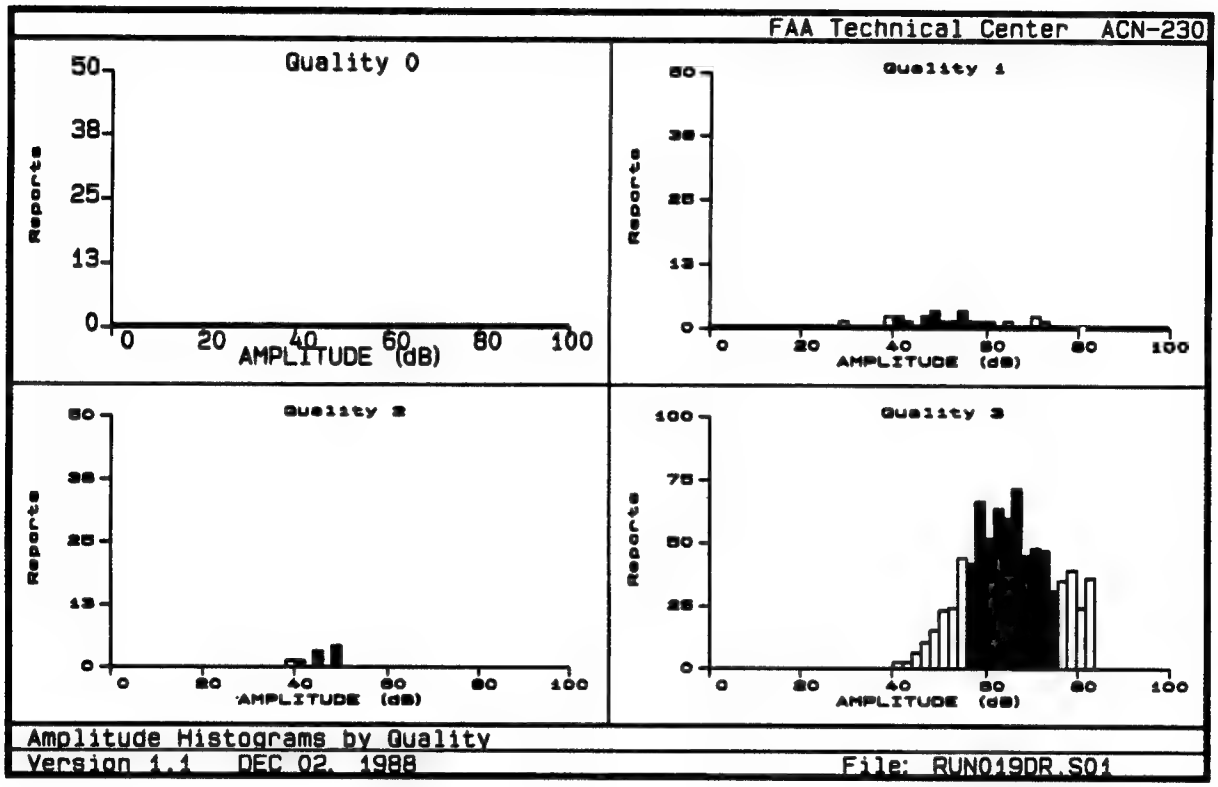

FIGURE 9.3-21. RUN019 - REPORT QUALITY DISTRIBUTION

9.4 RANGE RESOLUTION.

The purpose of the these tests was to measure the range resolution performance of the radar with the demonstration equipment installed. The effects of the pulse compressed waveform time sidelobes on the range resolution were measured.

Two range resolution flight tests were performed; RUN020 and RUN021. Resolution was determined using two dissimilar sized aircraft; a Beechcraft BE-200 and the Aero Commander. The aircraft flew tailchase patterns as shown in figure 9.4-1. The smaller aircraft (the Aero Commander) alternately overtook and dropped back from the larger aircraft in range in an attempt to generate enough range resolution data samples. The tests were performed between 30 and 50 nmi at approximately 230° azimuth at altitudes ranging from 9500 to 10500 feet AGL. The altitudes were not the same for each run due to the changing weather conditions (i.e., the planes had to fly above the clouds).

The beacon position of the two aircraft were used as a source of truth. In order to prevent garbling of the beacon replies from the two test aircraft, the aircraft replied to different modes of interrogation. The Beacon Interrogator (BI-5) was set up to interrogate with an interlace pattern of Mode 3/A and Mode B. The Aero Commander replied to Mode 3/A interrogations and the Beechcraft replied to Mode B interrogations.

Since the ASR-9 does not process Mode B replies, a pulse generator delayed the mode pair triggers from the BI-5 and regenerated the Mode B triggers as Mode 3/A. The two waveforms in the top of figure 9.4-2 represent the Mode 3/A and Mode B interrogations from the beacon interrogator. Mode 3/A pulses are separated by 8 μs. Mode B pulses are separated by 17 μs.

The two waveforms in the bottom of figure 9.4-2 are Mode 3/A triggers after delay and regeneration by the pulse generator. The pulse generator triggered on the P1 pulse and introduced a 19-μs delay to each mode pair trigger. The generator then output double pulses with the separation and characteristics of Mode 3/A.

Since the reply time from the aircraft is referenced to the P3 pulse in the range determination process, the use of the pulse generator in degarbling introduced a fixed offset in the beacon range. Since the aircraft codes were known at flight time, the range offset was subtracted from the beacon range during data analysis.

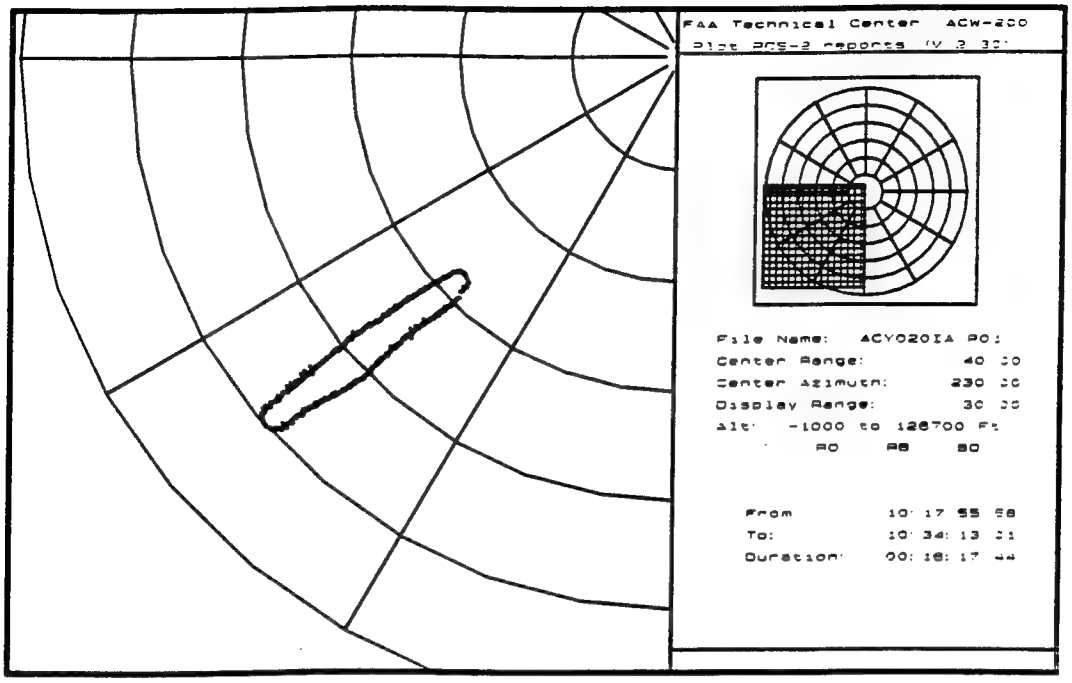

FIGURE 9.4-1. RANGE RESOLUTION FLIGHT TEST PATTERN

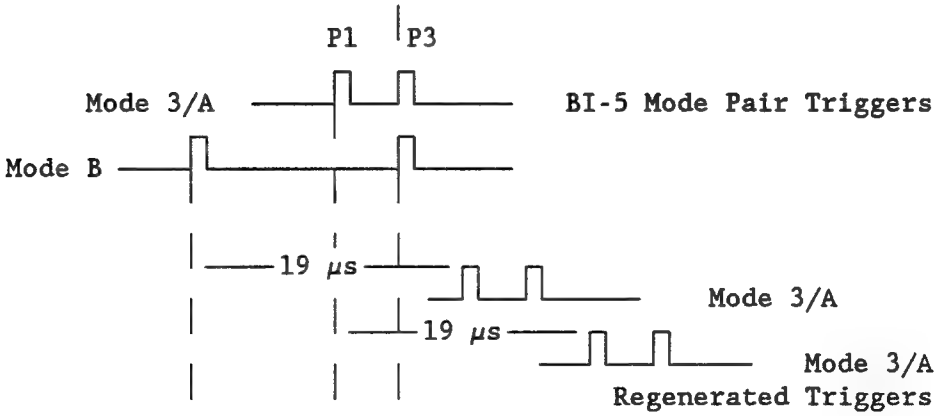

FIGURE 9.4-2. MODE PAIR TRIGGER REGENERATION

Several sources of error exist with the use of beacon reports as truth. Since the beacon range is measured by time reference to the lead edge of the P3 pulse, jitter in the P3 pulse may cause range ambiguities in the beacon system. The effect of P3 jitter is reduced in the ASR-9 beacon processor since the lead and trail edges of the pulse are used in the detection process.

There is also a small quantization error introduced to the measurement since the ASR-9 samples the beacon replies at a 85-ns rate. The jitter and quantization errors are considered negligible for the range resolution determination.

The range resolution data collected is shown in table 9.4-1. Data was recorded using IRES, the demonstration I/Q recorder and the ASR-9 digital recorder interface (DRI). However, data was not collected with the demonstration recorder for RUN020. Data was collected for each test using the demonstration 18-bit I/Q data recorder, however the recorder could collect data in only a small range-azimuth window and oftentimes the aircraft was not in the record window. Radar primitive data was collected with the ASR-9 digital recorder interface for runs 20 and 21.

TABLE 9.4-1. RANGE RESOLUTION FLIGHT TEST DATA COLLECTED

	IRES	Demonstration 18 bit I/Q	ASR-9 DRI
RUN020	ACY020IA.REC		RUN020X.RAP
RUN021	ACY021IA.REC	FLTEST60	RUN021X.RAP
		FLTEST61	
		FLTEST63	
		FLTEST64	
		FLTEST65	
		FLTEST66	
		FLTEST67	
		FLTEST68	

The results of the IRES data analysis are shown in figure 9.4-3. The figure shows the composite range resolution results for RUN020 and RUN021. The histogram on the left part of the figure shows the resolution as a function of range. The histogram on the right shows the number of data samples as a function of range. The error plot shows the mean difference in radar and beacon range as a function of range separation as well as the standard deviation.

The IRES resolution is a conditional probability based on the percent detection. The percent resolution calculation is as shown below. For the data presented in figure 9.4-3, the probability of radar splits was assumed to be zero and the percent of detection for each aircraft was set at 100 percent. This represents the worst possible resolution possibility. As different percent detections are used in the equation for each aircraft, the percent resolution is affected.

pct(res) = 100% * (p(two targets observed) - p(lead A/C

splits)pd(lead)[1-pd(trail)] - p(trail A/C splits)pd(trail)
[1-pd(lead)])/(pd(lead)pd(trail))

where:

pct(res) = percentage of resolution

p(two targets observed) = the measured probability of observing two reports

p(lead A/C splits) = the measured split probability for the lead aircraft

p(trail A/C splits) = the measured split probability for the trail aircraft

pd(lead) = the measured probability of detection for the lead aircraft

pd(trail) = measured probability of detection for the trail aircraft

Figure 9.4-3 shows that the largest number of samples were collected with the two aircraft within 5/64 nmi of each other. There were, however, a large number of samples (around 50 in each range bin) between 6/64 nmi and 10/64 nmi separation. The worst case percent resolution shows 80 percent resolution at 18/64 nmi.

Several factors affect the range resolution as determined from reports collected at the radar output. First, the ASR-9 resolution algorithms are matched to the ASR-9 pulse shape. The use of the long pulse with the standard ASR-9 algorithms may not produce optimum results.

The CFAR process described in the detection section of this report is incomplete. In addition to the near range and far range windows previously described, the ASR-9 CFAR process also uses a straddle window in threshold determination. The straddle window is centered on the target cell and contains 12 range cells (1/16 nmi). The introduction of the straddle window into the CFAR can potentially decrease the system range resolution (i.e., when the straddle window is active, resolution of two targets necessitates one target being outside the straddle window).

Disable and override variable site parameters in the ASR-9 are used to define areas where the three-window CFAR is disabled and the two-window CFAR is used for improved range resolution (i.e., parallel runway case). If the power level in the straddle window exceeds the levels in each of the other windows by the override Variable Site Parameter (VSP) amount, the three-window CFAR is overridden and the two-window CFAR is used.

The demonstration recorded data for the range resolution test is shown in table B-2 in appendix B. The data shows signal amplitudes of the collected data for each aircraft. The IRES beacon range and azimuth are shown for each aircraft as a source of truth.

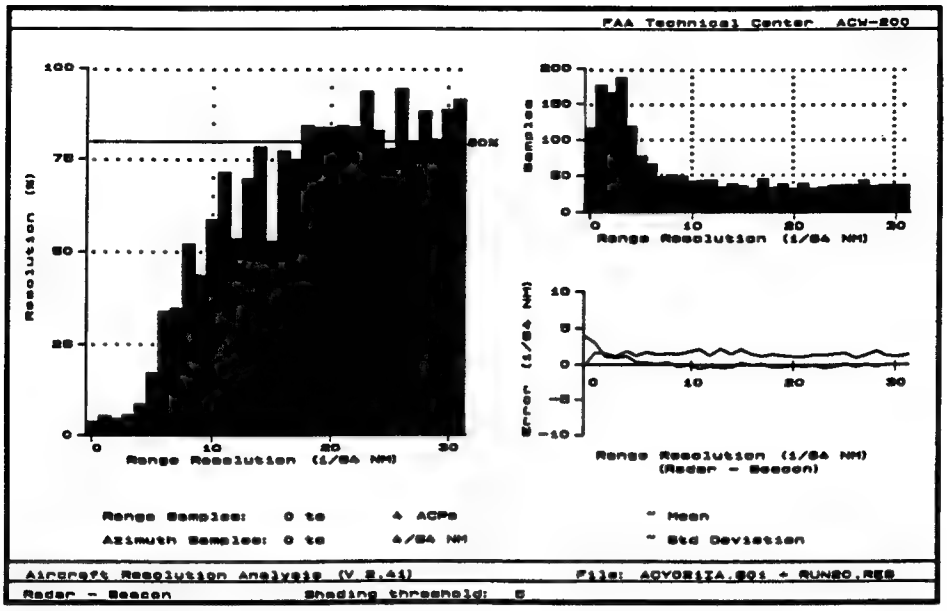

FIGURE 9.4-3. IRES PERCENT RESOLUTION

The record window set up for each file is shown in table 9.4-2. As was the case for the detection tests, the demonstration data recorder was limited in its ability to record the aircraft in the tailchase pattern. For Fltest68, both aircraft were out of the record window in azimuth for the entire record time. For Fltest64, the aircraft were out of the record window in range for the entire record time. For the remaining data files, the data shows that for much of the time the aircraft were flying "on the edge" of the record window. Those PRIs which have no radar returns, are not included in the tables. Fltest67 data were collected while the aircraft were turning. Therefore, there is a wide separation in azimuth relative to the data in other files.

TABLE 9.4-2. DEMONSTRATION RECORD WINDOWS

	Start Range (1/16 nmi)	Stop Range (1/16 nmi)	Start Azimuth (Degrees)	PRIs	Scans
Fltest60	400	660	223.59	38	1
Fltest61	400	660	223.59	38	1
Fltest63	400	660	229.00	38	1
Fltest64	400	660	229.00	63	19
Fltest65	400	660	229.00	64	15
Fltest66	400	560	220.78	102	17
Fltest67	400	560	220.78	102	28
Fltest68	720	880	220.78	102	26

The difference between the beacon range and azimuth for the two test aircraft for the scans in table B.2 in appendix B is plotted in figure 9.4-4. The figure shows a small number of opportunities for interesting range resolution data.

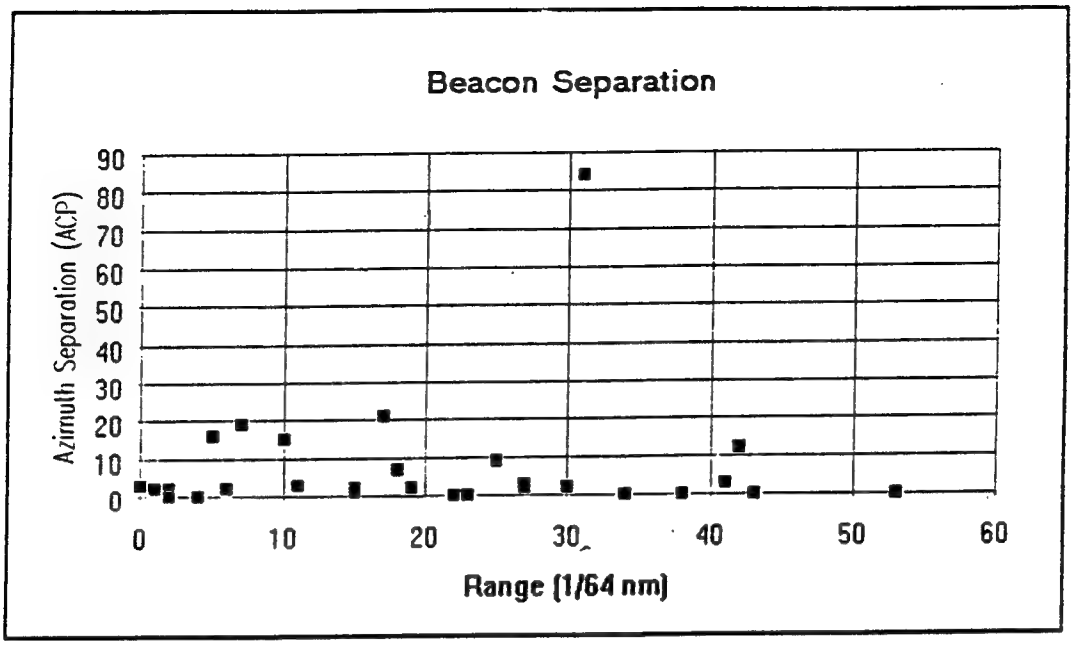

FIGURE 9.4-4. AIRCRAFT SEPARATION CORRESPONDING TO DEMONSTRATION DATA

9.5 FALSE ALARM ANALYSIS.

Data from RUN015 of the detection flight tests were analyzed for false alarms. There was a large number of radar correlated false alarms noticed on the maintenance display during the flight test with the demonstration equipment installed.

Figure 9.5-1 shows 30 scans of IRES recorded data which was filtered to contain only radar correlated reports. The figure shows a large number of false alarms particularly at the short-pulse/long-pulse transition.

The data was filtered to remove all radar only reports, sorted in range-azimuth order and tracked using an alpha beta tracker in IRES. The tracks generated were then passed through a track qualifier. The track qualifier contains user defined criteria (i.e., values for track age, aircraft speed, etc.) used in "true track" and "false track" determination. The percentage of true tracks was determined and a statistical base was developed.

The results of the analysis indicated that 48 percent of all radar correlated reports, recorded at the output of the ASR-9 processor, were false reports. Comparison of the IRES false alarm data with raw, unfiltered I and Q data from the demonstration recorder failed to show any correlation between the two data sets.

The false reports recorded at the output of the radar are largely due to the interface problems between the demonstration system and the ASR-9 processor and the incompatibility of the ASR-9 algorithms and the dual pulse waveform. The false alarm data is included in the report to show the reader the state of the interface. A true assessment of the false alarm performance of the demonstration system should be made with a radar fully compatible with and optimized to the demonstration transmitter and receiver.

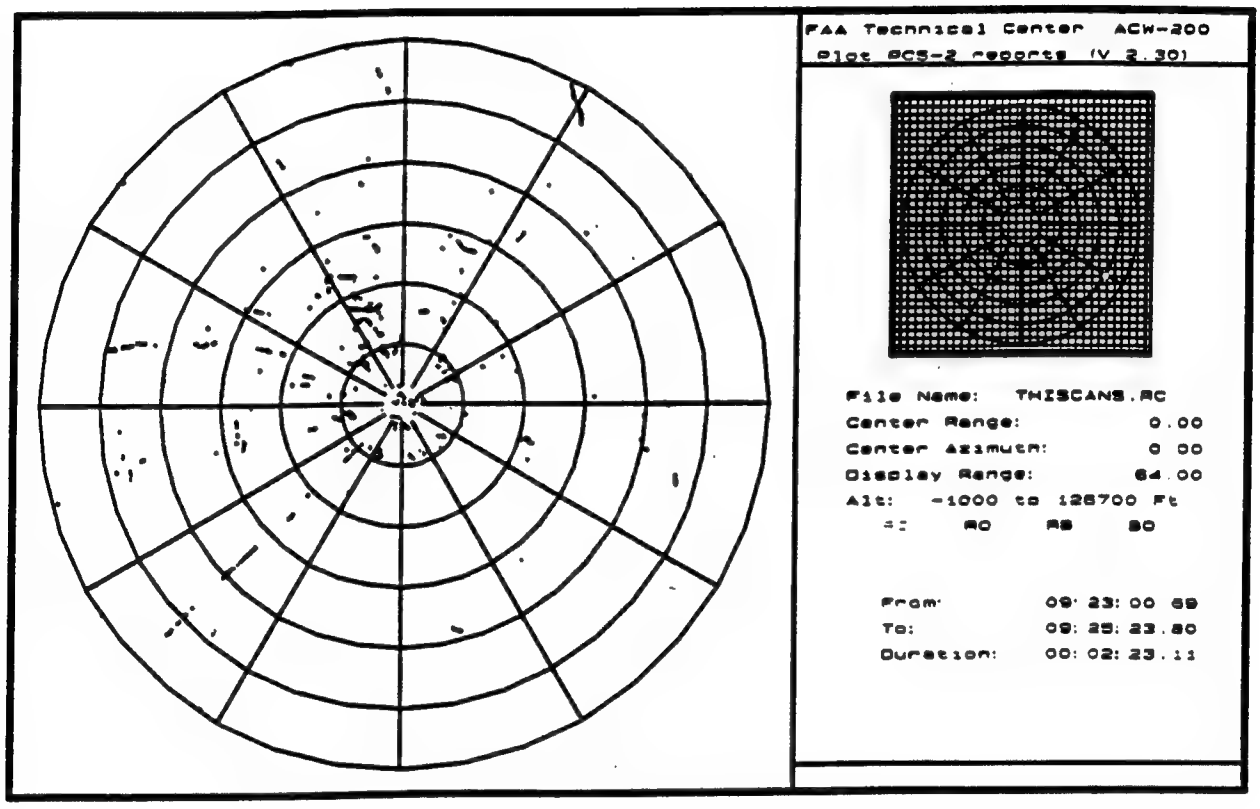

FIGURE 9.5-1. RUN015 - RADAR CORRELATED FALSE ALARMS (THIRTY SCANS)

10. SUMMARY OF RESULTS.

Table 10-1 summarizes the essential technical characteristics of the demonstration system. Table 10-2 summarizes the results of the detection flight tests.

TABLE 10-1. ESSENTIAL TECHNICAL CHARACTERISTICS

Parameter	Measured Value	Notes
Output Power	19 kW short pulse 22 kW long pulse	
Pulse Widths	.85 μs short pulse 74 μs long pulse	
Output Power Degradation	< 0.5 dB with two failed RF output modules	
Receiver Noise Figure	1.46 dB	
Receiver Dynamic Range	78.6 dB long pulse 61.8 dB short pulse	MDS to approx. 1 dB compression.
I and Q Image Rejection	Average ~ 60 dB	
Time Sidelobes	-55 to -51 dB peak	At doppler shifts up to the equivalent of a 130 m/sec target speed, with or without delay, with transmitter compensation, no STC. Independent of cold module swaps.
System Stability	61 to 62 dB	Field measurement with or without pulse stagger; pulse stagger requires pulse group amplitude compensation. (This figure does not include the gain associated with MTI Stability)

TABLE 10-2. SUMMARY OF IRES DETECTION EVALUATION

Flight No. Config: Aircraft: Scenario: Results:	RUN011 ASR-9 with demonstration equipment installed AC680E Aerocommander Radials from 0 to 60 nmi at 230°, 9500 ft AGL Overall poor detection. The cause of poor detection was traced to an interface problem between the demonstration receiver and the ASR-9 post-processor. The test was repeated in RUN015.
Flight No. Config: Aircraft: Scenario: Results:	RUN012 Standard ASR-9 (klystron) AC680E Aerocommander Radials from 0 to 60 nmi at 230°, 9500 ft AGL Overall good detection.
Flight No. Config: Aircraft: Scenario: Results:	RUN015 ASR-9 with demonstration equipment installed AC680E Aerocommander Radials from 0 to 60 nmi at 230°, 9500 ft AGL Good outer range detection. A hole in the coverage area at the short/long pulse transition may have been due to a combination of incompatibility with the ASR-9 processor and antenna pattern effects.
Flight No. Config: Aircraft: Scenario: Results:	RUN016 ASR-9 with demonstration equipment installed Beechcraft BE-200 Figure Eight Pattern from 0 to 15 nmi at 17500 ft AG Poor detection. The poor detection was most likely the result of incompatibility of the demonstration system with the cosecant squared beam pattern of the ASR-9. The pattern was chosen with a higher peak pulse in mind.
Flight No. Config: Aircraft: Scenario: Results:	RUN018 ASR-9 with demonstration equipment installed Beechcraft BE-200 Figure Eight Pattern from 0 to 15 nmi at 9500 ft AGL Better detection than in RUN016.
Flight No. Config: Aircraft: Scenario: Results:	RUN019 ASR-9 with demonstration equipment installed Beechcraft BE-200 Figure Eight Pattern from 0 to 15 nmi at 4500 ft AGL Good detection. The aircraft flew close to the peak of the beam at short range.

11. CONCLUSIONS AND RECOMMENDATIONS.

The ITT Gilfillan/Thomson-CSF solid-state radar system has impressive stability and time sidelobe performance. The field tests show an instability residue capability nearly an order of magnitude better than is claimed in current Federal Aviation Administration (FAA) radar systems. However, to take full advantage of this improved performance, the radar signal processor must remove the deterministic effects of the transmitter's thermal time constants during staggered pulse repetition frequency (PRF) operation.

The very low-time sidelobe performance measured during the demonstration shows much promise for target and weather detection without range smearing or other undesired artifacts from the compression process. First-order simulations of weather detection using a Thomson-CSF-like compressed waveform have shown that these low sidelobe levels, if maintained for a complex extended target, can provide adequate weather detection. However, a doppler-varying high-reflectivity gradient weather event (like a thunderstorm cell) could cause smeared responses due to the radar's integrated sidelobe levels. In addition, at close ranges (where airport runways are located), the short-pulse waveform may not have enough energy to detect low-reflectivity events such as gust fronts or dry microbursts. No weather data addressing these issues were taken during the FAA Technical Center demonstration. In addition, the radar signal processor must compensate for the (deterministic) staggered PRF step phase changes in order to maintain radar waveform performance across pulse repetition intervals (PRI).

Although the sidelobe levels measured during the demonstration were low, range resolution test results were inconclusive because of a lack of flight test samples at the range separation of interest. Most of the data was collected at the output of the radar. Therefore, it is difficult to distinguish the effects of the Airport Surveillance Radar, Model 9 (ASR-9) processor on the resolution performance.

As expected, detection at far range is adequate since sufficient energy is transmitted in the long pulse. Detection at higher altitudes, in close, is still in question. Theoretically, the short pulse should be able to provide enough energy, however, the ASR-9 cosecant squared beam pattern was not designed with the lower peak power of the short pulse in mind. A more suitable beam pattern should be selected for use with the demonstration system. The detection at the short-pulse/long-pulse transition as measured at the output of the radar was largely influenced by the ASR-9 processor. New processor algorithms, customized to the dual pulse waveform must be developed to maximize detection while maintaining a low false alarm rate. Also, the STC curve and the range for the short-pulse/long-pulse transition must be carefully selected to complement these algorithms.

The transmitter maintainability demonstration showed that the solid-state transmitter is much more maintainable than the conventional tube transmitters. The time needed to replace modules is minimal. Also, the graceful degradation of transmitter performance when a limited number of modules fail is an advantage over tube-based transmitters.

The FAA Technical Center ASR-9 radio frequency and processor hardware were not optimum for a complete demonstration of the solid-state radar's performance capabilities. As mentioned above, more thorough demonstration, test, and analysis require optimized, independent high/low-beam switching, independent STCs for the two waveform channels, and much more extensive, high dynamic range data recording and real-time display capabilities. From the very limited data available from the FAA Technical Center demonstration, however, the radar's raw target detection capability appears to match its predicted performance.

The FAA Technical Center solid-state radar demonstration marks a promising milestone in advancing air traffic control (ATC) radar technology. Serious questions remain, however, concerning the new technology's performance in severe and low-reflectivity weather, in extended clutter, and in a real-world interference environment. In addition, algorithms for optimization of the radar hardware configuration, the STC, the constant false alarm rate (CFAR), and transmitter thermal effects compensation all need to be developed and tested. The recommended path for such testing and development is a combination of detailed simulation, extensive hardware-in-the-loop testing, and stressing field measurement with weather and target truthing and thorough instrumentation. Following such a set of recommendations will ensure that solid-state technology feeds into Terminal Area Surveillance System (TASS) or other radar procurements with minimum technological risk, while maximizing the potential maintenance and performance benefits offered by solid-state radar.

12. ACRONYMS AND ABBREVIATIONS.

AC	alternating current
AGL	Above Ground Level
APD	Amplitude/Phase Detection
ARSR	Air Route Surveillance Radar
ASR	Airport Surveillance Radar
ATC	Air Traffic Control
BW	Bandwidth
CFAR	Constant False Alarm Rate
CPI	Coherent Processing Interval
CRDA	Cooperative Research and Development Agreement
CRO	Cooperative Research Organization
CW	Continuous Wave
dB	decibel
dBc	decibel referenced to the carrier
dBi	decibel referenced to an isotropic source
dBm	decibel referenced to 1 milliwatt
dBq	decibel referenced to 1 quantum of noise
dBw	decibel referenced to 1 watt
dc	direct current
DPC	Digital Pulse Compression
DRI	Digital Recorder Interface
FAA	Federal Aviation Administration
FFT	Fast Fourier Transform
GHz	GigaHertz
I	Inphase
IF	Intermediate Frequency
IRES	Integrated Radar Evaluation System
LED	Light Emitting Diode
LNA	Low Noise Amplifier
LO	Local Oscillator
LP	Long Pulse
MDS	Minimum Discernible Signal
MS	meters per second
MTD	Moving Target Detection
MTI	Moving Target Indicator
MTS	Moving Target Simulator
MW	megawatt
NF	Noise figure
nmi	nautical mile
ns	nanosecond
NTIA	National Telecommunications and Information Administration
PRF	Pulse Repetition Frequency
PRI	Pulse Repetition Interval
Q	Quadrature
RC	Range Cell
RCS	Radar Cross Section
RF	Radio Frequency
RMS	Route Mean Square
RSEC	Radio Spectrum Emissions Criteria

SP	Short Pulse
STC	Sensitivity Time Control
STDV	Standard Deviation
TASS	Terminal Area Surveillance System
TCSF	Thomson-CSF
Vac	Volts (AC)
VSP	Variable Site Parameter
WSR	Weather Surveillance Radar

APPENDIX A

DETECTION

TABLE A-1. RUN011 - IRES DETECTION DATA (DEMO EQUIPMENT) RADIALS AT 230 DEGREES AZIMUTH; 9500 FT ALTITUDE; 0-60 NM

	Inbound				Outbound			
Range (NM)	Opp	Hits	Raw %	Smooth %	Opp	Hits	Raw %	Smooth %
0	16	13	81	0	1	0	0	0
1	27	14	52	55	6	5	83	33
2	40	19	48	58	20	4	20	54
3	41	30	73	69	37	25	68	60
4	30	28	93	86	28	22	79	75
5	21	21	100	97	14	12	86	79
6	27	27	100	93	15	11	73	80
7	23	18	78	86	15	12	80	79
8	26	20	77	82	13	11	85	84
9	24	22	92	83	15	13	87	90
10	21	17	81	88	14	14	100	95
11	19	17	89	91	13	13	100	100
12	24	24	100	95	14	14	100	100
13	17	16	94	91	14	14	100	100
14	17	13	76	87	14	14	100	100
15	18	16	89	87	14	14	100	98
16	18	17	94	94	15	14	93	93
17	16	16	100	98	14	12	86	84
18	19	19	100	100	20	15	75	78
19	16	16	100	98	20	15	75	75
20	19	18	95	98	17	13	76	75
21	16	16	100	98	20	15	75	76
22	17	17	100	100	18	14	78	75
23	17	17	100	100	18	13	72	75
24	17	17	100	100	20	15	75	75
25	15	15	100	100	17	13	76	75
26	18	18	100	100	20	15	75	74
27	17	17	100	96	17	12	71	67
28	17	15	88	94	20	11	55	65
29	16	15	94	94	17	12	71	68
30	17	17	100	96	19	15	79	74
31	17	16	94	96	18	13	72	75
32	16	15	94	94	19	14	74	74
33	18	17	94	96	17	13	76	75
34	16	16	100	96	19	14	74	75
35	17	16	94	90	17	13	76	75
36	17	13	76	88	19	14	74	76
37	18	17	94	90	19	15	79	75
38	16	16	100	98	17	12	71	73
39	17	17	100	98	20	14	70	70
40	18	17	94	98	16	11	69	68
41	16	16	100	96	20	13	65	66
42	17	16	94	96	17	11	65	67
43	18	17	94	96	26	18	69	70

TABLE A-1. RUN011 - IRES DETECTION DATA (DEMO EQUIPMENT RADIALS AT 230 DEGREES AZIMUTH; 9500 FT ALTITUDE; 0-60 NM (Continued)

	Inbound				Outbound			
Range (NM)	Opp	Hits	Raw %	Smooth %	Opp	Hits	Raw %	Smooth %
44	17	17	100	94	23	17	74	74
45	16	14	88	94	20	16	80	75
46	18	17	94	90	22	16	73	75
47	17	15	88	83	22	16	73	73
48	17	11	65	74	23	17	74	74
49	16	11	69	69	17	13	76	73
50	18	13	72	69	20	14	70	66
51	17	11	65	63	16	8	50	63
52	17	9	53	59	20	13	65	63
53	17	10	59	52	18	13	72	66
54	16	7	44	45	18	11	61	67
55	18	6	33	34	18	12	67	66
56	16	4	25	31	20	14	70	67
57	17	6	35	31	17	11	65	55
58	18	6	33	34	19	6	32	39
59	15	5	33	33	20	5	25	33
60	0	0	0	0	7	4	57	0

TABLE A-2. RUN012 - IRES DETECTION DATA (STANDARD ASR-9) RADIALS AT 230 DEGREES AZIMUTH; 9500 FT ALTITUDE; 0-60 NM

	Inbound				Outbound			
Range (NM)	Opp	Hits	Raw %	Smooth %	Opp	Hits	Raw %	Smooth %
0	7	0	0	0	3	1	33	0
1	9	4	44	21	14	11	79	55
2	26	5	19	61	23	10	43	67
3	44	39	89	73	66	48	73	74
4	25	25	100	95	36	35	97	86
5	26	26	100	100	30	30	100	99
6	27	27	100	100	25	25	100	100
7	23	23	100	100	27	27	100	97
8	17	17	100	100	20	18	90	97
9	18	18	100	100	19	19	100	97
10	16	16	100	100	19	19	100	100
11	16	16	100	100	19	19	100	100
12	18	18	100	100	19	19	100	100
13	16	16	100	100	20	20	100	100
14	17	17	100	100	19	19	100	100
15	16	16	100	98	18	18	100	100
16	16	15	94	98	20	20	100	98
17	17	17	100	98	18	17	94	98
18	18	18	100	100	19	19	100	96
19	15	15	100	100	19	18	95	98
20	17	17	100	100	19	19	100	98
21	16	16	100	100	19	19	100	100
22	17	17	100	100	18	18	100	98
23	16	16	100	98	20	19	95	98
24	17	16	94	94	17	17	100	98
25	16	14	88	94	19	19	100	100
26	17	17	100	96	17	17	100	100
27	16	16	100	100	19	19	100	100
28	17	17	100	100	17	17	100	100
29	16	16	100	100	18	18	100	100
30	17	17	100	100	17	17	100	100
31	16	16	100	98	19	19	100	100
32	16	15	94	98	17	17	100	100
33	19	19	100	98	18	18	100	98
34	17	17	100	100	18	17	94	98
35	16	16	100	100	18	18	100	96
36	16	16	100	100	18	17	94	98
37	16	16	100	98	18	18	100	98
38	18	17	94	98	17	17	100	100
39	16	16	100	98	19	19	100	96
40	18	18	100	96	17	15	88	96

TABLE A-2. RUN012 - IRES DETECTION DATA (STANDARD ASR-9) RADIALS AT 230 DEGREES AZIMUTH; 9500 FT ALTITUDE; 0-60 NM (Continued)

	Inbound				Outbound			
Range (NM)	Opp	Hits	Raw %	Smooth %	Opp	Hits	Raw %	Smooth %
41	16	14	88	96	19	19	100	94
42	17	17	100	92	18	17	94	98
43	16	14	88	94	18	18	100	98
44	18	17	94	92	17	17	100	98
45	16	15	94	96	19	18	95	93
46	16	16	100	96	19	16	84	93
47	17	16	94	96	17	17	100	93
48	18	17	94	94	19	18	95	96
49	17	16	94	96	17	16	94	93
50	16	16	100	98	19	17	89	95
51	16	16	100	96	19	19	100	89
52	18	16	89	92	16	12	75	87
53	16	14	88	92	20	17	85	81
54	18	18	100	96	17	14	82	88
55	16	16	100	98	19	18	95	83
56	20	19	95	96	18	13	72	84
57	16	15	94	93	18	15	83	78
58	19	17	89	86	19	15	79	74
59	15	11	73	82	17	10	59	72
60	4	3	75	0	14	11	79	0

TABLE A-3. RUN015 - IRES DETECTION DATA (DEMO EQUIPMENT) RADIALS AT 230 DEGREES AZIMUTH; 9500 FT ALTITUDE; 0-60 NM

	Inbound				Outbound			
Range (NM)	Opp	Hits	Raw %	Smooth %	Opp	Hits	Raw %	Smooth %
0	23	17	74	0	1	0	0	0
1	31	27	87	81	10	7	70	68
2	90	72	80	83	42	29	69	75
3	28	25	89	84	20	18	90	77
4	24	22	92	86	19	15	79	89
5	21	16	76	84	18	18	100	87
6	19	16	84	78	16	13	81	82
7	19	14	74	82	15	9	60	53
8	19	17	89	88	18	4	22	52
9	20	20	100	97	15	12	80	65
10	19	19	100	97	15	15	100	93
11	20	18	90	97	15	15	100	100
12	21	21	100	97	18	18	100	100
13	19	19	100	100	15	15	100	100
14	21	21	100	100	15	15	100	98
15	19	19	100	100	17	16	94	98
16	21	21	100	100	15	15	100	94
17	19	19	100	100	15	13	87	96
18	15	15	100	100	15	15	100	96
19	14	14	100	100	15	15	100	100
20	15	15	100	98	17	17	100	100
21	13	12	92	98	15	15	100	100
22	15	15	100	98	16	16	100	100
23	13	13	100	100	15	15	100	100
24	15	15	100	100	16	16	100	100
25	13	13	100	100	15	15	100	100
26	14	14	100	98	16	16	100	100
27	14	13	93	98	15	15	100	100
28	14	14	100	95	16	16	100	100
29	14	13	93	98	15	15	100	100
30	14	14	100	98	16	16	100	100
31	14	14	100	95	15	15	100	98
32	14	12	86	90	17	16	94	98
33	13	11	85	88	14	14	100	98
34	14	13	93	90	16	16	100	100
35	15	14	93	93	17	17	100	100
36	15	14	93	93	15	15	100	98
37	15	14	93	95	15	14	93	96
38	14	14	100	95	16	15	94	96
39	14	13	93	93	15	15	100	98

TABLE A-3. RUN015 - IRES DETECTION DATA (DEMO EQUIPMENT) RADIALS AT 230 DEGREES AZIMUTH; 9500 FT ALTITUDE; 0-60 NM (Continued)

	Inbound				Outbound			
Range (NM)	Opp	Hits	Raw %	Smooth %	Opp	Hits	Raw %	Smooth %
40	13	11	85	92	14	14	100	100
41	10	10	100	91	10	10	100	100
42	10	9	90	97	11	11	100	100
43	9	9	100	97	11	11	100	100
44	10	10	100	100	10	10	100	97
45	10	10	100	100	9	8	89	93
46	9	9	100	100	10	9	90	93
47	10	10	100	97	10	10	100	97
48	10	9	90	97	12	12	100	100
49	10	10	100	90	10	10	100	88
50	10	8	80	77	11	7	64	83
51	10	5	50	71	9	8	89	80
52	8	7	88	75	10	9	90	93
53	10	9	90	93	10	10	100	93
54	10	10	100	93	10	9	90	97
55	10	9	90	97	10	10	100	94
56	10	10	100	93	12	11	92	94
57	9	8	89	97	9	8	89	78
58	11	11	100	85	11	6	55	71
59	7	4	57	86	8	6	75	61
60	3	3	100	0	4	2	50	0

TABLE A-4. RUN016 - IRES RADIAL DETECTION DATA FIGURE EIGHT PATTERN; 17500 FT ALTITUDE

	Inbound				Outbound			
Range (NM)	Opp	Hits	Raw %	Smooth %	Opp	Hits	Raw %	Smooth %
0	1	0	0	0	0	0	0	0
1	11	10	91	74	2	1	50	88
2	19	13	68	60	23	21	91	85
3	23	9	39	34	16	13	81	41
4	75	18	24	32	48	2	4	19
5	69	27	39	43	60	9	15	22
6	66	45	68	52	59	25	42	35
7	59	28	47	62	53	27	51	44
8	61	43	70	66	55	22	40	49
9	59	47	80	76	54	31	57	57
10	56	43	77	80	53	40	75	73
11	21	19	90	81	47	42	89	82
12	0	0	0	0	7	6	86	89

TABLE A-5. RUN018 - IRES RADIAL DETECTION DATA FIGURE EIGHT PATTERN; 9500 FT ALTITUDE

	Inbound				Outbound			
Range (NM)	Opp	Hits	Raw %	Smooth %	Opp	Hits	Raw %	Smooth %
0	46	14	30	0	1	1	100	0
1	22	11	50	55	11	7	64	36
2	106	71	67	73	35	9	26	60
3	79	70	89	81	66	51	77	69
4	61	58	95	92	61	52	85	85
5	58	55	95	94	62	57	92	85
6	66	60	91	92	61	48	79	84
7	66	60	91	89	59	48	81	74
8	64	54	84	91	60	38	63	78
9	53	53	100	93	57	52	91	84
10	50	49	98	99	63	62	98	95
11	37	37	100	99	39	37	95	98
12	19	19	100	100	22	22	100	97
13	2	2	100	100	13	13	100	100
14	0	0	0	0	3	3	100	100

TABLE A-6. RUN019 - IRES RADIAL DETECTION DATA FIGURE EIGHT PATTERN; 4500 FT ALTITUDE

	Inbound				Outbound			
Range (NM)	Opp	Hits	Raw %	Smooth %	Opp	Hits	Raw %	Smooth %
0	9	4	44	0	1	1	100	0
1	86	42	49	70	52	17	33	58
2	97	88	91	77	80	59	74	70
3	66	61	92	92	70	66	94	86
4	75	71	95	96	72	67	93	96
5	68	68	100	98	68	68	100	98
6	70	70	100	97	70	70	100	100
7	69	63	91	91	70	69	99	97
8	64	52	81	87	72	67	93	97
9	52	46	88	87	62	61	98	96
10	44	41	93	93	57	55	96	97
11	46	45	98	92	33	31	94	97
12	43	37	86	93	36	36	100	98
13	13	13	100	90	34	34	100	100
14	6	6	100	100	15	15	100	100
15	5	5	100	100	8	8	100	100
16	6	6	100	100	4	4	100	100
17	6	6	100	100	6	6	100	100
18	5	5	100	100	5	5	100	100
19	6	6	100	100	5	5	100	100
20	0	0	0	0	3	3	100	100

TABLE A-7. RUN011 - FLTEST1 DATA

	Scan 1 BRC = 322 BAZ = 2618		Scan 2 BRC = 329 BAZ = 2619		Scan 3 BRC = 336 BAZ = 2618		Scan 4 BRC = 343 BAZ = 2616		Scan 5 BRC = 350 BAZ = 2617	
PRI	AMP.	RC	AMP.	RC	AMP.	RC	AMP.	RC	AMP.	RC
1	43.58	321	44.6	328	47.86	335	43.27	341	28.88	348
2	40.91	321	46.66	328	46.23	335	40.83	341	40.28	348
3	40	321	42.73	328	48.18	335	34.19	341	34.88	348
4	41.15	321	42.47	328	47.29	335	34.35	341	35.98	348
5	42.73	321	40.68	328	44.9	335	38	341	37.5	348
6	32.78	321	41.06	328	44.03	335	34.51	341	37.4	348
7	37.23	321	38.46	328	43.98	335	29.41	341	33.76	348
8	37.59	321	37.03	328	40.03	335	29.54	341	26.9	348
9	35.96	321	37.76	328	41.45	335	30.43	341	23.82	348
10	35.1	321	35.22	328	37.63	335	31.18	341	27.79	348
11	31.58	321	31.16	328	37.27	335	23.52	342	28.57	348
12	30.51	321	30.16	328	35.8	335	27.46	341	22.55	349
13	28.31	321	29.45	328	34.17	335				
14	26.99	321	27.96	328	32.3	335	23.12	341	23.01	349
15	29.37	321	25.59	328	28.23	335	20.64	341	18.63	348
16	20.37	320	25.12	328	28.88	335			18.13	348
17	23.98	321	22.94	327	24.15	335				
18	20.68	321			21.37	334				
19					18.69	335				

	Scan 6 BRC = 357 BAZ = 2617		Scan 7 BRC = 363 BAZ = 2615		Scan 8 BRC = 371 BAZ = 2617		Scan 9 BRC = 377 BAZ = 2614		Scan 10 BRC = 384 BAZ = 2613	
PRI	AMP.	RC	AMP.	RC	AMP.	RC	AMP.	RC	AMP.	RC
1	42.07	355	31.14	362			34.19	376	40.1	383
2	37.91	355	34	362			34.5	376	36.96	383
3	35.16	355	28.9	362			34.57	376	36	383
4	31.78	355	33.68	362	23.87	369	27.5	376	35.28	383
5	32.15	355	24.62	362	27.11	369	30.59	376	34.58	383
6	30.04	355			24.62	369	23.44	376	32.58	383
7	30.37	355	18.57	362			19.54	376	27.99	383
8	26.79	355	28.43	362					27.36	383
9	24.84	355							22.3	383
10	27.27	355							21.64	383
11	23.44	355							20	384
12	23.65	355								
13	20.04	355								
14	17.24	355								
15	17.85	355								

BRC = Beacon Range Cell (1/16 nm) BAZ = Beacon Azimuth (ACP)

PRI = Pulse Repetition Interval AMP. = Signal Amplitude RC = Range Cell (1/16 nm

TABLE A-7. RUN011 - FLTEST1 DATA (Continued)

	Scan 11 BRC = 391 BAZ = 2613		Scan 12 BRC = 398 BAZ = 2613		Scan 13 BRC = 405 BAZ = 2610		Scan 14 BRC = 412 BAZ = 2611		Scan 15 BRC = 419 BAZ = 2610	
PRI	AMP.	RC	AMP.	RC	AMP.	RC	AMP.	RC	AMP.	RC
1	29.21	390	34.15	397	36.97	405	34.89	411	21.14	418
2	25.01	390	37.38	398	38.54	405	34.97	412	23.82	418
3	31.6	390	33.46	398	36.02	405	30.28	412	23.26	418
4	25.29	390	30.16	397	30.62	405	29.71	412		
5	29.04	390	26.45	398	32.35	405				
6	21.7	390	25.01	398	30.12	405	26.39	412		
7	23.05	390	24.86	398	25.89	405	22.86	412		
8			21.61	397	23.52	405				
9					20	405				

	Scan 16 BRC = 426 BAZ = 2611		Scan 17 BRC = 433 BAZ = 2611		Scan 18 BRC = 440 BAZ = 2608		Scan 19 BRC = 447 BAZ = 2610		Scan 20 BRC = 454 BAZ = 2608	
PRI	AMP.	RC	AMP.	RC	AMP.	RC	AMP.	RC	AMP.	RC
1	33.12	425	35.49	432	28.17	439	28.52	446	34.04	453
2	34.68	425	34.51	432	30.97	439	24.74	446	36.06	453
3	35.17	425	33.45	432	28.07	439	24.15	446	34.57	453
4	30.45	425	32.04	432					28.28	453
5	26.53	425	28.4	432					27.24	453
6	22.38	425	28.68	432					26.61	453
7			21.34	432					20	453
8									25.76	453
9									19.29	453
10									17.63	453

	Scan 21 BRC = 461 BAZ = 2609		Scan 22 BRC = 468 BAZ = 2609	
PRI	AMP.	RC	AMP.	RC
1	25.62	460	32.69	467
2	29.66	460	31	467
3	29.03	460	26.28	467
4	24.17	460	24.17	467
5	26.93	460	17.24	467
6			22.38	467

BRC = Beacon Range Cell (1/16 nm)
BAZ = Beacon Azimuth (ACP)
PRI = Pulse Repetition Interval
AMP. = Signal Amplitude
RC = Radar Range Cell

TABLE A-8. RUN011 - FLTEST2 DATA

	Scan1 Missed		Scan2 BRC = 642 BAZ = 2615		Scan3 BRC = 649 BAZ = 2617		Scan4 BRC = 656 BAZ = 2618		Scan5 BRC = 662 BAZ = 2617	
PRI	AMP.	RC	AMP.	RC	AMP.	RC	AMP.	RC	AMP.	RC
1	33.05	635	28.97	642	26.86	649	28.17	656	33.77	663
2	37.25	635	36.19	642	33.27	649	29.57	656	27.36	663
3	35.51	635	38.89	642	25.29	649	19.29	656	30.28	663
4	31.34	635	35.98	642	30.34	649	25.12	656	34.65	663
5	35.71	635	33.42	642	31.3	649	31.03	656	33.67	663
6	33.18	635	34.68	642	32.48	649	28.81	656	27.03	663
7	31.01	635	29.93	642	27.63	649	23.12	656	24.3	663
8	30.09	635	29.71	642	27.66	649	26.9	656	24.3	663
9	25.59	635	20.64	642			26.68	656	26.28	663
10	24.17	636	25.43	642	23.44	649	23.01	656	25.68	663
11	26.28	635	25.39	642	22.86	649				
12	17.16	635	25.12	642					19.29	662
13									25.05	663

	Scan6 BRC = 669 BAZ = 2617		Scan7 BRC = 676 BAZ = 2617		Scan8 BRC = 683 BAZ = 2619		Scan9 BRC =690 BAZ = 2617		Scan10 BRC = 697 BAZ = 2618	
PRI	AMP.	RC	AMP.	RC	AMP.	RC	AMP.	RC	AMP.	RC
1	26.99	670	31.6	677	34.52	684			37.07	698
2	30.4	670	25.72	677	33.12	684			35.76	698
3	35.35	670	25.72	677	32.48	684	24.97	691	37.2	698
4	32.73	670	30.48	677	29.68	684	27.85	691	35.21	698
5	32.68	670	28.63	677	31.05	684	19.49	690	35.8	698
6	28.69	670			28.52	684	25.31	691	36.19	698
7	25.11	670	21.34	677	32.42	684	24.49	691	32.86	698
8	29.57	670	24.61	677	31.34	684	20.97	691	33.26	698
9	29.72	670	23.52	677	32	66	21.64	691	34.02	698
10	25.62	670			28.15	684	18.69	691	31.25	698
11	24.1	670			23.38	684	21.37	691	28.46	698
12	18.57	670			24.3	684			29.77	698
13			24.62	677	23.52	684			27.97	698
14			19.14	677					26.24	698
15									22.1	698
16									21.96	698
17			18.33	678					21.61	698
18			19.08	677					20.17	698
19									18.63	698
20									18.57	697

BRC = Beacon Range Cell (1/16 nm)
PRI = Pulse Repetition Interval
BAZ = Beacon Azimuth (ACP)
AMP. = Signal Amplitude (dB)
RC = Radar Range Cell (1/16 nm)

TABLE A-8. RUN011 - FLTEST2 DATA (Continued)

	Scan11 BRC = 704 BAZ = 2618		Scan12 BRC = 711 BAZ = 2618		Scan13 BRC = 718 BAZ = 2617		Scan14 BRC = 726 BAZ = 2617		Scan15 BRC = 733 BAZ = 2617	
PRI	AMP.	RC	AMP.	RC	AMP.	RC	AMP.	RC	AMP.	RC
1	39.32	705	38.7	712	33.67	719	30.61	726	25.87	734
2	38.87	705	40.12	712	38.79	719	33.47	726	26.64	734
3	41.36	705	40.1	712	30.51	719	27.16	727	28.17	734
4	36.47	705	40.4	712	36.92	719	27.17	727	26.64	734
5	39.57	705	40.32	712	36.69	719	32.27	727	27.66	734
6	37.87	705	38.24	712	35.21	719	27.39	726	24.84	734
7	36.13	705	38.31	712	34.26	719	24.74	727	23.44	734
8	37.05	705	35.84	712	30.83	719	26.13	726	19.29	734
9	34.57	705	35.83	712	31.39	719	23.89	726	27.72	734
10	36.13	705	35.63	712	29.29	719				
11	37.42	705	31.89	712	28.04	719	22.92	727		
12	31.06	705	29.37	712	28.02	719	23.18	726		
13	31.18	705	31.01	712	25.68	719	20.37	726	18.06	734
14	27.72	705	27.44	712	25.72	719	22.88	726	18.69	735
15	20.64	705	24.61	712	21.58	719			23.44	734
16	26.79	705	24.17	712	22.04	719				
17	20.25	705	21.7	712	20.17	719				
18	23.18	705			19.14	719				
19	19.29	705								
20	19.14	705								

	Scan16 BRC = 740 BAZ = 2616		Scan17 BRC = 747 BAZ = 2616		Scan18 BRC = 755 BAZ = 2614		Scan19 BRC = 762 BAZ = 2614		Scan20 BRC = 769 BAZ = 2614	
PRI	AMP.	RC	AMP.	RC	AMP.	RC	AMP.	RC	AMP.	RC
1	34.49	741	34.65	748	32.58	755	27.97	762	32.36	770
2	32.15	741	35.98	748	25.72	755	22.92	762	33.81	769
3	33.87	741	34.39	748	25.43	755	32.78	762	31.81	769
4	31.41	741	26.6	748	31	755	29.57	762	32.1	770
5	31.67	741	33.1	748	25.89	755	19.29	762	32.08	770
6	29.66	741	29.55	748	26.06	755	22.58	763	30.64	769
7	27.36	741	26.27	748	25.68	755	25.56	762	26.02	769
8	27.82	741	28.77	748	23.26	755	20	762	28.94	770
9	23.26	741	28.69	748	21.85	755	23.01	763	24.74	770
10	23.01	741	24.97	748			18.69	763	25.39	770
11	23.67	741	23.26	748						
12	20.83	741	19.87	748					20	770
13	21.64	741	24.1	748					21.58	769
14			19.29	748						

BRC = Beacon Range Cell (1/16 nm)
PRI = Pulse Repetition Interval
BAZ = Beacon Azimuth (ACP)
AMP. = Signal Amplitude (dB)
RC = Radar Range Cell (1/16 nm)

TABLE A-8. RUN011 - FLTEST2 DATA (Continued)

	Scan21 BRC = 776 BAZ = 2615		Scan22 BRC = 783 BAZ = 2616		Scan23 BRC = 790 BAZ = 2615		Scan24 BRC = 797 BAZ = 2615		Scan25 BRC = 804 BAZ = 2615	
PRI	AMP.	RC	AMP.	RC	AMP.	RC	AMP.	RC	AMP.	RC
1	25.51	777	25.31	783	20.97	791	28.33	797	26.55	804
2	27.27	776	24.15	783	20.68	790	23.98	797	30.39	804
3	29.46	777	27.03	783			20.64	798	28.57	804
4	24.96	776	23.01	783	19.14	791			23.01	804
5	19.54	777			20.97	790			21.73	804
6	18.33	777	19.14	784			19.29	798	25.56	804
7	18.13	776	17.24	784	17.63	790	22.5	797		
8			20.68	783	16.99	790	26.28	798	25.89	804
9	24.35	777	22.3	783			17.63	797	20.17	804
10	21.37	776								

	Scan26 BRC = 811 BAZ = 2616		Scan27 BRC = 818 BAZ = 2615		Scan28 BRC = 825 BAZ = 2617		Scan29 BRC = 832 BAZ = 2614		Scan30 BRC = 839 BAZ = 2613	
PRI	AMP.	RC	AMP.	RC	AMP.	RC	AMP.	RC	AMP.	RC
1	31.96	811	35.27	819					28.6	840
2	29.37	811	32.61	819					27.11	840
3	29.03	811	31.32	819					23.18	840
4	26.79	811	30.61	819	20.04	826	18.13	833	21.37	840
5	23.87	812	28.77	819	22.28	826	21.73	833	20.17	840
6	25.67	811	26.12	819					20.68	840
7	20.37	811	26.9	819					21.37	840
8	20.86	812	26.13	818					18.33	839
9	21.14	812							21.96	839
10	23.98	812	19.03	819						
11			24.17	819						
12			19.08	818						

BRC = Beacon Range Cell (1/16 nm)
PRI = Pulse Repetition Interval
BAZ = Beacon Azimuth (ACP)
AMP. = Signal Amplitude (dB)
RC = Radar Range Cell (1/16 nm)

TABLE A-8. RUN011 - FLTEST2 DATA (Continued)

	Scan31 BRC = 846 BAZ = 2612		Scan32 BRC = 853 BAZ = 2613		Scan33 BRC = 860 BAZ = 2613		Scan34 BRC = 867 BAZ = 2612		Scan35 BRC = 875 BAZ = 2612	
PRI	AMP.	RC	AMP.	RC	AMP.	RC	AMP.	RC	AMP.	RC
1			33.64	854	23.05	861	23.12	868	29.04	875
2			32.5	854	20	861	26.53	868	24.67	875
3			28.3	854	26.48	861	24.62	868	28.4	875
4			31.39	854	24.71	861	23.6	868	27.07	875
5			29.13	854	22.38	861			23.82	875
6			28.6	854	18.63	861			26.85	875
7			23.44	854					23.54	875
8									20.68	875
9			20.53	854					20.17	875
10			18.33	854						

	Scan36 BRC = 881 BAZ = 2615		Scan37 BRC = 888 BAZ = 2614	
PRI	AMP.	RC	AMP.	RC
1	26.82	882	30.45	889
2	25.72	882	28.43	889
3	24.71	882	30.17	889
4	22.58	882	26.02	889
5			26.19	889
6			20.97	889
7			18.63	889
8			22.38	889

BRC = Beacon Range Cell (1/16 nm)
PRI = Pulse Repetition Interval
BAZ = Beacon Azimuth (ACP)
AMP. = Signal Amplitude (dB)
RC = Radar Range Cell (1/16 nm)

TABLE A-9. RUN015 - FLTEST6 DATA

	Scan 13 BRC: 702 BAZ :2626		Scan 14 BRC: 708 BAZ: 2625		Scan 15 Missed		Scan 16 BRC: 723 BAZ: 2626		Scan 17 BRC: 729 BAZ: 2626	
PRI	AMP.	RC	AMP.	RC	AMP.	RC	AMP.	RC	AMP.	RC
2			17.63	708						
3			16.13	709						
8	19.03	704								
9	15.68	705								
10										
11			18.69	709						
12			16.02	710						
13	16.99	705								
14	16.53	704								
15	18.69	703	18.57	710						
16	20.25	704	20	710			19.49	722		
17	16.99	704	22.88	710			19.03	722		
18	22.5	704	25.51	710	16.99	716	21.64	722	21.37	728
19	26.27	704	24.3	710	18.69	716	21.61	723	19.03	729
20	26.06	704	26.6	710	24.62	716	28.3	722	24.71	728
21	26.13	704	31.05	710	28.46	716	19.54	722	24.3	729
22	31.78	704	31.5	710	19.14	716	21.14	722	26.27	729
23	36.26	704	30.74	710	30.8	716	29.68	722	28.6	728
24	35.18	704	28.69	710	31.05	716	28.44	722	26.27	728
25	36.18	704	33.86	710	31.19	716	30.51	722	31.31	728
26	34.83	704	31.61	710	26.99	716	33.27	722	30.83	728
27	36.58	704	31.71	710	31.41	716	33.11	722	27.46	729
28	34.38	704	36.46	710	33.26	716	33.98	722	33.01	728
29	33.74	704	34.5	710	31.41	716	31.83	722	27.72	728
30	37.33	704	31.61	710	23.87	716	33.86	722		
31	38.17	704	32.44	710	21.7	716	31.6	722	28.38	728
32	36	704	34.15	710	27.85	716	29.99	722	33.57	728
33	31.29	704	33.61	710	32.58	716	34.57	722	30.14	728
34	32.51	704	34.19	710	33.6	716	27.63	722	33.26	728
35	35.55	704	37.33	710	26.79	716	29.19	722	34.22	728
36	31.34	704	33.92	710	28.36	716	29.14	722	24.49	728
37	31.56	704	32.69	710	21.61	716	30.59	722	30.53	728
38	35.03	704	27.09	710	29.77	716	28.77	722	27.16	728
39	34.1	704	28.3	710	30.25	716	28.31	722	29.93	728
40	30.37	704	27.07	710	24.15	716	28.84	722	27.24	729
41	29.31	704	24.35	710	23.18	716	25.43	722	22.3	728
42	25.28	704	26.28	710	22.28	716	26.93	722	23.98	728
43	22.94	704	24.42	710			16.02	722	21.07	728
44	23.05	704	19.14	710			20.25	722	21.14	728
45	23.12	704	18.33	710			19.29	722	22.3	728
46			19.14	710			19.08	723	16.53	729
47			21.7	710			17.85	722		

TABLE A-9. RUN015 - FLTEST6 DATA (Continued)

	Scan 18 BRC: 736 BAZ: 2625		Scan 19 BRC: 742 BAZ: 2627		Scan 20 BRC: 748 BAZ: 2625		Scan 21 BRC: 754 BAZ: 2621		Scan 22 BRC: 761 BAZ: 2622	
PRI	AMP.	RC	AMP.	RC	AMP.	RC	AMP.	RC	AMP.	RC
9							15.56	754	18.13	760
10							18.13	755		
11										
12										
13									18.13	759
14			20.17	741					21.14	760
15	20	735	19.14	741						
16	18.33	735	21.61	741					18.33	760
17	18.13	735			21.61	747	20.04	753	20	760
18	24.15	735	26.28	741	20	747	23.38	753	28.68	760
19	17.63	735	28.84	741	23.52	747	29.29	753	24.15	760
20	27.33	735	27.52	741	23.6	747	24.49	753	20.86	760
21	28.23	735	27.82	741			25.28	753	26.02	760
22	26.55	735	26.82	741	22.94	747	23.65	753	29.07	760
23	33.35	735	31.53	741	30.24	747	31.14	753	31.06	760
24	28.44	735	30.64	741	35.58	747	31.71	753	33.05	760
25	31.83	735	31.82	741	30.91	747	26.99	753	36.65	760
26	31.05	735	34.54	741	22.3	747	23.26	753	32.02	760
27	32	735	35.29	741	29.69	747	21.73	754	35.67	760
28	32.79	735	34.1	741	28.81	747	30.07	753	30.59	760
29	30.91	735	25.01	741	32	747	30.68	753	29.08	760
30	32.17	735	32.38	741	33.94	747	22.38	753	34.71	760
31	31.14	735	35.1	741	33.75	747	33.63	753	31.97	760
32	32.73	735	32.81	741	28.6	747	32	753	30.63	760
33	32.8	735	27.55	741	30.37	747	27.67	753	27.66	760
34	35.96	735	32.66	741	22.15	747	29.83	753	27.67	760
35	28.17	735	29.21	741	25.68	747	27.52	753	29.79	760
36	35.72	735	28.33	741	29	747	27.66	753	28.95	760
37	30.28	735	33.76	741	33.74	747	29.25	753	29.79	760
38	26.48	735	30.11	741	34	747	29.08	753	30.56	760
39	32.84	735	28.3	741	26.12	747	23.67	753	29.57	760
40	27.63	735	28.97	741	20	747	19.29	753	20.68	760
41	26.53	735	28.33	741	20	747	16.9	753	22.04	760
42	27.63	735	23.38	741	23.12	747	21.34	753	18.13	760
43	19.54	735			24.3	747	17.24	754		
44	24.35	735			21.58	747	16.99	753	18.33	759
45									19.29	759

BRC = Beacon Range Cell (1/16 nm)
PRI = Pulse Repetition Interval
BAZ = Beacon Azimuth (ACP)
AMP. = Signal Amplitude (dB)
RC = Range Cell (1/16 nm)

TABLE A-9. RUN015 - FLTEST6 DATA (Continued)

	Scan 23 BRC: 767 BAZ: 2623		Scan 24 BRC: 773 BAZ: 2624		Scan 25 BRC: 779 BAZ: 2624		Scan 26 BRC: 785 BAZ: 2625		Scan 27 BRC: 792 BAZ: 2625	
PRI	AMP.	RC	AMP.	RC	AMP.	RC	AMP.	RC	AMP.	RC
12					15.68	781				
13					17.24	781				
14										
15			19.49	772						
16			19.54	772						
17										
18	18.13	766	16.9	772	16.13	779			17.24	791
19	21.07	766	21.61	772	20.37	778	18.13	784	18.57	790
20	24.65	766	23.65	772			26.06	784	19.29	790
21	30.53	766	30.18	772			22.3	784	17.24	790
22	27.99	766	27.24	772	17.85	778	27.16	784	22.04	790
23	31.83	766	31.14	772	17.24	778	23.52	784	23.65	791
24	27.98	766	29.27	772	29.65	778	25.31	784	27.5	790
25	27.66	766	32.71	772	26.64	778	26.28	784	28.84	790
26	26.82	766	34.06	772	23.26	778	27.61	784	31.09	790
27	24.65	766	33.31	772	21.14	778	28.84	784	30.81	790
28	31.64	766	32.93	772	21.73	778	28.81	784	29.55	790
29	27.62	766	28.29	772	21.7	778	27.39	784	27.31	791
30	29.85	766	31.19	772			28.63	784	29.83	790
31	29.77	766	17.16	772	23.01	778	31.08	784	21.34	791
32	16.99	766	27.82	772	25.68	778	22.38	784	30.66	790
33	26.27	766	30.43	772			28.84	784	28.13	790
34	31.61	766	34.51	772			27.03	784	27.82	790
35	29.83	766	30.28	772			25.76	784	27.27	790
36	27.44	766	29.08	772	24.96	778	20.86	784	22.15	790
37	18.13	765	28.06	772	23.44	778	25.12	784	19.54	791
38	21.61	766	24.71	772	27.16	778	25.11	784	24.67	790
39	16.99	766	28.06	772	24.96	778	21.96	784	25.68	790
40	16.13	766	26.28	772	18.13	777	23.54	784	23.52	790
41	17.16	765	20.68	772	19.29	778	21.61	784		
42	20.97	766	17.63	772			22.5	784	21.7	791
43							18.13	784	18.63	790

BRC = Beacon Range Cell (1/16 nm)
PRI = Pulse Repetition Interval
BAZ = Beacon Azimuth (ACP)
AMP. = Signal Amplitude (dB)
RC = Range Cell (1/16 nm)

TABLE A-9. RUN015 - FLTEST6 DATA (Continued)

	Scan 28 BRC: 798 BAZ: 2623		Scan 29 BRC: 804 BAZ: 2625		Scan 30 Missed		Scan 31 BRC: 817 BAZ: 2621		Scan 32 BRC: 823 BAZ: 2621	
PRI	AMP.	RC	AMP.	RC	AMP.	RC	AMP.	RC	AMP.	RC
10	16.99	797								
11	19.03	796								
12	20.86	796								
13	21.73	797								
14	23.84	797					20	816		
15	24.3	797	16.53	803			25.31	816		
16	26.82	797	19.14	803			19.49	816	23.44	822
17	25.48	797	19.14	803			20	816	20.64	822
18	26.28	797	19.54	803			16.99	816	17.24	822
19	28.51	797	22.1	803			28.99	816	23.69	822
20	31.66	797	24.74	803	24.17	810	21.34	816	26.28	822
21	34.88	797	23.38	803	17.85	810	17.16	816	28.07	822
22	33.86	797	28.2	803	19.87	810	26.27	816	30.06	822
23	32.3	797	25.29	803	19.54	809	28.72	816	30.29	822
24	33.26	797	29.38	803			32.08	816	25.76	822
25	37.85	797	25.87	803	22.28	809	34.74	816	34.55	822
26	37.3	797	32.03	803	24.23	809	32.75	816	27.98	822
27	37.66	797	32.51	803	24.62	810	31.01	816	31	822
28	35.92	797	23.05	803	27.96	810	29.72	816	29.86	822
29	35.89	797	28.49	803			30.62	816	28.69	822
30	36.26	797	34.67	803	27.24	809	20.64	816	30.14	822
31	35.5	797	31.34	803	24.49	809	33.57	816	31.61	822
32	38.37	797			24.97	810	30.17	816	29.41	822
33	34.46	797	30.51	803	23.44	810	28.49	816	28.6	822
34	37.43	797	24.35	803	20	809			29.31	822
35	34.84	797	22.28	803			32.28	816	26.24	822
36	33.02	797	28.88	803			24.35	816	29.45	822
37	34.9	797	24.67	803			24.62	816	27.9	822
38	30.8	797	26.88	803			28.68	816	21.61	822
39	33.09	797					26.86	816	30.45	822
40	30.37	797	23.87	803					25.28	822
41	27.87	797	23.52	803						
42	25.67	797	18.33	803						
43	22.04	797								
44	21.37	797								
45	21.14	797								
46										
47										
48										
49										

TABLE A-9. RUN015 - FLTEST6 DATA (Continued)

	Scan 33 BRC: 829 BAZ: 2620		Scan 34 BRC: 836 BAZ: 2624		Scan 35 BRC: 842 BAZ: 2622		Scan 36 BRC: 848 BAZ: 2620		Scan 37 BRC: 854 BAZ: 2621	
PRI	AMP.	RC	AMP.	RC	AMP.	RC	AMP.	RC	AMP.	RC
13							16.99 .	847		
14			19.08	834	19.29	841	19.54	847		
15	20.37	828	17.16	835	18.33	841			15.05	853
16	24.86	828	21.14	835	18.13	841	21.64	847	21.7	853
17	20.83	828	21.58	835	25.28	841	22.3	847	24.23	853
18	23.89	828	23.54	835	22.86	841	27.27	847	21.64	853
19	20	828	20.25	835	27.63	841	26.53	847	18.63	853
20	28.46	828	19.29	835	26.55	841	28.6	847	22.15	853
21			26.13	835	18.13	841	26.27	847	22.38	854
22	24.62	829	28.73	835			28.33	847		
23	30.76	828	32.92	835	19.54	841	27.75	847		
24	32.57	828	28.46	835	28.23	841	21.73	847	26.99	853
25	33.08	828	25.67	835	27.03	841	30.37	847	28.46	853
26	27.24	829	25.12	835	23.44	841	29.33	847	27.55	853
27	31	828	30.85	835	24.15	841	31.44	847	27.63	853
28	35.25	828	26.55	835	24.15	841	32.26	847	31.64	853
29	29.04	828	25.39	835	25.22	841	32.69	847	18.06	853
30	33.72	828	29.14	835	30.85	841	31.81	847	17.24	853
31	29.84	828	24.23	835	27.18	841	29.92	847	25.89	853
32	25.31	828	22.28	835	23.67	841	30.37	847	21.07	853
33	28.57	829	26.28	835	25.87	841	30.68	847	26.24	853
34	29.91	828	28.9	835	22.04	841	26.28	847	24.71	853
35	29.46	828	26.82	835	23.67	841	28.6	847	16.53	724
36	31.47	828	26.45	835	24.96	841	24.74	847	20.04	853
37	28.43	828	26.53	835			29.2	847	25.56	853
38	27.85	828	25.11	835	19.87	841			22.28	853
39	28.29	829	17.85	835	17.63	841	23.87	847	20.68	854
40	21.07	828	19.49	835			19.49	847	17.85	853
41	21.7	828					21.73	847	18.06	853
42	23.01	828					19.87	847	19.14	853
43	17.85	828					16.99	847		

BRC = Beacon Range Cell (1/16 nm)
PRI = Pulse Repetition Interval
BAZ = Beacon Azimuth (ACP)
AMP. = Signal Amplitude (dB)
RC = Range Cell (1/16 nm)

TABLE A-9. RUN015 - FLTEST6 DATA (Continued)

	Scan 38 BRC: 860 BAZ: 2625		Scan 39 BRC: 867 BAZ: 2623		Scan 40 BRC: 873 BAZ: 2623		Scan 41 BRC: 879 BAZ: 2624		Scan 42 BRC: 885 BAZ: 2624	
PRI	AMP.	RC	AMP.	RC	AMP.	RC	AMP.	RC	AMP.	RC
12					19.29	872				
13					18.13	872	17.85	878		
14					19.87	872	23.01	878	19.49	884
15					22.04	872	23.52	878	19.49	884
16					25.28	872	26.07	878	19.87	884
17					28.36	872	25.31	878	19.03	884
18					29.33	872	29.25	878	23.52	884
19					28.77	872	25.29	878	20.53	884
20	19.87	859			31.92	872	28.63	878	25.76	884
21	21.37	860			33.02	872	31.7	878	30.22	884
22					33.71	872	32.6	878	28.84	884
23			22.15	865	33.72	872	32.19	878	26.88	884
24	21.64	859	27.67	866	37.11	872	36.26	878	26.28	884
25	24.17	859	24.42	866	38.19	872	34.96	878	28.3	884
26	23.69	859	25.01	865	38.03	872	34.56	878	28.91	884
27	25.01	859	28.04	866	37.04	872	36.99	878	29.85	884
28	27.36	859	23.69	866	36.82	872	35.77	878	28.63	884
29	20.97	859	20.25	866	38.52	872	36.64	878	30.66	884
30	20.64	860			37.54	872	35.93	878	30.09	884
31	29.79	859			38.86	872	35.05	878	28.86	884
32	23.6	859	26.06	866	36.53	872	35.81	878	24.84	884
33	24.61	859	24.97	865	38.1	872	32.17	878	28.79	884
34	21.37	859	17.24	865	37.74	872	34.53	878	33.47	884
35	23.52	859			35.94	872	33.73	878	29.66	884
36	19.87	859	20.68	865	36.46	872	32.75	878	26.28	884
37	16.13	859	16.9	866	33.93	872	30.62	878	24.86	884
38			25.05	865	35.03	872	33.03	878	26.06	884
39			18.13	866	33.92	872	28.43	878	25.12	884
40					31.98	872	27.52	878	22.3	885
41					29.84	872	26.13	878	21.73	884
42					26.13	872	23.89	878	17.16	885
43					25.12	872	18.13	878		
44					24.61	872	19.49	878		
45					19.87	872				
46					20.25	872				
47					18.33	872				
48									16.99	884
49									20.25	884

TABLE A-9. RUN015 - FLTEST6 DATA (Continued)

	Scan 43 BRC: 892 BAZ: 2623		Scan 44 BRC: 898 BAZ: 2621		Scan 45 BRC: 904 BAZ: 2624		Scan 46 BRC: 910 BAZ: 2623		Scan 62 BRC: 914 BAZ: 2607	
PRI	AMP.	RC	AMP.	RC	AMP.	RC	AMP.	RC	AMP.	RC
1									27.33	912
2									20.64	912
3									19.54	912
4									26.68	912
5									29.27	912
6									26.44	913
7									22.28	912
8									24.42	913
9									25.16	912
10									30.63	912
11									28.06	912
12			17.24	898					27.85	912
13			19.49	897			18.33	909	26.13	912
14							17.85	909	28.63	913
15			19.29	897			22.15	909	23.52	913
16	18.13	891	24.49	897			22.3	909	23.82	913
17	20	891	26.19	897					16.99	912
18	22.15	891	25.51	897	19.54	904	21.14	909	18.13	912
19	18.33	891	28.2	897	20.68	903	22.15	909	23.44	912
20	24.62	891	27.61	897	18.33	903	22.88	910	22.86	912
21	25.31	890	28.06	897	20.04	903	24.23	910		
22	29.27	891	31.01	897	23.84	903	30.91	909		
23	24.62	891	28.72	897	26.45	903	30.43	909		
24	28.15	891	27.17	897	21.07	903	30.22	909		
25	28.68	891	27.67	897	29.93	903	28.68	909		
26	27.67	891	31.4	897	17.63	903	30.77	909		
27	23.84	891	27.55	897	20.64	903	30.91	910		
28	23.44	891	31.87	897	25.16	903	26.85	910		
29	29.01	891	30.37	897	24.61	903	28.65	910		
30	27.18	891	31.14	897	18.13	903				
31	26.28	891	33.22	897			28.81	909		
32	25.43	891	28.68	897	22.86	903	27.63	909		
33	27.63	891	29.66	897	24.71	903	24.23	909		
34	24.84	891	27.85	897	22.5	903	25.58	909		
35	26.93	891	30.34	897	22.55	903	27.39	910		
36	23.89	891	22.1	897	21.14	903	28.6	910		
37	23.44	891	26.52	897			25.31	909		
38	25.68	891	19.87	897	23.69	903	23.52	909		
39	23.38	891	21.37	897	25.05	903	23.44	910		
40	21.7	891	19.14	897	18.63	903	23.12	909		
41	20	892	20.68	897			19.14	910		
42			19.49	897						

TABLE A-9. RUN015 - FLTEST6 DATA (Continued)

	Scan 63 BRC: 907 BAZ: 2608		Scan 64 BRC: 901 BAZ: 2606		Scan 65 BRC: 894 BAZ: 2608		Scan 66 BRC: 888 BAZ: 2607		Scan 67 BRC: 881 BAZ: 2606	
PRI	AMP.	RC	AMP.	RC	AMP.	RC	AMP.	RC	AMP.	RC
1	28.84	906	20.17	899			17.16	886	25.72	880
2	31.97	906	25.68	899			18.33	886	30.94	880
3			27.72	899	23.44	893	28.2	886	31.73	880
4	27.96	906	29.77	899	27.9	893	24.74	886	31.09	879
5	21.14	906	25.68	899	30.11	893	26.12	886	33.84	880
6	20.97	906	26.68	899	30.74	893	27.87	886	33.41	880
7	32.3	906	28.3	899	23.69	893	30.22	886		
8	34.67	906	28.63	899	25.16	893	30.98	886	33.58	879
9	31.01	906	27.55	899	26.7	893	33.31	886	34.22	880
10	27.85	906	32.15	899	29.43	893	36.81	886	34.81	880
11	32.15	906	31.21	899	29.68	893	27.18	886	32.92	880
12	28.91	906	29.14	899	30.53	893	35.23	886	33.86	880
13	33.1	906	28.57	899	26.07	893	27.27	886	29.69	880
14	30.9	906	20.04	899	25.12	893	20	886		
15	33.01	906	27.31	900	21.85	893			27.16	880
16	22.58	906	25.16	899	22.1	893	25.51	886	28.73	880
17	21.61	906	18.33	899	20.97	893	19.87	886	29.55	880
18	23.52	906	27.18	899	22.92	893	22.92	886	24.74	879
19	18.06	906	19.54	899	23.44	893	22.94	886	25.95	879
20					22.67	893	20.97	886	23.82	880
21	23.26	906					21.34	886	21.85	879
22	17.63	906					18.57	886	19.29	880
23	18.13	906					18.13	886	18.33	879
24									18.13	879
25									19.08	880
26										
27										
28										
29										
30										
31										
32										
33										
34										
35										
36										
37										
38	16.99	906								
39	19.14	906								

TABLE A-9. RUN015 - FLTEST6 DATA (Continued)

	Scan 68 BRC: 874 BAZ: 2605		Scan 69 BRC: 867 BAZ: 2604		Scan 70 BRC: 861 BAZ: 2605		Scan 71 BRC: 854 BAZ: 2606		Scan 72 BRC: 847 BAZ: 2603	
PRI	AMP.	RC	AMP.	RC	AMP.	RC	AMP.	RC	AMP.	RC
1	23.84	873	30.39	866	23.12	859	29.03	853	27.5	846
2	31.1	873	29.2	866	19.54	860	29.71	853	21.7	846
3	28.28	873	28.02	866	24.86	859	31.14	853	31.51	846
4	29.66	873	34.95	866	27.52	859	32.86	853	20.17	846
5	28.9	873	33.07	866	25.89	859	31.87	853	32.39	846
6	29.84	873	25.59	866	23.12	859	31.98	853	32.04	846
7	26.45	873	28.18	866	33.64	859	32.44	853	31.41	846
8	26.39	873	28.97	866	27.79	859	32.35	853	35.68	846
9	24.86	873	31.82	866	26.67	859	32.15	853	28.33	846
10	24.62	873	26.48	866	29.33	859	34.58	853	28.51	846
11			28.6	866	27.5	859	32.53	853	27.67	846
12	31.6	873	29.49	866	25.93	859	33.13	853	30	846
13	31.95	873	29.54	866	26.48	859	33.22	853	26.03	846
14	24.23	873	30.97	866			29.25	853	24.15	846
15	29.49	873	27.63	866			26.24	853	22.88	846
16	26.28	873	28.31	866	22.3	859	30.45	853	23.05	846
17	25.59	873	29.66	866	22.3	859	26.9	853		
18	21.96	873	27.5	866			26.12	853		
19	21.14	873	23.6	866			22.3	853	23.69	846
20	21.85	873					22.3	853	19.87	846
21							18.69	853	19.29	846
22							18.33	853		
23							17.63	853		

BRC = Beacon Range Cell (1/16 nm)
PRI = Pulse Repetition Interval
BAZ = Beacon Azimuth (ACP)
AMP. = Signal Amplitude (dB)
RC = Range Cell (1/16 nm)

TABLE A-9. RUN015 - FLTEST6 DATA (Continued)

	Scan 73 BRC: 841 BAZ: 2603		Scan 74 BRC: 834 BAZ: 2604		Scan 75 BRC: 827 BAZ: 2604		Scan 76 BRC: 820 BAZ: 2605		Scan 77 Missed	
PRI	AMP.	RC	AMP.	RC	AMP.	RC	AMP.	RC	AMP.	RC
1	30.74	839	22.5	833	18.33	826	34.42	819	27.17	812
2	21.85	839	27.27	833	17.63	826	28.06	819	35.76	812
3	33.01	839	27.96	833	26.48	826	29.55	819	40	812
4	36.39	839	31.34	833	26.52	826	29.33	819	36.39	812
5	35.04	839	31.6	833	29.91	826	29.66	819	31.44	812
6	33.23	839	26.68	833	34.51	826	28.13	819	36.38	812
7	33.3	839	20.97	833	31.13	826	30.74	819	32.14	812
8	30.1	839	26.82	833	27.96	826	24.84	819		
9	24.42	839	29.14	833	18.13	826	23.01	819		
10	24.38	840	27.52	833	27.99	826	27.87	819	17.16	813
11	23.12	840	23.12	833	28.43	826	30.51	819	27.03	812
12	30.63	839	25.11	833	24.67	826	26.79	819	24.74	812
13	31.34	839	17.16	833	21.64	826	26.9	819	20.97	812
14	25.16	839					25.29	819		
15	17.16	840	20	833			22.04	819		
16	26.28	839	22.15	833			17.24	819	25.12	812
17	27.33	839	20.17	833					22.28	813
18	26.48	839	18.33	833			17.16	819	17.85	812
19	26.55	839	23.69	833			15.68	820		
20			17.16	833						
21	21.34	839								
22	19.49	839								

BRC = Beacon Range Cell (1/16 nm)
PRI = Pulse Repetition Interval
BAZ = Beacon Azimuth (ACP)
AMP. = Signal Amplitude (dB)
RC = Range Cell (1/16 nm)

TABLE A-9. RUN015 - FLTEST6 DATA (Continued)

	Scan 78 BRC: 807 BAZ: 2599		Scan 79 BRC: 800 BAZ: 2598		Scan 80 BRC: 794 BAZ: 2599		Scan 81 BRC: 787 BAZ: 2599		Scan 82 BRC: 781 BAZ: 2597	
PRI	AMP.	RC	AMP.	RC	AMP.	RC	AMP.	RC	AMP.	RC
1	34.22	806	35.26	799	38.99	792	30.14	786	30.85	779
2	31.54	806	36.83	799	34.15	792	34.47	786	32.7	779
3	21.61	806	30.97	799	33.59	792	32.42	786	24.96	779
4	27.82	806	23.65	799	36.65	792	32.09	786	33.11	779
5	31.19	806	32.26	799	35.42	792	30.04	786	29.55	779
6	31.47	806	33.44	799	34.67	792	31.21	786	30.63	779
7	26.03	806	28.02	799	35.57	793	28.17	786	21.14	779
8	27.27	806	21.85	799	34.71	792	28.06	786	24.84	779
9	20	806	23.67	799	33.71	792	27.24	786		
10	22.3	806	21.73	799	33.35	793	19.54	786		
11	25.59	806	20.04	799	29.77	792	22.04	786		
12	27.99	806	24.38	799	23.98	793	23.6	786	20.97	779
13	27.11	806	19.29	799	22.55	792	25.56	786	18.13	780
14	24.1	806	21.96	799	23.01	792				
15			17.24	799	22.67	792				
16										
17					17.16	792				
18					18.13	793				

BRC = Beacon Range Cell (1/16 nm)
PRI = Pulse Repetition Interval
BAZ = Beacon Azimuth (ACP)
AMP. = Signal Amplitude (dB)
RC = Range Cell (1/16 nm)

TABLE A-9. RUN015 - FLTEST6 DATA (Continued)

	Scan 83 BRC: 774 BAZ: 2598		Scan 84 BRC: 767 BAZ: 2598		Scan 85 Missed		Scan 86 BRC: 754 BAZ: 2599		Scan 87 BRC: 748 BAZ: 2597	
PRI	AMP.	RC	AMP.	RC	AMP.	RC	AMP.	RC	AMP.	RC
1	32.08	773	33.93	766	30.76	759	27.62	753	38.72	747
2	29.68	773	32.26	766	29.94	759	25.01	753	37.68	747
3	29.74	773	30.04	766	19.87	760	20	753	35.18	747
4	21.96	773	25.68	766	27.36	760	26.86	753	24.61	747
5	25.43	773	26.67	766	23.87	760	22.04	753	28.6	747
6	29.13	773	28.9	766	25.12	759	28.69	753	21.61	747
7	33.71	773	23.12	766	31.83	760	25.01	753	22.04	747
8	29.21	773			21.58	761	18.13	753	21.7	747
9	24.15	773			27.24	760	18.13	753	18.13	747
10	28.29	773			25.12	760				
11	25.11	773	21.34	766	29.57	760	18.13	753	18.13	746
12	22.28	773	18.63	766	26.28	760	19.03	754	18.57	747
13					26.48	760				
14					30.16	760				
15					25.48	760				
16					30.98	760				
17					28.36	760				
18					28.9	760				
19					25.59	760				
20					29.87	760				
21					23.54	760				
22					26.61	760				
23										
24					23.12	761				
25					18.13	761				
26					21.85	760				
27					19.87	761				
28					18.13	760				
29					18.13	761				

BRC = Beacon Range Cell (1/16 nm)
PRI = Pulse Repetition Interval
BAZ = Beacon Azimuth (ACP)
AMP. = Signal Amplitude (dB)
RC = Range Cell (1/16 nm)

TABLE A-9. RUN015 - FLTEST6 DATA (Continued)

	Scan 88 BRC: 742 BAZ: 2598		Scan 89 BRC: 736 BAZ: 2600		Scan 90 BRC: 730 BAZ: 2597		Scan 91 BRC: 723 BAZ: 2598		Scan 92 BRC: 717 BAZ: 2597	
PRI	AMP.	RC	AMP.	RC	AMP.	RC	AMP.	RC	AMP.	RC
1	22.15	741	27.87	734	29.45	728	29.79	722	35.06	716
2	18.63	741	27.63	734	26.82	728	23.05	722	36.68	716
3	24.15	740	24.62	734	23.98	728	31.91	722	28.91	716
4	21.7	741	25.31	734	35.15	728	24.62	722	28.57	716
5	27.33	740			30.84	728	27.62	722	27.03	716
6	26.13	741	26.82	735	26.07	728	24.1	722	28.77	716
7	17.24	740	25.29	734	21.64	729	26.53	722	25.56	716
8	20.86	740			20.53	728	23.18	722	18.63	716
9	22.67	740			22.28	728	24.71	722		
10					19.91	728	17.63	722		
11					22.04	728				
12									20.17	716
13									17.16	715

	Scan 93 BRC: 711 BAZ: 2598		Scan 94 BRC: 704 BAZ: 2602	
PRI	AMP.	RC	AMP.	RC
1			40.12	703
2	30.09	709	39.61	703
3	25.01	710	29.86	703
4	26.13	710		
5	20	710	29.85	703
6			29.66	703
7			29.45	703
8			24.35	703
9			21.37	703
10	18.13	709	21.37	703
11	19.29	709	22.3	703
12	18.13	709	16.9	704

BRC = Beacon Range Cell (1/16 nm)
PRI = Pulse Repetition Interval
BAZ = Beacon Azimuth (ACP)
AMP. = Signal Amplitude (dB)
RC = Range Cell (1/16 nm)

TABLE A-10. RUN015 - FLTEST7 DATA

	Scan 16 BRC: 517 BAZ: 2626		Scan 20 BRC: 541 BAZ: 2629		Scan 21 BRC: 547 BAZ: 2633		Scan 22 BRC: 553 BAZ: 2634		Scan 23 BRC: 559 BAZ: 2632	
PRT	AMP.	RC	AMP.	RC	AMP.	RC	AMP.	RC	AMP.	RC
1			43.26	539	34.32	546	41.62	552		
2			41.57	539	33.78	546	42.79	552		
3			40.33	539	34.12	546	44.02	552		
4			38.15	539	36.3	546	45.6	552	19.87	559
5			36	539	36.62	545	46.52	552	22.67	559
6			33.29	539	37.79	545	47.76	552	26.53	559
7			30.31	539	37.9	545	49.26	552	28.12	559
8			24.49	539	37.69	545	49.81	552	32.27	559
9			23.05	539	35.19	545	50.23	552	34.72	559
10			19.49	539	35.96	545	50.2	552	36.18	559
11	20.97	518			32.21	545	50.05	552	36.66	559
12	19.08	518			30.75	545	51.07	552	38.95	559
13	20.04	519			26.39	545	51.2	552	39.38	559
14	16.99	519			30.88	545	51.48	552	41.06	559
15					25.56	545	50.59	552	41.83	559
16	20.53	519			28.86	545	50.12	552	41.62	559
17	19.14	518					48.63	552	42.95	559
18							49.01	552	42.71	559
19							48.8	552	45.09	559
20							48.21	552	44.97	559
21							46.82	552	43.68	559
22							45.04	552	44.59	559
23							43.75	552	44.6	559
24							42.36	552	45.36	559
25							40.09	552	44.97	559
26							38.77	552	45	559
27							37.38	552	44.59	559
28							34.97	552	42.51	559
29							31.66	552	43.61	559
30							29.55	552	40.48	559
31							26.12	552	41.84	559
32							23.67	552	39.43	559

BRC = Beacon Range Cell (1/16 nm)
PRI = Pulse Repetition Interval

BAZ = Beacon Azimuth (ACP)
AMP. = Signal Amplitude (dB)
RC = Range Cell (1/16 nm)

TABLE A-10. RUN015 - FLTEST7 DATA (Continued)

	Scan 24 BRC: 565 BAZ: 2634		Scan 25 BRC: 570 BAZ: 2631		Scan 58 BRC: 776 BAZ: 2628		Scan 59 BRC: 782 BAZ: 2630		Scan 60 BRC: 789 BAZ: 2631	
PRT	AMP.	RC	AMP.	RC	AMP.	RC	AMP.	RC	AMP.	RC
8					23.18	780				
9					21.61	780				
10					25.29	780				
11					24.97	780				
12					22.86	780			20.37	790
13					30.07	780			22.3	790
14					24.65	780				
15					27.67	780				
16					27.09	780				
17	24.49	566			28.63	780			16.99	790
18	23.6	566			26.79	780			26.36	790
19	29.08	565			28.12	780	24.42	784	24.08	790
20	31.05	565			26.13	780	23.26	784	26.88	790
21	31.01	565			27.9	780			25.72	790
22	32.33	565			28.6	780	20.64	784	29.14	790
23	34.68	565			26.82	780	22.92	784	24.62	790
24	35.9	565	19.14	572	26.36	780	25.72	784	23.65	790
25	37.83	565	21.14	572	24.23	779	29	784	20.68	790
26	39.72	565	22.94	572	24.35	780			25.56	790
27	39.86	565	28.04	572	21.14	780				
28	39.93	565	29.27	572	23.05	780			24.35	790
29	41.8	565	31.47	572	21.96	780	18.13	784	17.16	790
30	41.08	565	35.15	572			17.85	783		
31	43.9	565	35.33	572					24.42	790
32	42.21	565	37.17	572					20.97	790

BRC = Beacon Range Cell (1/16 nm)
PRI = Pulse Repetition Interval
BAZ = Beacon Azimuth (ACP)
AMP. = Signal Amplitude (dB)
RC = Range Cell (1/16 nm)

TABLE A-10. RUN015 - FLTEST7 DATA (Continued)

	Scan 61 BRC: 795 BAZ: 2630		Scan 62 BRC: 801 BAZ: 2632		Scan 63 BRC: 807 BAZ: 2631		Scan 64 BRC: 814 BAZ: 2631		Scan 65 BRC: 820 BAZ: 2628	
PRT	AMP.	RC	AMP.	RC	AMP.	RC	AMP.	RC	AMP.	RC
3									18.13	821
4									19.49	821
5									21.85	821
6							21.64	816	28.13	821
7							23.44	815	28.28	821
8					24.74	809	24.65	815		
9					27.36	809	18.69	815	23.44	821
10					24.96	810	21.61	815	24.38	821
11			19.14	803	20.83	809			19.49	821
12			20	802	26.45	809			24.35	821
13	22.38	797			23.05	809			26.99	821
14	23.67	796	24.74	803	22.15	809			26.61	821
15	23.26	797	28.23	803	21.34	809			24.17	821
16			19.54	803	26.85	809			24.61	821
17					24.67	809			23.18	821
18					27.16	809			25.43	821
19	21.14	797			23.87	809			24.65	821
20	27.33	797	29.19	803	26.06	809			27.03	821
21	25.87	796	28.43	803	30.62	809	27.62	815	20.04	821
22	23.89	797	27.03	803	28.6	809	28.07	815	29.54	821
23	24.23	797	23.44	803	25.01	809	24.67	815		
24			22.04	803	24.3	809				
25	20	797	25.12	803	23.65	809				
26	24.23	797			25.12	809				
27	24.49	797	18.33	803	19.29	809				
28			24.84	803	19.29	879				
29					22.88	809				
30					17.63	809				

BRC = Beacon Range Cell (1/16 nm)
PRI = Pulse Repetition Interval
BAZ = Beacon Azimuth (ACP)
AMP. = Signal Amplitude (dB)
RC = Range Cell (1/16 nm)

TABLE A-10. RUN015 - FLTEST7 DATA (Continued)

	Scan 66 BRC: 826 BAZ: 2628		Scan 67 BRC: 833 BAZ: 2628		Scan 68 BRC: 839 BAZ: 2631		Scan 69 BRC: 845 BAZ: 2628		Scan 70 BRC:851 BAZ: 2626	
PRT	AMP.	RC	AMP.	RC	AMP.	RC	AMP.	RC	AMP.	RC
1	22.86	827							24.62	851
2	20.04	827			22.04	839			18.63	851
3	22.86	827	28.69	833	25.39	839	23.44	845	30.21	851
4	28.51	827	18.63	832	25.12	839	23.69	845		
5			18.13	833					18.06	851
6	21.64	827							26.28	851
7	24.17	827							23.05	851
8	22.94	827							20.97	851
9	23.87	827							19.08	851
10	32.36	827							19.91	851
11	27.09	827								
12	21.7	827	28.4	833						
13	25.12	827	21.61	832						
14	25.16	827	18.69	833						
15	19.91	827	19.87	833						
16	25.76	827	18.13	834						
17			24.35	833						
18	25.68	827								
19	26.24	827								
20	21.96	827								
21	23.44	827								
22										
23										
24										
25										
26			19.14	832						
27			17.24	833						
28										
29			18.13	832						
30			19.08	833						

BRC = Beacon Range Cell (1/16 nm)
PRI = Pulse Repetition Interval

BAZ = Beacon Azimuth (ACP)
AMP. = Signal Amplitude (dB)
RC = Range Cell (1/16 nm)

TABLE A-10. RUN015 - FLTEST7 DATA (Continued)

	Scan 71 BRC: 857 BAZ: 2630		Scan 72 BRC: 864 BAZ: 2627		Scan 73 BRC: 870 BAZ: 2630		Scan 74 BRC: 876 BAZ: 2630		Scan 75 BRC: 882 BAZ: 2631	
PRT	AMP.	RC	AMP.	RC	AMP.	RC	AMP.	RC	AMP.	RC
1	22.04	857							19.14	882
2	24.62	857							19.29	882
3	26.02	857	19.03	864	22.28	870				
4			19.91	863	21.7	870				
5	22.38	857			22.88	870				
6	22.1	857			23.01	870			25.11	882
7	22.55	857	17.16	864	19.54	870	18.63	876	22.38	882
8	24.23	857	20.25	863	26.45	870	23.69	876		
9	22.38	857	17.85	863	19.14	869	20.53	876	23.01	882
10	18.33	857	20.53	863	24.15	870	19.03	876	26.02	882
11	23.82	857	18.63	863	26.64	870	22.5	876	27.07	882
12	19.14	857	18.33	864			19.03	876	25.95	882
13	20.97	857			18.33	870	22.28	876	19.14	882
14	22.3	857			20.17	870			25.48	882
15	20.83	857			20	870			22.92	882
16	17.24	857								
17					18.06	869				
18					19.54	870				
19										
20										
21										
22										
23										
24							17.85	877		
25							19.87	877		

	Scan 76 BRC: 888 BAZ: 2630		Scan 77 BRC: 894 BAZ: 2630		Scan 79 BRC: 906 BAZ: 2629	
PRT	AMP.	RC	AMP.	RC	AMP.	RC
9	20.97	888				
10	27.16	888				
11	18.69	888				
12	22.15	888	19.54	893	21.73	904
13	19.91	888	21.14	893	21.73	904
14	19.29	888				
15	22.1	888				
16						
17						
18					19.87	904
19					18.63	905
20					18.69	904
21					22.67	904
22					20.17	904

BRC = Beacon Range Cell
PRI = Pulse Repetition Interval
BAZ = Beacon Azimuth (ACP)
AMP. = Signal Amplitude (dB)
RC = Range Cell (1/16 nm)

APPENDIX B

RESOLUTION

TABLE B-1. RUN021 - FLTEST61 AND FLTEST62 DATA

	Fltest60				Fltest61			
	Beacon 1		Beacon 2		Beacon 1		Beacon 2	
	BRC: 2216	BAZ: 2261	Missed		BRC: 1812	BAZ: 2557	BRC:1816	BAZ: 2557
PRT	AMP1	RC1	AMP2	RC2	AMP1	RC1	AMP2	RC2
8					26.45	453		
9					26.13	453		
10					32.9	452		
11					30.63	452		
12					37.19	453		
13	26.53	565	26.86	553	30.88	452		
14	32.7	565	26.28	553	37.18	453		
15	34.81	565	28.15	553	26.19	452		
16	33.29	565	29.19	553	42.95	453		
17	32.63	565	27.85	553	36.82	453		
18	30.66	565	31.49	553	35.22	452		
19	35.94	565	27.46	553	36	452		
20	39.55	565	27.82	553	37.26	453		
21	41.51	565	35.67	553	31.66	452		
22	40.08	565	43.01	553	33.9	452		
23	43.63	565	44.75	553	46.89	452		
24	41.9	565	41.48	553	39.7	453		
25	42.87	565	45.85	553	45.51	452		
26	47.95	565	44.43	553	42.09	452		
27	47.99	565	44.42	553	40.04	452		
28	44.36	565	39.98	553	38.2	453		
29	40.99	565	41.98	553	41.14	452		
30	42.18	565	38.08	553	38.08	452		
31	45.19	565	34.45	553	40.34	452		
32	44.74	565	36.09	553	36	452		
33	45.6	565	41.8	553	32.47	452		
34	42.29	565	46.05	553	27.85	452		
35	44.06	565	46.86	553	34.14	452		
36	42.74	565	43.64	553	32	452		
37	41.22	565	41.78	553	30.62	453		
38	40.21	565	43.83	553	33.52	452		

Beacon Separation: Fltest60 - N/A ; Fltest61 - Range 4/64 nm; Azimuth 0 ACP

BRC = Beacon Range (1/64 nm)
AMP = Signal Amplitude (dB)
BAZ = Beacon Azimuth (ACP)

PRI = Pulse Repetition Interval
RC = Radar Range (1/16 nm)

TABLE B-2. RUN021 - FLTEST63 DATA

	Beacon 1 Missed		Beacon 2 Missed	
PRT	AMP1	RC1	AMP2	RC2
1				
2	20.25	546		
3	23.01	546		
4	29.84	546	23.52	556
5	27.67	546	27.46	556
6	30.45	546	30.86	556
7	28.68	546	28.49	556
8	34.04	546	27.17	556
9	34.04	546	30.59	556
10	31.95	546	32.95	556
11	34.98	546	25.93	556
12	37.13	546	35.79	556
13	37.78	546	28.84	556
14	35.27	546	37.42	556
15	35	546	36.04	556
16	33.14	546	40.64	556
17	34.81	546	36.55	556
18	36.94	546	38.41	556
19	38.5	546	40.73	556
20	30.88	546	39.42	556
21	37.44	546	41.64	556
22	35.31	546	41.95	556
23	35.01	546	35.81	556
24	33.17	546	37.93	556
25	34.19	546	35.16	556
26	29.71	546	38.28	556
27	32.03	546	37.98	556
28	33.26	546	35.44	556
29	29.49	546	34.95	556
30	27.6	546	33.56	556
31	23.52	546	34.04	556
32	25.72	546	33.38	556
33	24.97	546	33.81	556
34	20.04	546	33.22	556
35			30.69	556
36	18.06	546	22.04	556
37	18.33	546	24.74	556
38			21.61	556

PRI = Pulse Repetition Interval
AMP = Signal Amplitude
RC = Radar Range Cell

TABLE B-3. RUN021 - FLTEST65 DATA

	Scan 1				Scan 2			
	Beacon 1		Beacon 2		Beacon 1		Beacon 2	
	BRC:2190	BAZ:2578	BRC:2189	BAZ:2580	BRC:2159	BAZ:2582	BRC:2159	BAZ:2579
PRI	AMP1	RC1	AMP2	RC2	AMP1	RC1	AMP2	RC2
9					18.63	539		
10					22.5	539		
11	20.97	546			21.64	539		
12	20	546			18.33	539		
13	22.86	546			20.25	539		
14	27.52	546			22.3	539		
15	25.95	547			21.61	539		
16	28.73	546			21.61	539		
17	25.58	547			20.97	539		
18	34.06	546			33.61	539		
19	33.23	546			29.92	538		
20	38.35	546			39.52	539		
21	39.94	546			41.56	539		
22	40.33	546			41.98	539		
23	38.83	546			47.28	539		
24	41.52	546			46.04	539		
25	42.36	546			44.36	539		
26	41.3	546			46.37	539		
27	39.55	546			46.41	539		
28	45.94	546			43.27	539		
29	38.43	546			39.16	539		
30	46.36	546			40.75	538		
31	47.2	546			42.3	539		
32	44.84	546			45.2	539		
33	48.76	546			39.21	539		
34	47.5	546			35.42	539		
35	43.57	546			46.17	539		
36	43.32	546			48.45	539		
37	46.4	546			47.11	539		
38	42.57	546			45.19	539		
39	42.1	546			46.4	539		
40	40.97	546			45.91	539		
41	42.63	546			42.6	539		
42	40.11	546			38.86	539		
43	38.25	546			41.39	539		
44	33.52	546	17.16	541	38.38	539		
45	34.95	546	16.99	540	28.51	539		

Beacon Separation: Scan 1: Range 1/64 nm; Azimuth 2 ACPs
Scan 2: Range 0/64 nm; Azimuth 3 ACPs

BRC = Beacon Range Cell (1/64 nm)
RC = Radar Range Cell (1/16 nm)
BAZ = Beacon Azimuth (ACP)
AMP = Signal Amplitude (dB)

TABLE B-3. RUN021 - FLTEST65 DATA (Continued)

	Scan 1				Scan 2			
	Beacon 1		Beacon 2		Beacon 1		Beacon 2	
	BRC:2190	BAZ:2578	BRC:2189	BAZ:2580	BRC:2159	BAZ:2582	BRC:2159	BAZ:2579
PRI	AMP1	RC1	AMP2	RC2	AMP1	RC1	AMP2	RC2
46	26.93	546			30.4	539		
47	20.04	546			26.99	539		
48	23.26	546			25.58	539		
49	20.86	546			20.83	539		
50	19.29	545			21.64	539		
51					21.14	539		
52					18.06	539		

	Scan 3				Scan 4			
	Beacon 1		Beacon 2		Beacon 1		Beacon 2	
	BRC: 2127	BAZ:2577	BRC:2129	BAZ:2579	BRC:2079	BAZ:2577	BRC:2102	BAZ:2579
PRI	AMP1	RC1	AMP2	RC2	AMP1	RC1	AMP2	RC2
6	18.57	531						
7	17.63	530						
8	19.14	530						
9					19.91	523		
10					19.29	523		
11	18.57	531			21.07	523		
12	24.15	531			26.19	523		
13					25.43	523		
14	21.37	531			26.67	523		
15	17.85	532			26.64	523	24.84	525
16	27.99	532			32.8	523	27.27	525
17	28.79	531			33.76	523		
18	30.32	531			34.15	523		
19	29.93	532			30.11	523	32.88	525
20	36.42	531			36.8	523	32.08	525
21	39.12	531			41.26	523	30.94	525
22	36.67	531			43.67	523	18.69	515
23	41.27	531			45.29	523		
24	38.99	531			42.61	523	38.5	525
25	35.83	530			42.62	523	38.52	525
26	44.46	531			44.35	523		
27	39.98	532			43.83	523		
28	43.68	532			45.95	523	43.55	525
29	41.47	531			43.92	523	41.86	525

Beacon Separation: Scan 3: Range 2/64 nm; Azimuth 2 ACPs
Scan 4: Range 6/64 nm; Azimuth 2 ACPs

BRC = Beacon Range Cell (1/64 nm)
RC = Radar Range Cell (1/16 nm)
BAZ = Beacon Azimuth (ACP)
AMP = Signal Amplitude (dB)

TABLE B-3. RUN021 - FLTEST65 DATA (Continued)

	Scan 3				Scan 4			
	Beacon 1		Beacon 2		Beacon 1		Beacon 2	
	BRC: 2127	BAZ:2577	BRC:2129	BAZ:2579	BRC:2079	BAZ:2577	BRC:2102	BAZ:2579
PRI	AMP1	RC1	AMP2	RC2	AMP1	RC1	AMP2	RC2
30	45.87	531			41.78	523	43.2	525
31	46.61	531			43.8	523		
32	41.47	530			45.07	523		
33	41.29	530			46.54	523		
34	37.16	531			46.41	523		
35	42.17	531			47.38	523		
36	46.27	531			45.97	523		
37	44.56	531			44.54	523		
38	42.23	531			42.05	523		
39	36.9	530			41.1	523	33	525
40	37.25	532			37.2	523	37.5	525
41	39.56	532			39.54	523		
42	36.36	532			35.64	523	36.32	525
43	30.94	532			28.97	523	25.62	525
44	37.03	531			31.64	523	30.88	525
45	34.88	531			33.18	523		
46	29.84	531			32.28	523		
47	26.03	531			27.44	523		
48	22.58	530			23.12	523	19.29	525
49	20.64	530			18.13	523	20.04	525
50	20.97	531			18.57	523		

	Scan 5				Scan 6			
	Beacon 1		Beacon 2		Beacon 1		Beacon 2	
	BRC: 2065	BAZ:2577	BRC:2076	BAZ:2580	BRC:2034	BAZ:2578	BRC:2049	BAZ:2580
PRI	AMP1	RC1	AMP2	RC2	AMP1	RC1	AMP2	RC2
7					19.49	511		
8					17.85	512		
9								
10								
11			19.54	518				
12			20	518	24.23	507		
13					19.29	508		
14	24.15	518			24.62	507		
15	21.85	515	23.12	518	28.15	507	30.04	511
16	17.85	515	26.67	518	31.16	507	28.97	511

Beacon Separation: Scan 5: Range 11/64 nm: Azimuth 3 ACPs
Scan 6: Range 15/64 nm: Azimuth 2 ACPs

BRC = Beacon Range Cell (1/64 nm) BAZ = Beacon Azimuth (ACP)
RC = Radar Range Cell (1/16 nm) AMP = Signal Amplitude (dB)

TABLE B-3. RUN021 - FLTEST65 DATA (Continued)

	Scan 5				Scan 6			
	Beacon 1		Beacon 2		Beacon 1		Beacon 2	
	BRC: 2065	BAZ:2577	BRC:2076	BAZ:2580	BRC:2034	BAZ:2578	BRC:2049	BAZ:2580
PRI	AMP1	RC1	AMP2	RC2	AMP1	RC1	AMP2	RC2
17			22.3	518	30.94	507	32.26	511
18	21.85	515	26.39	518	30.75	507	34	511
19	28.72	515	36.82	518	33.62	507	36.48	511
20	30.94	515	30.17	518	34.51	507	39.55	511
21	34.45	515	39.93	518	33.05	507	38.97	511
22	34.55	515	33.26	518	31.55	507	38.41	511
23	36.78	515	39.49	518	34.02	507	40.32	511
24	40.63	515	40.51	518	37.9	507	36.62	511
25	32.68	515	36.65	518	41.61	507	39.85	511
26	21.64	515	41.07	518	41.85	507	25.89	511
27	35.65	515	41.09	518	42.71	507	41.9	511
28	30	515	36.01	518	46.62	507	41.61	511
29	36.24	515	37.08	518	40.93	507	43	511
30	32.26	515	45.68	518	43.13	507	43.97	511
31	42.37	515	42.69	518	41.56	507	44.69	511
32	32.32	515	41.72	518	43.53	507	41.91	511
33	42.03	515	44.3	518	37.82	507	44.92	511
34	36.96	515	38.55	518	36.93	507	41.54	511
35	42.56	515	39.98	518	40.05	507	37.82	511
36	35.19	515	43.77	518	26.99	507	40.79	511
37	40.04	515	40.8	518	40.14	507	28.63	511
38	32.56	515	37.27	518	41.07	507	35.61	511
39	26.13	515	38.21	518	39.79	507	29.25	511
40	34.2	515	37.47	518	38.69	507	33.29	511
41	28.51	515	25.12	518	40.29	507	32.73	511
42	26.13	515	32.69	518	33.67	507	31.48	511
43	30.26	515	35.37	518	34.64	507	32.88	511
44	23.98	515	31.22	518	33.32	507	28.23	511
45	28.81	515	29.8	518	25.72	507	28.6	511
46	24.38	515	24.23	518	26.27	507		
47	22.04	515	23.52	518	20.97	507		
48	23.65	515	23.12	518	16.99	507		
49	20.37	515	20.04	518	22.92	507		
50					19.29	507		

BRC = Beacon Range Cell (1/64 nm)
RC = Radar Range Cell (1/16 nm)
BAZ = Beacon Azimuth (ACP)
AMP = Signal Amplitude (dB)

TABLE B-3. RUN021 - FLTEST65 DATA (Continued)

	Scan 7				Scan 8			
	Beacon 1		Beacon 2		Beacon 1		Beacon 2	
	BRC: 2002	BAZ:2577	BRC:2021	BAZ:2579	BRC:1971	BAZ:2577	BRC:1993	BAZ:2577
PRI	AMP1	RC1	AMP2	RC2	AMP1	RC1	AMP2	RC2
12			19.54	499				
13			22.04	499				
14	19.03	504	20	499			20	491
15	25.39	504	25.39	499	25.68	498	22.28	492
16	20	505	23.05	499	25.48	497	25.31	492
17	25.28	504	31.16	499	26.7	498	20.04	491
18			34.65	499	25.62	497	25.31	492
19			32.73	499	32.91	498	25.76	491
20			34.45	499	31.78	498	26.55	492
21	32.14	504	38.93	499	35.68	498		
22	36.18	504	41.14	499	34.74	497	37.06	491
23	28.38	504	41.93	499	35.4	497	31.54	491
24	29.53	504	42.1	499	26.82	498	36.54	491
25	36.93	504	43.45	499	38.95	497	37.8	491
26			41.16	499	26.82	497	39.52	491
27	41.89	504	44.96	499	41.84	497	41.77	491
28	36.49	504	42	499	37.2	498	32.82	491
29	37.42	504	47.54	499	36.94	497	36.79	491
30	38.46	504	45.52	499	42.05	498	38.35	491
31	33.92	504	44.09	499	41.66	497	29.46	491
32	35.37	504	46.51	499	34.82	497	41.61	491
33	37.28	504	47.46	499	42.57	497		
34	40.95	504	46.57	499	38.38	497	45.18	491
35	35.31	504	47.13	499	40.54	497	43.03	491
36	35.33	504	44.13	499	34.15	498	34.7	492
37	30.11	504	43.62	499	33.27	497	41.66	491
38	35.48	504	44.08	499	39.08	497	40.51	491
39	31.6	504	39.78	499	29.74	497	40.06	491
40	36.42	504	42.96	499	39.08	497	40.99	491
41	30.94	504	38.51	499	33.2	498	30.18	491
42	28.91	504	41.74	499	30.97	497	34.49	491
43	29.37	504	37.85	499	34.74	498	25.67	491
44	23.89	504	35.12	499	24.84	498	33.03	492
45	19.29	505	35.83	499	29.66	498	21.96	491
46	23.44	504	33.12	499	28.99	498	33.92	491

Beacon Separation: Scan 7: Range 19/64 nm; Azimuth 2 ACPs
Scan 8: Range 22/64 nm; Azimuth 0 ACPs

BRC = Beacon Range Cell (1/64 nm)
RC = Radar Range Cell (1/16 nm)
BAZ = Beacon Azimuth (ACP)
AMP = Signal Amplitude (dB)

TABLE B-3. RUN021 - FLTEST65 DATA (Continued)

	Scan 7				Scan 8			
	Beacon 1		Beacon 2		Beacon 1		Beacon 2	
	BRC: 2002	BAZ:2577	BRC:2021	BAZ:2579	BRC:1971	BAZ:2577	BRC:1993	BAZ:2577
PRI	AMP1	RC1	AMP2	RC2	AMP1	RC1	AMP2	RC2
47			27.16	499			23.87	492
48			27.63	499			24.35	491
49							23.98	491
50			24.61	499			21.7	492
51	19.49	499						
52								
53								
54					17.63	497		
55					16.53	498		

	Scan 9				Scan 10			
	Beacon 1		Beacon 2		Beacon 1		Beacon 2	
	BRC: 1939	BAZ:2577	BRC:1966	BAZ:2579	BRC:1908	BAZ:2582	BRC:1938	BAZ:2580
PRI	AMP1	RC1	AMP2	RC2	AMP1	RC1	AMP2	RC2
4							17.24	476
5							16.53	477
6								
7								
8					17.63	484		
9					18.13	484		
10					21.61	484		
11					20.86	484		
12					23.01	484		
13	22.67	491			21.34	484	19.54	476
14	20.83	491			25.28	484	22.28	476
15	19.14	491	19.29	484	30.07	484	25.62	476
16	27.31	491	21.07	484	27.31	484	22.94	476
17	21.64	491	23.87	484	34.44	484	25.95	476
18	24.84	491	30.37	484	36.27	484	27.55	476
19	26.19	491	27.33	484	36.39	484	23.98	476
20	23.01	491	32.67	484	38.55	484	30.16	476
21	27.61	491	33.25	484	42.03	484	33.1	476
22	30.8	491	35.91	484	41.95	484	30.51	476
23	29.56	491			46.55	484	38.34	476
24	27.36	491	40.76	484	45.32	484	31.87	476
25	36.54	491	41.47	484	44.21	484	41.25	476
26	35.59	491	39.56	484	45.51	484	42.77	476

Beacon Separation: Scan 9: Range 27/64 nm; Azimuth 2 ACPs
Scan 10: Range 30/64 nm; Azimuth 2 ACPs

BRC = Beacon Range Cell (1/64 nm)
RC = Radar Range Cell (1/16 nm)
BAZ = Beacon Azimuth (ACP)
AMP = Signal Amplitude (dB)

TABLE B3. RUN021 - FLTEST65 DATA (Continued)

	Scan 9				Scan 10			
	Beacon 1		Beacon 2		Beacon 1		Beacon 2	
	BRC: 1939	BAZ:2577	BRC:1966	BAZ:2579	BRC:1908	BAZ:2582	BRC:1938	BAZ:2580
PRI	AMP1	RC1	AMP2	RC2	AMP1	RC1	AMP2	RC2
27	41.33	491	38.64	484	45.14	484	40.13	476
28	36.06	491	40.91	484	48.4	484	44.32	476
29	36.2	491	42.23	484	49.91	484	42.76	476
30	36.58	491	41.14	484	42.75	484	39.74	476
31	27.73	491	43.22	484	48.24	484	41.71	476
32	24.42	491	44.52	484	48.04	484	40.26	476
33	32.42	491	42.45	484	49.48	484	42.84	476
34	35.56	491	43.39	484	47.27	484	37.74	476
35	25.67	491	42.41	484	51.84	484	43.14	476
36	33.63	491	41.25	484	48.18	484	41.2	476
37	28.36	491	44.05	484	47.63	484	36.99	476
38	38.03	491	44.54	484	44	484	43.23	476
39	31.52	491	41.19	484	44.69	484	42.63	476
40	38.37	491	38.26	484	41.78	484	38.99	476
41	27.36	491	38.28	484	43.86	484	42.28	476
42	33.35	491	39.68	484	41.11	484	38.6	476
43	20	491	35.76	484	39.02	484	33.42	476
44	19.14	490	39.81	484	37.92	484	33.27	476
45			34.12	484	37	484	32.87	476
46			33.17	484	37.19	484	26.79	476
47			20.25	483	32.35	484	30.68	476
48			29.77	484	30.72	484	19.87	476
49	20	491	25.28	484	26.28	484	21.96	476
50	17.85	491	26.82	484	20.97	484	18.13	476
51			23.65	484	22.38	484	26.19	476
52							18.13	476

	Scan 11				Scan 12			
	Beacon 1		Beacon 2		Beacon 1		Beacon 2	
	BRC: 1877	BAZ:2579	BRC:1911	BAZ:2579	BRC:1846	BAZ:2579	BRC:1884	BAZ:2579
PRI	AMP1	RC1	AMP2	RC2	AMP1	RC1	AMP2	RC2
11					19.87	470		
12					25.59	470		
13	25.68	477			21.96	470		
14	24.86	477			29.03	470		
15	29.01	477	18.13	468	32.56	470		
16	30.62	477	20.83	468	33.05	470	25.12	460

Beacon Separation: Scan 11: Range 34/64 nm: Azimuth 0 ACPs
Scan 12: Range 38/64 nm: Azimuth 0 ACPs

BRC = Beacon Range Cell (1/64 nm)
RC = Radar Range Cell (1/16 nm)
BAZ = Beacon Azimuth (ACP)
AMP = Signal Amplitude (dB)

TABLE B-3. RUN021 - FLTEST65 DATA (Continued)

	Scan 11				Scan 12			
	Beacon 1		Beacon 2		Beacon 1		Beacon 2	
	BRC: 1877	BAZ:2579	BRC:1911	BAZ:2579	BRC:1846	BAZ:2579	BRC:1884	BAZ:2579
PRI	AMP1	RC1	AMP2	RC2	AMP1	RC1	AMP2	RC2
17	32.3	477	22.67	468	33.65	470	22.1	460
18	31.7	477	23.82	468	35.42	470	25.68	460
19	34.36	477	27.18	468	38.97	470	26.88	460
20	35.35	477	30.88	468	39.39	470	28.81	460
21	34.32	477	35.16	468	41.39	470	34.42	460
22	32.39	477	39.15	468	40.12	470	28.28	460
23	41.85	477	38.5	468	43.64	470	32.6	460
24	39.47	477	40.48	468	45.37	470	37.05	460
25	45.3	477	38.56	468	45.25	470	41.16	460
26	44.34	477	38.86	468	49.93	470	45.98	460
27	46.02	477	41.55	468	48.95	470	41.25	460
28	45.97	477	41.71	468	47.42	470	40.85	460
29	45.53	477	41.57	468	48.03	470	43.19	460
30	46	477	39.37	468	49.24	470	39.45	460
31	46.54	477	44.22	468	49.34	470	39.75	460
32	44.94	477	44.76	468	49.77	470	43.17	460
33	41.87	477	45.77	468	48.98	470	45.95	460
34	41.78	477	48.08	468	46.04	470	40.41	460
35	45.73	477	47.96	468	47.05	470	40.18	460
36	44.89	477	46.33	468	46.49	470	46.27	460
37	42.55	477	44.76	468	49.27	470	42.97	460
38	45.99	477	42.81	468	45.59	470	45.97	460
39	44	477	40.51	468	49.07	470	48.8	460
40	43.49	477	41.02	468	46.27	470	42.97	460
41	42.21	477	40.46	468	43.2	470	40.66	460
42	38.06	477	37.97	468	41.56	470	39.2	460
43	39.75	477	40	468	42.1	470	38.07	460
44	35.8	477	36.12	468	39.96	470	35.53	460
45	31.29	477	37.45	468	37.45	470	38.38	460
46	31.4	477	37.79	468	31.37	470	25.58	460
47	31.36	477	34.88	468	31.69	470	33.02	460
48	26.28	477	32.71	468	31.4	470	30.25	460
49	27.85	477	28.23	468	27.87	470	35.63	460
50	23.12	477	26.82	468	27.98	470	29.83	460
51	24.74	477	22.5	468	24.97	470	33.22	460
52	16.02	477	20.53	468	21.37	470	23.67	460
53	18.13	477	17.85	468			22.3	460
54			19.29	468			20.68	460

BRC = Beacon Range Cell (1/64 nm)
RC = Radar Range Cell (1/16 nm)
BAZ = Beacon Azimuth (ACP)
AMP = Signal Amplitude (dB)

TABLE B-3. RUN021 - FLTEST65 DATA (Continued)

	Scan 13				Scan 14			
	Beacon 1		Beacon 2		Beacon 1		Beacon 2	
	BRC: 1815	BAZ:2582	BRC:1856	BAZ:2579	BRC:1785	BAZ:2580	BRC:1828	BAZ:2580
PRI	AMP1	RC1	AMP2	RC2	AMP1	RC1	AMP2	RC2
13	20	463					20.53	456
14	27.97	463					25.12	456
15	28.77	463					24.17	456
16	31.05	463					28.46	456
17	32.68	463	18.69	453			32.19	456
18	32.75	463	19.08	452	20	445	30.37	456
19	37.5	463	24.3	453	19.14	445	34.2	456
20	33.05	463	21.34	453			32.28	456
21	38.3	463	34	452	18.69	445	31.82	456
22	41.67	463	33.26	453	26.02	445	40.83	456
23	40.41	463	34.6	452	26.06	445	39.68	456
24	41.63	463	31.29	452	22.15	445	42.67	456
25	43.83	463	36.71	453	32.1	445	41.66	456
26	49.26	463	40	453	34.14	445	45.33	456
27	45.11	463	39.09	453	29.31	445	45.35	456
28	47.15	463	39.26	453	29.41	445	46.63	456
29	44.54	463	38.6	453	33.9	445	43.09	456
30	48.92	463	35.67	452	25.31	445	46.92	456
31	38.35	463	41.22	452	29.04	445	39.09	456
32	47.2	463	38.38	452	30.69	445	44.64	456
33	46.2	463	44.77	453	38.67	445	43.05	456
34	47.84	463	42.4	453	32.99	445	48.03	456
35	46.43	463	43.94	453	39.39	445	41.6	456
36	45.19	463	42.2	452	34.72	445	48.26	456
37	44.85	463	38.79	453	34.16	445	45.33	456
38	44.62	463	41.53	453	39.32	445	42.7	456
39	49.13	463	43	453	41.17	445	45.25	456
40	43.54	463	39.87	453	32.86	445	43.72	456
41	43.18	463	39.28	453	29.85	445	43.3	456
42	40.8	463	34.92	452	34.88	445	40.07	456
43	37.96	463	37.59	453	36.66	445	34.93	456
44	37.87	463	31.51	453	27.73	445	35.99	456
45	34.68	463	37.48	452	38.55	445	33.81	456
46	34.86	463	35.45	452	34.71	445	29.94	456
47	31.62	463	34.02	453	30.48	445	33.81	456
48	29.89	463	21.7	452	24.08	445	29.59	456
49	24.35	463			27.11	445	26.27	456
50	27.03	463	24.96	453	18.69	445	25.22	456
51	24.23	463	29.79	453	22.86	456		
52	22.28	463	23.12	453	20.68	456		
53	18.57	463	24.96	453				
54			16.53	452				

Beacon Separation: Scan 13: Range 41/64 nm: Azimuth 3 ACPs
Scan 14: Range 43/64 nm: Azimuth 0 ACPs

TABLE B-3. RUN021 - FLTEST65 DATA (Continued)

Scan 15

	Beacon 1		Beacon 2	
	BRC: 1758	BAZ:2592	BRC:1800	BAZ:2580
PRI	AMP1	RC1	AMP2	RC2
14			18.06	449
15			20.53	449
16			18.63	449
17			20.97	449
18			23.05	449
19			26.9	449
20				
21			22.94	449
22			32.75	449
23			31.78	449
24			40.17	449
25	20.97	438	32.49	449
26	23.84	439	34.92	449
27	31.22	439	42.93	449
28			40.1	449
29	21.73	438	40.9	449
30	21.7	439	38.9	449
31	25.59	438	39.77	449
32	27.27	438	29.46	449
33	35.42	439	34.51	449
34	30.88	439	40.63	449
35	29.83	438	41.96	449
36	33.47	438	40.79	449
37	33.43	439	44.93	449
38	39.01	439	37.75	449
39	38.56	438	35.69	449
40	44.03	439	42.08	449
41	33.29	438	40.16	449
42	33.33	438	37.06	449
43	33	439	35.48	449
44	36.19	438	27.63	449
45	38.99	438	27.18	449
46	37.27	438	32.11	449
47	35.9	438	28.28	449
48	32.55	438	31.5	449
49	34.9	438	24.84	449

Beacon Separation: Scan 15: Range 42/64 nm: Azimuth 12 ACPs

BRC = Beacon Range Cell (1/64 nm)
RC = Radar Range Cell (1/16 nm)
BAZ = Beacon Azimuth (ACP)
AMP = Signal Amplitude (dB)

TABLE B-3. RUN021 - FLTEST65 DATA (Continued)

Scan 15

	Beacon 1		Beacon 2	
	BRC: 1758	BAZ:2592	BRC:1800	BAZ:2580
PRI	AMP1	RC1	AMP2	RC2
50	35.2	439	23.54	449
51	32.26	438	18.57	449
52	34.84	439	23.01	449
53	19.03	438	19.08	449
54	27.98	438	18.63	449
55	26.68	439		
56	24.3	438		
57	24.65	438		
58	25.87	439		
59	20.04	438		
60	18.13	438		

BRC = Beacon Range Cell (1/64 nm)
RC = Radar Range Cell (1/16 nm)
BAZ = Beacon Azimuth (ACP)
AMP = Signal Amplitude (dB)

TABLE B-4. RUN021 - FLTEST66 DATA

	Scan 1				Scan 2			
	Beacon 1		Beacon2		Beacon 1		Beacon2	
	BRC:2095	BAZ:2564	BRC:2097	BAZ:2564	BRC:2064	BAZ:2562	BRC:2070	BAZ:2564
PRT	AMP1	RC1	AMP2	RC2	AMP1	RC1	AMP2	RC2
25					15.31	519		
26					16.9	518		
49					18.13	517		
50					20.25	517		
51					21.37	517	17.85	515
52							24.15	516
53					18.57	515		
54	17.63	523					23.12	517
55	23.44	523					27.67	517
56	23.6	522					29.55	517
57	29.07	523					33.59	517
58					32.42	515	31.22	517
59	30.19	524			36.65	515		
60	32.33	524			33.84	515	33	517
61	35.3	523					40.47	517
62	30.25	522	30.31	524			40.76	517
63	38.15	523					42.49	517
64	37.82	524					43.2	517
65	33.16	523					40.9	517
66	36.48	524					40.99	517
67	46.88	523					41.65	517
68	39.32	524					44.83	517
69	27.24	523			40.66	515	43.49	517
70	37.25	523			43.31	515	41.36	517
71	38.92	523			46.5	515	36.45	517
72	42.61	523			43.73	515		
73	38.79	524					42.67	517
74	37.27	523					43.82	517
75	42.61	523					42.53	517
76	38.32	524					42.79	517
77	41.31	523					41.58	517
78	36.43	523					37.42	517
79	38.65	523					36.65	517
80	34.26	524					37.99	517
81	30.88	523					35.73	517
82	29.08	524			35.44	515	31.5	517
83	32.9	523			33.81	515	27.07	517
84	29.84	524			27.99	515		
85	27.23	523					29.14	517
86	20.53	524			24.49	515	24.49	517
87	23.69	523			25.28	515	24.3	517
88	22.67	524			18.33	515	19.14	517

Beacon Separation: Scan 1: Range 2/64 nm; Azimuth 0 ACPs
Scan 2: Range 6/64 nm; Azimuth 2 ACPs

TABLE B-4. RUN021 - FLTEST66 DATA (Continued)

	Scan 3				Scan 4			
	Beacon 1		Beacon2		Beacon 1		Beacon2	
	BRC:2032	BAZ:2564	BRC:2043	BAZ:2561	BRC:2001	BAZ:2561	BRC:2016	BAZ:2562
PRT	AMP1	RC1	AMP2	RC2	AMP1	RC1	AMP2	RC2
3	16.99	509						
4	15.68	509						
32							17.16	499
33							16.53	500
47					18.13	503		
48					22.38	503		
49	16.99	506			24.84	503		
50	19.14	507			28.33	503		
51	17.63	507			30.72	503	24.3	499
52	17.16	507	17.63	510	33.3	503	26.13	499
53	24.62	507	24.15	510	36.11	503	26.03	499
54	28.28	507	18.13	510	37.73	503	26.28	499
55	26.52	507	25.12	510	37.18	503	27.9	499
56	29.29	507	28.68	510	40.15	503	25.99	499
57	27.99	507	25.12	510	40.79	503	31.8	499
58	31.56	507	26.24	510	39.93	503	35.21	499
59	30.48	507	34.64	510	43.58	503	35.06	499
60	30.66	507	34.66	510	46.31	503	36.2	499
61	35.51	507	36.9	510	46.43	503	39.37	499
62	41.91	507	25.05	510	48.12	503	41.33	499
63	35.74	507	36.11	510	49.25	503	41.3	499
64	36.82	507	39.65	510	50.56	503	42.92	499
65	43.56	507	39.14	510	51.37	503	35.45	499
66	40.16	507	37.75	510	49.61	503	36.38	499
67	42.24	507	41.29	510	51.06	503	34.35	499
68	39.41	507	38.6	510	50.6	503	42.04	499
69	40.1	507	31.39	510	49.1	503	44.44	499
70	40.75	507	42.41	510	47.86	503	41.27	499
71	35.16	507	41.16	510	50.02	503	41.32	499
72	37.69	507	39.72	510	51.11	503	40.28	499
73	40.72	507	40.35	510	49.63	503	39.98	499
74	45.39	507	38.31	510	48.44	503	43.06	499
75	44.26	507	20.68	510	49.34	503	40.55	499
76	36.28	507	36.36	510	48.36	503	39.26	499
77	35.67	507	37.97	510	48.32	503	39.71	499
78	40.24	507	35.39	510	47.51	503	31.78	499
79	36.58	507	32.47	510	43.61	503	28.99	499

Beacon Separation: Scan 3: Range 11/64 nm; Azimuth 3 ACPs
Scan 4: Range 15/64 nm; Azimuth 1 ACP

BRC = Beacon Range Cell (1/64 nm)
AMP = Signal Amplitude (dB)
BAZ = Beacon Azimuth (ACP)
RC = Radar Range Cell (1/16 nm)

TABLE B-4. RUN021 - FLTEST66 DATA (Continued)

	Scan 3				Scan 4			
	Beacon 1		Beacon2		Beacon 1		Beacon2	
	BRC:2032	BAZ:2564	BRC:2043	BAZ:2561	BRC:2001	BAZ:2561	BRC:2016	BAZ:2562
PRT	AMP1	RC1	AMP2	RC2	AMP1	RC1	AMP2	RC2
80	35.28	507	32.6	510	43.48	503	27.99	499
81	30	507	23.12	510	40.24	503	32.92	499
82	31.39	507	32.67	510	37.1	503	29.69	499
83	25.89	507	28.36	510	36.4	503	27.11	499
84	22.92	507	26.28	510	35.38	503	24.62	499
85	25.87	507	24.67	510	31.14	503	23.98	499
86	25.95	507			30.37	503	22.58	499
87	20.04	507			27.97	503	18.63	500
88	20	507			24.71	503		
89					22.38	503		
90					20.37	503		

	Scan 5				Scan 6			
	Beacon 1		Beacon2		Beacon 1		Beacon2	
	BRC:1970	BAZ:2569	BRC:1988	BAZ:2562	BRC:1938	BAZ:2561	BRC:1961	BAZ:2561
PRT	AMP1	RC1	AMP2	RC2	AMP1	RC1	AMP2	RC2
39	18.13	498			18.33	483		
40	15.68	499			16.99	482		
47	18.69	496			16.13	484		
48	21.58	496			21.14	483		
49	22.86	496			21.14	484	26.36	490
50	24.62	496	20.68	492	23.12	483	23.82	490
51	23.01	496	20.53	491	17.85	482		
52	20.68	496	16.9	492			19.29	490
53	21.61	497					26.45	489
54	28.65	496	19.29	491	28.07	483	20.37	489
55	31.6	496	22.3	491	32.42	483	23.65	489
56	31.69	496	28.13	491	34.2	483	29.54	489
57	30.04	496	33.29	491	35.2	483	29.33	489
58	35.12	496	35.59	491	40.3	483	28.81	489
59	31.87	496	37.95	491	34.67	483	26.48	490
60	40.99	496	33.25	491	40.66	483	35.24	489
61	41.66	496	38.78	491	40.83	483	38.69	489
62	42.95	496	35.88	491	38.89	483	43.08	489
63	38.82	496	40.76	491	34.88	483	28.2	489

Beacon Separation: Scan 5: Range 18/64 nm: Azimuth 7 ACPs
Scan 6: Range 23/64 nm: Azimuth 0 ACPs

BRC = Beacon Range Cell (1/64 nm)
AMP = Signal Amplitude (dB)
BAZ = Beacon Azimuth (ACP)
RC = Radar Range Cell (1/16 nm)

TABLE B-4. RUN021 - FLTEST66 DATA (Continued)

	Scan 5				Scan 6			
	Beacon 1		Beacon2		Beacon 1		Beacon2	
	BRC:1970	BAZ:2569	BRC:1988	BAZ:2562	BRC:1938	BAZ:2561	BRC:1961	BAZ:2561
PRT	AMP1	RC1	AMP2	RC2	AMP1	RC1	AMP2	RC2
64	37.19	496	28.36	491	34.47	483	33.77	490
65	37.01	496	33.67	491	34.82	483	37.06	489
66	40.93	496	32.01	491	43.72	483	28.84	489
67	42.06	496	34.11	491	43.49	483	37.82	489
68	35.3	496	34.39	491	44.3	483	40.51	489
69	42.81	496	40.28	491	46.67	483	32.93	489
70	36.13	496	40.59	491	44.71	483	18.69	490
71	39.3	496	41.94	491	40.09	483	32.38	490
72	43.12	496	39.99	491	43.78	483	35.71	489
73	43.76	496	41.16	491	44.41	483	32.75	489
74	41.28	496	36.87	491	39.46	483	42.74	489
75	40.69	496	38.22	491	40.28	483	39.57	489
76	34.58	496	38.68	491	35.11	483	22.55	489
77	32.28	496	26.68	491	33.3	483	29.84	490
78	32.32	496	28.06	491	31.85	483	29.29	489
79	33.67	496	24.61	491	37.16	483	23.98	489
80	31.7	496	28.33	491	35.83	483	25.67	489
81	28.86	496	32.47	491	34.21	483		
82	23.12	496	28.02	491	34.88	483	16.99	490
83	25.95	496	26.99	491	24.74	483	19.87	489
84	24.38	496			28.95	483		
85	20.97	496			26.27	483		
86	22.38	496			23.52	483		
87					19.49	483		

	Scan 7				Scan 8			
	Beacon 1		Beacon2		Beacon 1		Beacon2	
	BRC:1907	BAZ:2564	BRC:1934	BAZ:2561	BRC:1882	BAZ:2568	BRC:1907	BAZ:2559
PRT	AMP1	RC1	AMP2	RC2	AMP1	RC1	AMP2	RC2
39	15.56	477						
40	17.85	476						
47					21.7	476		
48			23.12	483	18.13	476		
49			22.55	483	24.42	476		
50			24.23	483	23.05	476		
51			27.75	483	28.68	476		
52			31.96	483	30.21	476		
53	20.86	476	29.27	483	32.27	476		
54	20.25	476	26.45	483	32.05	476		

Beacon Separation: Scan 7: Range 27/64 nm: Azimuth 3 ACPs
Scan 8: Range 25/64 nm: Azimuth 9 ACPs

TABLE B-4. RUN021 - FLTEST66 DATA (Continued)

	Scan 7				Scan 8			
	Beacon 1		Beacon2		Beacon 1		Beacon2	
	BRC:1907	BAZ:2564	BRC:1934	BAZ:2561	BRC:1882	BAZ:2568	BRC:1907	BAZ:2559
PRT	AMP1	RC1	AMP2	RC2	AMP1	RC1	AMP2	RC2
55	26.83	476	33.61	483	34.62	476		
56	23.69	476	35.45	483	35.37	476	18.13	470
57	26.02	476	29.83	483	36.93	476	20.64	469
58	27.36	476	41.87	483	28.6	476	16.13	470
59	29.41	476	39.54	483	38.48	476	20	470
60	19.14	476	42.8	483	42.85	476	23.67	469
61	31.73	476	41.07	483	42.37	476	24.62	469
62			40.83	483	43.35	476	27.5	469
63	30.59	476	42.36	483	42.14	476	28.18	469
64	33.14	476	45.58	483	44.76	476	34.65	469
65	32.91	476	34.3	483	42.54	476	32.71	469
66	32.73	476	42.05	483	43.92	476	37.44	470
67	32.21	476	43.63	483	42.9	476	35.3	469
68	38.11	476	37.04	483	43.3	476	35.16	469
69	38.51	476	44.22	483	46.54	476	36.83	469
70	35.76	476	44.97	483	43.46	476	37.35	469
71	38.97	476	42.08	483	44.38	476	38.87	470
72	25.72	476	44.32	483	41.65	476	39.26	469
73	39.7	476	43.04	483	37.99	476	39.69	469
74	37.03	476	38.4	483	37.1	476	38.37	469
75	33.32	476	38.86	483	33.74	476	38.02	469
76	31.44	476	38.96	483	37.2	476	37.15	469
77	31.9	476	39.25	483	38.76	476	42.61	469
78	30.31	476	24.08	483	33.06	476	37.96	469
79	29.27	476	34.35	483	34.79	476	41.96	470
80	34.89	476	31.37	483	28.69	476	37.17	469
81	32.47	476	27.18	483	32.95	476	36.02	469
82	24.42	476	30.28	483	27.72	476	32.53	469
83	24.15	476	26.44	483	29.66	476	36.45	470
84			23.67	483	24.65	476		
85			20.53	483	20.37	476		
88							24.84	469
89							26.06	469
90							23.98	469
91							16.9	470
92							25.12	469
93							18.33	470
94							21.7	470
95							17.63	469
99	16.9	476						
100	19.03	476						

BRC = Beacon Range Cell (1/64 nm) BAZ = Beacon Azimuth (ACP)
AMP = Signal Amplitude (dB) RC = Radar Range Cell (1/16 nm)

TABLE B-4. RUN021 - FLTEST66 DATA (Continued)

	Scan 9				Scan 10			
	Beacon 1		Beacon2		Beacon 1		Beacon2	
	BRC:1865	BAZ:2580	BRC:1875	BAZ:2565	BRC:1857	BAZ:2587	BRC:1864	BAZ:2568
PRT	AMP1	RC1	AMP2	RC2	AMP1	RC1	AMP2	RC2
14					16.99	465		
15					15.68	466		
16					17.63	465		
17					16.13	464		
18					15.05	467		
49	20.17	470						
50	20.53	470						
51	23.44	470						
52	23.12	470						
53	29.27	470						
54	26.99	470						
55	32.28	470						
56	32.39	470						
57	37.38	470						
58	33.05	470						
59	36.82	470			21.61	465		
60	41.31	470			25.16	465		
61	44.11	470			31.34	465		
62	40.68	470			31.51	465		
63	40.01	470			35.11	465		
64	41.66	470	21.58	465	35.09	465		
65	42.77	470	21.37	465	38.14	465		
66	44.83	470	23.38	465	40.19	465		
67	43.85	470	26.93	465	40.62	465		
68	42.17	470	28.17	465	41.57	465		
69	48.75	470	31.39	465	42.91	465		
70	45.57	470	32.84	465	43	465		
71	42.45	470	33.47	465	43.01	465		
72	44.64	470	33	465	43.7	465		
73	34.15	470	36.53	465	43.25	465		
74	44.55	470	37.42	465	47.34	465		
75	38.33	470	38.69	465	45.06	465		
76	38.3	470	39.01	465	47.33	465		
77	39.02	470	44.25	465	45.47	465		
78	37.68	470	43.61	465	47.01	465		
79	38.77	470	43.23	465	47.5	465		

Beacon Separation: Scan 9: Range 10/64 nm: Azimuth 15 ACPs
Scan 10: Range 7/64 nm: Azimuth 19 ACPs

BRC = Beacon Range Cell (1/64 nm)
AMP = Signal Amplitude (dB)
BAZ = Beacon Azimuth (ACP)
RC = Radar Range Cell (1/16 nm)

TABLE B-4. RUN021 - FLTEST66 DATA (Continued)

	Scan 9				Scan 10			
	Beacon 1		Beacon2		Beacon 1		Beacon2	
	BRC:1865	BAZ:2580	BRC:1875	BAZ:2565	BRC:1857	BAZ:2587	BRC:1864	BAZ:2568
PRT	AMP1	RC1	AMP2	RC2	AMP1	RC1	AMP2	RC2
80	34.16	470	43.34	465	45.07	465		
81	35.76	470	46.03	465	47.62	465		
82	33.89	470	46.39	465	45.28	465	43.39	463
83	28.23	470	46.09	465	42.14	465	45.39	463
84	31.45	470	44.58	465	47.4	463		
85	26.86	470	44.78	465	48.42	463		
86	24.17	470	44.83	465	49.8	463		
87	20	470	43.85	465	51.06	463		
88	18.63	470	43.09	465	51.36	463		
89	20.97	470	45.35	465	51.79	463		
90			44.99	465	53.07	463		
91			43.43	465	53.82	463		
92			43.29	465	54.09	463		
93			41.12	465	54.08	463		
94			42.15	465	54.36	463		
95			40.46	465	54.19	463		
96			40.25	465	54.69	463		
97			36.18	465	54.67	463		
98			34.26	465	54.36	463		
99			32.58	465	53.79	463		
100			27.99	465	53.32	463		
101			31.06	465	51.79	463		
102			26.02	465	51.73	463		

	Scan 11				Scan 12			
	Beacon 1		Beacon2		Beacon 1		Beacon2	
	BRC:1859	BAZ:2596	BRC:1854	BAZ:2580	BRC:1870	BAZ:2605	BRC:1853	BAZ:2584
PRT	AMP1	RC1	AMP2	RC2	AMP1	RC1	AMP2	RC2
57	17.63	466						
58	18.69	465						
59								
60								
61								
62								
63	22.86	463						
64	26.27	463						
65	31.1	463						
66	32.2	463						

Beacon Separation: Scan 11: Range 5/64 nm; Azimuth 16 ACPs
Scan 12: Range 17/64 nm; Azimuth 21 ACPs

BRC = Beacon Range Cell (1/64 nm)
AMP = Signal Amplitude (dB)
BAZ = Beacon Azimuth (ACP)
RC = Radar Range Cell (1/16 nm)

TABLE B-4. RUN021 - FLTEST66 DATA (Continued)

	Scan 11				Scan 12			
	Beacon 1		Beacon2		Beacon 1		Beacon2	
	BRC:1859	BAZ:2596	BRC:1854	BAZ:2580	BRC:1870	BAZ:2605	BRC:1853	BAZ:2584
PRT	AMP1	RC1	AMP2	RC2	AMP1	RC1	AMP2	RC2
67	34.46	463						
68	35.98	463						
69	37.83	463						
70	39.04	463						
71	40.69	463						
72	42.95	463						
73	44.11	463						
74	45.62	463						
75	46.91	463			20.97	463		
76	47.28	463			21.96	462		
77	49.52	463			25.16	463		
78	50.45	463			26.79	463		
79	50.99	463						
80	51.07	463			33.54	463		
81	51.88	463			35.8	463		
82	51.83	463			37.56	463		
83	52.02	463			39.85	463		
84	52.64	463			42.08	462		
85	53	463			43.65	463		
86	51.92	463			44.98	463		
87	50.64	463			45.99	462		
88	51.62	463			47.09	463		
89	51.83	463			48.33	462		
90	50.55	463			47.57	463		
91	49.43	463			47.73	463		
92	49.52	463			48.25	463		
93	46.04	463			49.22	463		
94	47.65	463			48.77	463		
95	45.12	463			48.8	463		
96	42.72	463			49.61	463		
97	39.39	463			50.27	463		
98	42.71	463			50.34	463		
99	43.01	463			49.68	463	18.63	467
100	40.47	464			48.8	463	22.28	467
101	41.38	464			48.73	463	23.98	466
102	44.39	464			46.26	463	22.1	467

BRC = Beacon Range Cell (1/64 nm)
AMP = Signal Amplitude (dB)
BAZ = Beacon Azimuth (ACP)
RC = Radar Range Cell (1/16 nm)

TABLE B-4. RUN021 - FLTEST66 DATA (Continued)

	Scan 13				Scan 14			
	Beacon 1		Beacon2		Beacon 1		Beacon2	
	BRC:1888	BAZ:2609	BRC:1857	BAZ:2693	Missed		BRC:1867	BAZ:2601
PRT	AMP1	RC1	AMP2	RC2	AMP1	RC1	AMP2	RC2
78					15.31	466		
79					19.54	466		
86	16.13	456						
87	19.49	464						
88	16.99	464						
89								
90	26.12	464						
91	25.43	464						
92	29.49	464						
93	29.85	464						
94	32.84	464			17.24	466		
95	32.42	464			19.14	466		
96	32.55	464			23.01	466		
97	27.99	464			24.3	466		
98	35.3	464			20	466		
99	40.06	464			27.03	466		
100	34.98	464			29.27	466		
101	35.76	464			31.07	466		
102	38.77	464			34.45	466		

Beacon Separation: Scan 13: Range 31/64 nm; Azimuth 84 ACPs
Scan 14: N/A

	Scan 15				Scan 16			
	Beacon 1		Beacon2		Beacon 1		Beacon2	
	BRC:1936	BAZ:2605	BRC:1883	BAZ:2605	Missed		Missed	
PRT	AMP1	RC1	AMP2	RC2	AMP1	RC1	AMP2	RC2
5					16.99	450		
6					19.08	451		
7								
8					16.99	538		
9					16.9	538		
10								
11								
12								
13					15.56	416		
14					16.53	415		
15					19.03	492		
16					19.08	492		

Beacon Separation: Scan 15: Range 53/64 nm; Azimuth 0 ACPs
Scan 16: N/A

BRC = Beacon Range Cell (1/64 nm)
AMP = Signal Amplitude (dB)
BAZ = Beacon Azimuth (ACP)
RC = Radar Range Cell (1/16 nm)

TABLE B-4. RUN021 - FLTEST66 DATA (Continued)

	Scan 15				Scan 16			
	Beacon 1		Beacon2		Beacon 1		Beacon2	
	BRC:1936	BAZ:2605	BRC:1883	BAZ:2605	Missed		Missed	
PRT	AMP1	RC1	AMP2	RC2	AMP1	RC1	AMP2	RC2
20					16.53	515		
21					18.33	516		
22					16.99	515		
31					21.96	405		
32					15.56	406		
33								
34					16.99	496		
35					18.69	496		
50					17.63	409		
51	22.3	466			16.13	409		
52	24.15	466						
53	23.69	466						
54	24.23	466						
55	26.7	466			19.54	520		
56	18.63	462	28.99	466	16.99	521		
57	16.53	461	28.99	466	16.13	516		
58					15.31	517		
59								
60								
61								
62								
63					16.99	530	16.02	465
64					18.13	529	14.15	464
65					17.63	499		
66					17.16	499	20.64	483
67	32.99	466			22.3	482		
68	34	466			22.3	483	17.24	462
69	33.68	466			16.02	462		
70	31.47	466			22.94	483		
71	32.01	466			19.03	483		
72	31	466			19.91	483		
73	31.08	466			20	483		
74	27.36	466			15.68	483		
75	27.61	466						
76	28.77	466						
77								

BRC = Beacon Range Cell (1/64 nm)
AMP = Signal Amplitude (dB)
BAZ = Beacon Azimuth (ACP)
RC = Radar Range Cell (1/16 nm)

TABLE B-4. RUN021 - FLTEST66 DATA (Continued)

	Scan 15				Scan 16			
	Beacon 1		Beacon2		Beacon 1		Beacon2	
	BRC:1936	BAZ:2605	BRC:1883	BAZ:2605	Missed		Missed	
PRT	AMP1	RC1	AMP2	RC2	AMP1	RC1	AMP2	RC2
78	17.24	467						
79	16.02	466			16.02	477		
80	18.57	467			15.56	476		
81	17.24	467						
82	16.99	467						
83								
84					16.53	483		
85					19.03	482		
86								
87								
88								
89								
90								
91					19.54	415		
92					15.56	414	17.63	423
93					18.33	417	19.91	422
94					17.63	487	16.13	417
95					16.99	487		
96					15.05	488		
97								
98								
99								
100								
101					16.99	508		
102					16.13	509		

BRC = Beacon Range Cell (1/64 nm)
AMP = Signal Amplitude (dB)
BAZ = Beacon Azimuth (ACP)
RC = Radar Range Cell (1/16 nm)

TABLE B-4. RUN021 - FLTEST66 DATA (Continued)

Scan 17

	Beacon 1		Beacon2	
	Missed		Missed	
PRT	AMP1	RC1	AMP2	RC2
2	18.13	423		
3	17.16	423		
4	15.31	422	15.31	464
5	16.99	438	16.13	464
6	14.62	439		
7				
8	15.68	412		
9	14.62	413		
12	16.13	445		
13	16.02	444		
14	16.9	457		
15	18.69	457	18.06	459
16	16.99	458		
19	16.99	495		
20	17.16	494		
21	16.99	536		
22	16.53	536		
30	19.87	539		
31	16.99	539		
32	18.06	539		
33	18.57	490		
34	16.53	489	17.85	425
35	16.53	424	14.62	412
36	17.24	402	16.13	411
37	14.62	401		
38	16.99	481		
39	18.57	480		
40				
41				
42	15.68	462		
43	16.13	461	16.13	478
44	17.16	479		
48	19.29	500		
49	16.13	500		
50	16.9	499		
51	19.14	500		
52	20.25	500	17.16	474

Beacon Separation: Scan 17: N/A

BRC = Beacon Range Cell (1/64 nm)
AMP = Signal Amplitude (dB)
BAZ = Beacon Azimuth (ACP)
RC = Radar Range Cell (1/16 nm)

TABLE B-4. RUN021 - FLTEST66 DATA (Continued)

Scan 17

	Beacon 1		Beacon2			
	Missed		Missed			
PRT	AMP1	RC1	AMP2	RC2		
53	20.53	500	16.99	475		
54	20.86	499				
55	23.98	499	16.99	556		
56	22.3	500	22.1	555	20.04	546
57	23.98	499	16.13	428	16.53	545
58	14.62	427				
59						
60	16.13	433				
61	18.57	433				
62						
63	14.62	450				
64	16.53	551	15.31	449		
65	18.13	551				
66						
67	30.16	500	17.24	508		
68	34.28	500	28.86	509		
69	28.72	500				
70	29.13	500				
71	28.46	500				
72	26.19	500	16.13	467		
73	26.86	499	17.63	467		
74	25.39	500	15.56	467		
75	23.26	500				
76	23.98	500				
77						
78	17.16	446				
79	16.99	447				
84	15.68	536				
85	16.99	535				
86	19.14	422				
87	21.61	422				
88	20.04	422				
89	17.24	422				
90	21.07	422	16.53	430		
91	19.08	422	19.87	431		
92	18.57	422				
93	20.04	422	18.13	450		
94	18.69	422	17.16	449		
95	20.97	422				
100	15.68	430	16.99	456		
101	16.13	431	16.13	456		

BRC = Beacon Range Cell (1/64 nm)
AMP = Signal Amplitude (dB)
BAZ = Beacon Azimuth (ACP)
RC = Radar Range Cell (1/16 nm)